

**Computer assisted surgery for
fracture reduction and deformity correction of
the pelvis and long bones**

A Dissertation

Submitted to the Faculty of Mathematics and Computer Science
of the University of Mannheim
for the Degree of Doktor der Naturwissenschaften (Dr. rer .nat)

by

matematik - sistemnyj programmist Aleh Kryvanos
from Minsk/Belarus

Mannheim, 2002

**Computer assisted surgery for
fracture reduction and deformity correction of
the pelvis and long bones**

Inauguraldissertation
zur Erlangung des akademischen Grades
eines Doktors der Naturwissenschaften
der Universität Mannheim

vorgelegt von
matematik - sistemnyj programmist Aleh Kryvanos
aus Minsk/Belarus

Mannheim, 2002

Dekan: Professor Dr. Herbert Popp, Universität Mannheim
Referent: Privatdozent Dr. Jürgen Hesser, Universität Mannheim
Korreferent: Professor Dr. Mikhail M. Makhaniok, National Academy of
Belarus, Minsk/Belarus

Tag der mündlichen Prüfung 23. Mai 2002

Zusammenfassung

Viele Knochenoperationen, wie beispielsweise Osteotomien, werden nicht präoperativ geplant, so dass das Operationsergebnis weitgehend von der Erfahrung des Operateurs abhängt. In der Industrie sind Neuentwicklungen ohne CAD-Planungen oder Computersimulationen nicht mehr denkbar, lediglich in der Medizin hat sich die Operationstechnik bei den Korrekturosteotomien in den letzten 30 Jahren nur unwesentlich weiterentwickelt. Nach wie vor wird die Fehlstellung zweidimensional analysiert und darauf basierend im Operationssaal die Operation durchgeführt. Die präoperative Information über die aktuelle Knochensituation erhält der Chirurg durch Röntgenaufnahmen. Bei komplexeren Operationen (dazu gehört beispielsweise auch die Implantatsetzung) sind Planungen unerlässlich. Planungen basierend auf Röntgenaufnahmen haben einige systembedingte Nachteile wie geringe Genauigkeit, hoher Zeitbedarf (um die Verzeichnungen aufgrund der Projektion zu korrigieren) und Einschränkungen, wenn komplexe Korrekturen notwendig werden.

Als Lösung dient heute die Computertomographie. Sie ist momentan die einzige Modalität, um hinsichtlich der Genauigkeit und der Auflösung den Anforderungen einer guten 3D-Planung zu genügen. Sie hat allerdings den gravierenden Nachteil einer höheren Dosisbelastung für den Patienten, so dass beim Abwägen zwischen der Dosisbelastung und einer adäquaten Planung oftmals erstere entscheidend ist. Zukünftig wird aber erwartet, dass für Operationsergebnisse Garantien übernommen werden, was nur mit einer guten 3D-Planung möglich ist. MR-Systeme liefern zwar Bilder, aus denen sich indirekt Knochen extrahieren lassen, aber aufgrund der groben Verzeichnungen (Suszeptibilität, Magnetfeldinhomogenitäten), geringer räumlicher Auflösung und der hohen Kosten ist nicht zu erwarten, dass sie in nächster Zeit eine Alternative darstellen.

Der Ausweg aus diesem Dilemma ist die Nutzung anderer bildgebender Modalitäten. Ultraschall ist hier sowohl von den Kosten, als auch von der Genauigkeit ein guter Kompromiss. In dieser Arbeit entwickelte ich einen Algorithmus, mit dem man aus Ultraschalldaten 3D-Knochenmodelle erzeugen kann, die von der Geometrie sowohl von Auflösung, als auch von der Genauigkeit mit denen aus CT vergleichbar sind und daher in 3D-Planungsaufgaben genutzt werden können. Zur Lösung der Arbeit wird ein verbessertes Verfahren zum Segmentieren von Knochenoberflächen realisiert in Kombination mit Methoden zur Fusion zu einem dreidimensionalen Modell.

Das Besondere der Arbeit ist die Kombination eines von mir entwickelten 3D-Operationsplanungssystems und eines Ultraschall-basierten Trackingsystems. Zum Verwirklichen dieser Ideen, ist es notwendig, die folgenden Aufgaben zu lösen:

- Segmentierung von Knochen aus CT Daten;
- Extraktion der Knochenoberflächen aus Ultraschallbildern in Echtzeit;
- Tracking der Knochenoberfläche relativ zum CT-Datensatz;
- Integration der oben genannten Ergebnisse zu einem Planungssystem für Osteotomie-Korrekturen, das on-line Messungen unterstützt, verschiedene Typen der Deformität korrigiert (unter Verwendung eines anatomischen Modells) und dabei noch einen hohen Grad von Automatisierung mitbringt.

Das entwickelte Osteotomie Planungssystem ermöglicht die Untersuchung und Analyse der Pathologie. Das System berechnet eine optimale Planung und ermöglicht eine präzise visuelle und quantitative Begutachtung des post-operativen Ergebnisses. Daher kann dieses System als ein zusätzliches und sinnvolles Werkzeug für die orthopädische Chirurgie betrachtet werden. Die Hauptteile sind dabei die Knochenmodellierung anhand von 3D-Daten aus CT, MRI oder anderen Modalitäten, deren Visualisierung in Echtzeit und die geometrische Modellierung von Knochenfragmenten. Ein hoher Grad an Automatisierung ermöglicht dabei eine erhebliche Reduzierung der gesamten Planungszeit für die Operation.

Abstract

Intensive evolution of computer industry has been affecting almost all spheres of human activity. The appearance of fast, compact, reliable computer systems and successful implementation of information technologies in science and industry have promised new perspectives for engineers and physicians to start active developments in computerized medicine. This joint cooperation stimulates such application areas as medical image processing and visualisation.

Numerous computer applications have been developed to optimise the work of physicians. Many of them are addressed to the problems of improving the quality or/and analysing biological signals of response, e.g. electrocardiogram (ECG), electroencephalogram (EEG), and etc. Such systems are implemented in cardiology, neurology, gynaecology and other medical branches. However, not only one-dimensional signals are used to measure biological activity of different organs and tissues.

For a long time a variety of scanners has been applied in medicine to form 2D signals, i.e. image, to display the patient's anatomy or physiological functionality of different organs. The most popular and widely used scanners are found in radiology. The appearance of opportunities to acquire digital signals from X-ray imaging systems and optical cameras has challenged active developments in a new application area, called medical image processing. It provides accurate, frequently very fast diagnostic, reduces clinical routine work and offers new opportunities for physicians in investigating and developing new treatment methods.

In typical radiological applications, medical image processing is used to improve the X-ray image quality, create and maintain image databases and etc. However, in orthopaedic practice, many actual tasks are addressed not only to visual investigation of current skeleton's state. Surgical planning is frequently required for reducing fractures or correcting deformities, i.e. detecting the degree of the existing deformity and analysing an appropriate corrective method to provide a high degree of precision. Moreover, there are modern requirements for surgical interventions to be as little invasive, as possible so that surgery would lead to a minimal secondary damage for the patient and therefore to a lower risk and cost of the operation, and to a shorter rehabilitation period. Thus, the planning and implementation of such surgical procedures are becoming increasingly complex and expensive.

This complexity requires engaging experienced staff. However, the efficient planning and executing modern orthopaedic operations can be carried out with the aid of computers, i.e. with the implementation of Computer Assisted Orthopaedic Surgery (CAOS).

Human skeleton is a biomechanical system with very complex three dimensional (3D) geometry. Implementation of traditional planning methods based on the processing conventional X-ray images does not allow to achieve good accuracy both in planning and surgical procedures. The reasons are difficulties in the interpretation of anatomy by a limited number of X-ray projections, the necessity for a surgeon to keep in his/her mind numerous 3D reconstructions, which depend on the individual abilities and experience of the surgeon, and existence of X-ray projective errors. Another major limitation in current surgical practice is the lack of accurate quantitative measurements.

Since the development of computer tomography (CT) in 1974, computers have been increasingly used in medical practice. The manipulation of CT data has become popular in medical image processing. Compared with radiography, which operates on 2D images, CT gives an opportunity to process 3D data, by stacking up continuous parallel 2D slices. Recent developments in 3D computer graphics have led to 3D visualisation methods, which are able to work in real- or near real-time on a conventional personal computer (PC). Thus, the orthopaedic surgeon can obtain promising tools for improving the interpretation of biological structures, for increasing the diagnostic quality and in this way the effectiveness of the treatment. However, as discussed above, computer systems for preoperative planning and intraoperative control are complicated and therefore require sophisticated software, such as segmentation algorithms for bone modelling, virtual reality methods for simulating surgery steps and results, in order to analyse the skeleton in near real- or real-time. These technologies have been applied in industry for more than twenty years, but the field of CAOS is still in its infant stage. Recent CAOS developments have started to appear in clinical practice and promise both to help surgeons and to improve patient's treatment. They challenges the development of orthopaedic applications for fast processing and analysis of visual information.

The dissertation is devoted to the realisation of an exact 3D planning system and operation support system in orthopaedic surgery for the treatment of pelvis and long bone fractures and post-traumatic deformities. The work describes new methods in medical image processing,

including tools for image segmentation, computer-aided design, and system engineering that provide a solution for a variety of problems both in planning and supporting orthopaedic surgery.

Nowadays, traditional planning is carried out on 2D films, i.e. bone projections. Planning on CT data is just in its development. In principle, the traditional planning is not accurate because it inherits projection errors, and usually gives good results only in case of simple deformities. For instance, the procedure of osteotomy planning becomes extremely difficult in the case of 3D torsion and, of course, it is time-consuming. Moreover, the whole process is carried out by hand drawings and therefore even small deviations of the ideal position of the cutting plane can result in a failure of the whole operation. Thus, the whole process of preoperative planning becomes difficult even for experienced surgeons.

Accurate planning helps medical staff significantly to increase the quality of surgery, but still does not guarantee the success of the operation. Orthopaedic surgeons widely use methods like fluoroscopy, computer tomography and magnetic resonance imaging (MRI) for diagnose and CAOS. However, in practice their usage is frequently limited. Neither CT nor MRI provide information about the position of bones in real-time when their reposition might occur. In this case, the realisation of the operation plan is difficult (or even impossible). The implementation of fluoroscopy does not guarantee rather a good navigation after the reposition of skeleton parts, because of the complex anatomy and the limited number of X-ray sources. In case of pelvis surgery, the treatment is almost not possible without real-time intraoperative navigation. To perform the operation, the surgeon has to be navigated (i.e. to be oriented with respect to anatomy). The navigation allows to make the right correction and the fixation as accurate as possible. During the operation screws should be placed very precisely, because the thickness of the pelvis bone is frequently comparable with the diameter of the screws. For instance, an open pelvic fracture reduction causes a severe tissue damage and it is not possible in many cases of pelvis surgery. Implementation of less-invasive percutaneous surgery provides minimal damage. However, it requires an experienced surgeon and usually leads to high radiation doses both for the patient and the staff.

In my research I analysed a new structure of CAOS systems. The novelty of the presented work is in new approaches to realising an operation planning system, based on 3D computations, and implementing the intraoperative control by a guided ultrasound system for bone tracking. To realise these

ideas it is necessary to solve the following tasks:

- bone modelling from CT data. It includes the investigation and the development of segmentation methods for the extraction of bone surfaces from the sequences of CT images;
- partial real-time extraction of bone surfaces from guided ultrasound imaging. This task assumes the development of fast techniques for segmentation and classification of bone surfaces on the sequences of 2D ultrasound images;
- tracking the bone. Tracking is achieved by a real-time registration to obtain the pose of ultrasound (US) bone surfaces with respect to CT bone model.
- integrating and implementing the above results in the development of an operation planning system for osteotomy corrections (osteotomy planning system) that supports on-line measurements, different types of deformity correction, a bone geometry design and a high level of automation.

Bone modelling from CT data is carried out by using flexible segmentation tools, in an automatic or interactive mode. Different techniques are proposed to optimise the work of a surgeon, such as interactive multi-thresholding and automatic optimal thresholding based on the method of discriminant analysis, an entropy method or their combination, and morphological segmentation enhanced by the region growing algorithm. The selection of the segmentation techniques depends on the decision of the surgeon and the complexity of the pathology.

The heart of the operation support system is an ultrasound based navigation. The goal consists of intraoperative bone tracking and can be reached by using 3D ultrasound: highly accurate, minimal invasive and riskless medical equipment. The research was focused on the problem of B-mode US image segmentation, mostly in real-time. First, a classification of ultrasound artefacts to investigate the types of artefacts which influence the segmentation process is proposed. Then a preprocessing strategy is discussed and a new algorithm of automatic segmentation and classification of bones from US data is presented (the rainfall algorithm). Finally, a cadaveric validation study to investigate the robustness of the algorithm was carried out.

The tracking of bones is done by intraoperative registration of surfaces extracted from US and CT. To satisfy the requirements of real-time processing, the acceleration of the registration algorithm over the precalculation of 3D distances for data extracted from CT is proposed. Several experiments to calculate the accuracy of the registration algorithm were carried out. Their results showed that the accuracy is suitable for clinical use (mean distance error being less than 1.6 mm, rotation being less than 2 degrees).

The developed osteotomy planning system allows to investigate the pathology, makes its analysis, finds an optimal way to realise surgery and provides visual and quantitative information about the results of the virtual operation. Therefore, the implementation of the proposed system can be considered as an additional significant tool for the diagnosis and orthopaedic surgery. The major parts of the planning system are: bone modelling from 3D data derived from CT, MRI or other modalities, visualisation of the elements of the 3D scene (virtual surgical space) in real-time, and the geometric design of bone elements. A high level of automation allows the surgeon to reduce significantly the time of the operation plane development.

Prototypes of the developed systems were tested in the clinic of Ulm, Trauma department. Planning was done on different saw-bones and real patients (CT, MRI data). The algorithms of bone tracking were tested on saw-bones and cadaveric bones.

Organization

This thesis is organised as following:

- Chapter 1 discusses the state of computer assisted surgery art and gives an overview of the proposed operation planning and supporting system (intraoperative navigation system) for the surgery of long bones and pelvis. The main concepts, the structure of the proposed system and the visualisation principles are presented.
- Chapter 2 is concerned with an overview of the segmentation methods for bone extraction from CT images. The methods that can be implemented interactively or in automatic mode are described. Finally, the methodology of the segmentation for orthopaedic operation planning and supporting systems is given.
- Chapter 3 presents the solution of the problem of the extraction and classification of bone surfaces from ultrasound images. First, the classification of artefacts produced during ultrasonic scanning is done. Then an overview describing those filter and segmentation methods that allow to reduce or even eliminate the presence of artefacts on B-mode ultrasound images is shown. Fully developed automatic algorithm of the extraction and classification of bone surfaces (the rainfall algorithm) is described. Finally, two validation studies of the rainfall algorithm are investigated.
- Chapter 4 analyses the method for CT and US registration. It starts from the discussion of existing methods and the description of the application of the Iterative Closest Point (ICP) algorithm for surface registration of CT and US and its disadvantages. Acceleration techniques of the ICP algorithm, which are based on a 3D distance coding are discussed. Next, an algorithm to calculate the internal distance function is presented. The validation of the registration accuracy for a synthetic data set and for two medical phantoms of femur and pelvis bones (saw-bones) is proposed.
- Finally, Chapter 5 presents a description and a clinical implementation of an osteotomy planning system. The available methods of correction

are discussed and numerous examples are presented. Also, the current state of the ultrasound based navigation system is given and future perspective research directions are suggested.

- Summary of the results is given in Conclusion.
- The major tools for image processing such as basic morphological operators are described in the Appendix.

Acknowledgements

The author thanks all his colleagues, who have taken a part in author support and assistance during the work. I would like to express personal gratitude to:

PD Dr. J. Hesser, Institute for Computer Medicine, Germany, my fellow who supervised the work, for motivation, expertise and sharing his ideas;

special thanks must be given to Dr. Sc. A.V. Tuzikov, Information Technologies Centre of the National Academy of Sciences of Belarus. He participated significantly and supervised in development of segmentation techniques, based on mathematical morphology;

Dr. S. Sheynin and Y. Prokopchuk from the Information Technologies Centre of the National Academy of Sciences of Belarus, for their numerous consultations in mathematics;

Dr. V. Kovalev, Max-Plank Institute for Neuropsychology, Germany, for sharing his experience;

My personal grateful is directed to Dr. Keppler, clinic of Ulm, Germany. His inspiration, assistance in understanding of medical problems and big attention to this work help me significantly;

PD Dr. F. Gebhard, clinic of Ulm, for advising and technical support of the work;

Prof. Dr. M.M. Makhaniok, Information Technologies Centre of the National Academy of Sciences of Belarus, for the general supervision, initiation and support of my research, as well as for openness and friendliness through the years of its execution;

Prof. Dr. R. Maenner, Lehrstuhle fuer Informatik V, University of Mannheim, for his encouragement, establishment of excellent working equipment and research atmosphere;

Volume Graphics GmbH (www.volumegraphics.com) team for its assistance in implementing the volume graphic library (VGL) in author's software; AO research foundation for financial support of the presented work (99-K43) and also administration staff both the Clinic of Ulm and the University of Mannheim.

Contents

1	Computer Assisted Orthopaedic Surgery	15
1.1	Introduction	15
1.1.1	Why CAOS is so important?	19
1.1.2	Dissertation goals	20
1.2	Methods overview	21
1.2.1	Planning systems	21
1.2.2	Navigation systems	22
1.3	Proposed method	25
1.3.1	Planning	25
1.3.2	Bone tracking based on ultrasound imaging	26
1.3.3	System overview	26
1.3.4	Visualisation	27
1.4	Summary	29
2	Modelling bone surfaces from CT	31
2.1	Thresholding methods	33
2.1.1	Segmentation of bones by histogram based thresholding	34
2.1.2	Adaptive thresholding	38
2.1.3	Limitations of the thresholding techniques	39
2.2	Edge based segmentation	39
2.3	Region based segmentation	41
2.4	Shape based segmentation	44
2.5	Proposed morphological segmentation	45
2.6	Error estimation	49
2.7	Application of the morphological segmentation	51
2.8	Summary	52

3	Segmentation of bone surfaces from US	53
3.1	Backgrounds of ultrasound	53
3.1.1	Physical principles of ultrasonic imaging	55
3.1.2	Types of ultrasonic instrumentation	56
3.1.3	Transducers	57
3.2	Artefacts in ultrasound	58
3.2.1	Artefacts produced by equipment	59
3.2.2	Artefacts produced by ultrasound interaction	60
3.3	Image processing B-mode ultrasound	64
3.3.1	Methods overview	65
3.3.2	Proposed method	69
3.3.3	The rainfall algorithm	76
3.3.4	Validation of the rainfall algorithm	81
3.4	Improvement of the rainfall algorithm	85
3.5	Summary	86
4	Registration	87
4.1	Introduction in image registration	87
4.1.1	Types of registration	87
4.1.2	Methods of registration	88
4.1.3	Rigid body registration	91
4.2	Iterative closest point algorithm	93
4.2.1	Principles	93
4.2.2	Why <i>ICP</i> ?	93
4.3	Distance map	94
4.4	Validation of the modification of the <i>ICP</i> algorithm	97
4.4.1	Registration of synthetic data	98
4.4.2	Phantom accuracy validation	102
4.5	Summary	106
5	System integration	113
5.1	Introduction	113
5.2	Operation planning system	118
5.2.1	Workflow	118
5.2.2	Anatomical landmarks	120
5.2.3	Measurements	120
5.2.4	Virtual osteotomy	123
5.2.5	Supported types of osteotomies	124

<i>CONTENTS</i>	13
5.2.6 Rearrangement of bone segments	127
5.2.7 Clinical applications	128
5.2.8 Comparison with other systems	131
5.3 Operation support system	134
5.4 Future steps	134
5.5 Summary	135
6 Conclusion	137
7 Appendix: Background of the image processing	139
7.1 Basic mathematical tools for the image processing	139
7.2 Binary operations	140
7.3 Gray-level morphology	142
8 Glossary	147

Chapter 1

Computer Assisted Orthopaedic Surgery

1.1 Introduction

In recent years computer assistance has become more and more useful and popular in medicine not only for diagnostic purposes, but also for surgery [21]. The applications in the field of computer assisted orthopaedic surgery can be functionally divided into two classes, i.e. preoperative planning and intraoperative control. The operation planning and control systems are developed to optimise the performance of a surgeon, i.e. to increase the quality of surgery and to make it minimal-invasive.

The purpose of the planning procedure is the determination of the information that is vitally important for the realisation of the surgical operation. The preoperative planning can be defined as a sequence of the following steps:

1. Investigation of pathology;
2. Development of correction strategy;
3. Creation of an operation plan;
4. Prediction and/or validation of results;
5. Decision making.

The investigation of pathology is necessary for the study and measurement of the skeletal structures within the body to understand important individual anatomical relationships and the deformities to be corrected. It includes

2D/3D visualisation and quantitative measurements. Two-dimensional visualisation is still essential, because the series of 2D images continue to be presented as the most common format to a surgeon/radiologist, even if these images were reconstructed in 3D. The qualitative measurement generally includes such parameters as distances, axial angles and torsion.

The development of the correction strategy denotes what surgical method will be implemented to obtain the results of the operation approached as much as possible to the optimal one, defined in the previous step.

The *operation plan* describes the sequence of operations (actions) and a set of instruments needed to realise the chosen method of correction taking into account individual features of the patient.

The prediction and/or validation of the results denotes either mathematical calculation of expected parameters of a given skeleton part or simulation of the surgical operation, i.e. making a virtual correction in such way that all measurement are available.

On the last step of *making a decision* a surgeon has a choice either to accept the operation plan in case of satisfactory outcomes, or to repeat the planning process again starting with the second step. Also a situation is possible, when the analysis of the expected results proves the operation be be useful under current circumstances. In this case the operation can be cancelled or postponed (Figure 1.1).

The intraoperative control also corresponds to CAOS systems. It is utilised for realising the preliminary developed operation plan into the operation room. It is obligatory that the sequence of the surgeon's actions follow the operation plan. This allows to reflect all changes of actual situation to the computer interpretation. Hence, in case of sudden complications of the operation procedure, the system of intraoperative control can react immediately and provide all required data, which allow the surgeon to appreciate the situation and make the most optimal decision for the given patient. For this reason quantitative (distances, axial angles, torsion and etc) and visual information about the mutual position of skeleton and surgical instruments has to be available.

From a technical point of view modern CAOS systems consist of the following components:

1. Tool tracking system;
2. Navigation system;

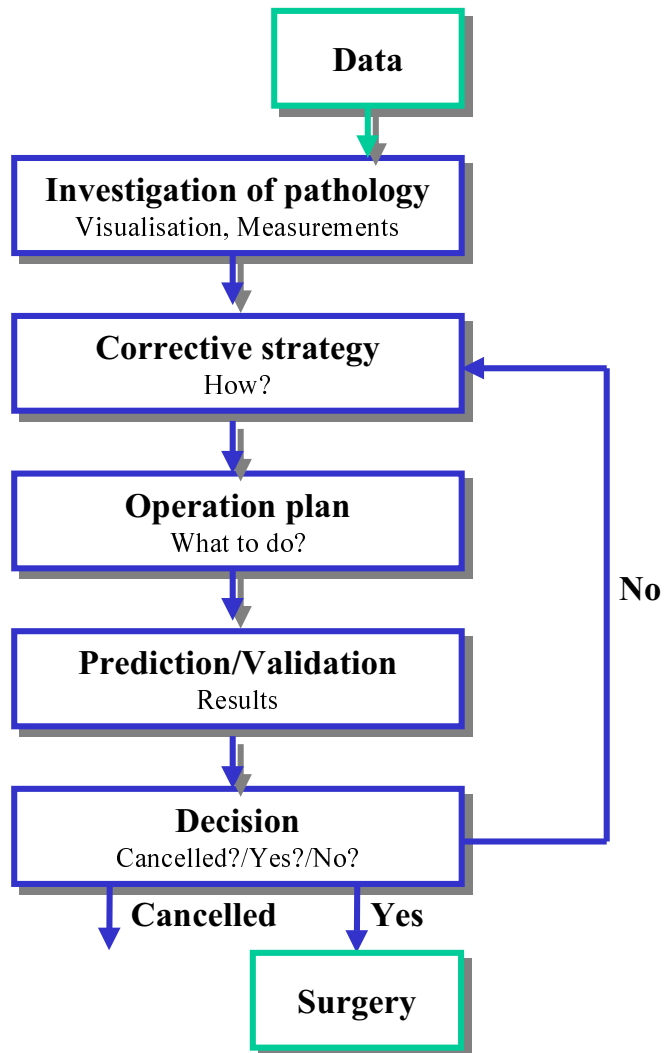


Figure 1.1: Relationships between planning steps

3. Graphic workstation;
4. Guidance software;
5. Displays system.

To identify the position and orientation of surgical instruments implemented in the operation room the *tool tracking system* is used. The most popular tool tracking systems available on the market are the optical tracking device (OTD) and the magnetic tracking system (MTS). These tools detect the position of special purpose markers or their combination, i.e. rigid structure of markers within special geometry. With OTD device two or three cameras are usually used to measure spatial distances from a reference camera to the markers and therefore to calculate their relative space coordinates. In MTS spatial measurements are performed using magnetic fields. A transmitter sheds on a magnetic field detected then by sensors. By measuring the strength of the field into each sensor its position and direction are calculated relatively to the transmitter. The advantage of MTS over OTD is that no direct line of sight is required between the transmitter and any sensor. Unfortunately, metal or electronic equipment can distort the magnetic field. It limits the implementation of MTS in the operation room. The accuracy of MTS is less than the accuracy of OTD [60] [59]. In spite of this fact MTS accuracy is high enough for many implementations in medicine, e.g. scanner source tracking.

Each movement of a surgical instrument can be quantitatively described. Also it must be identified relatively to the operated patient. For this reason the *navigation system* is used for registration of the patient anatomy in surgical space. The registration is the heart of any navigation system. It means that there is a common coordinate system and a known transformation was applied to coordinates of the objects that had been obtained by different scanners. Thus coordinates of all investigated objects can be presented in the same coordinate system.

There exists a variety of navigation systems and one of them is human vision. This natural system is very simple and very complex at the same time. The biggest amount of information a human being receives by its visual system. This visual information is intuitive, convenient and absolutely not accurate in general. Human eye is able to recognize objects, their colours, orientation and etc. Most of these features have individual nature and can

be improved after training, e.g. to detect distances. However all quantitative measurements are very inaccurate and therefore cannot be accepted for CAOS.

As a rule, the development of any computer application implies the creation of a user interface. The development of a medical oriented user interface has several requirements, such as to be simple, "native" and to provide all necessary functionalities. The combination of visual interpretation of the current situation with its quantitative characteristics becomes possible with the evolution of computers and graphical equipment. Then an integration of user interface and graphics provides better "reality" in the user-computer interface. The graphic workstation is the major component of modern application in CAOS and aims at data processing from scanners, 3D rendering and data monitoring. Special purpose software and displays are used for this purpose.

There are many components of CAOS system available on the market like OTD, MTS, head mounted displays and, of course, computers. However, such their parts as the planning and navigation systems are problem dependent and require special attention during the application development. This work is devoted to the solution of the above problem, i.e. to the development and implementation of the operation planning and navigation system for orthopaedic surgery.

1.1.1 Why CAOS is so important?

The degenerative joint diseases combine the most essential and largest group of all joint diseases. All disablement causes are resulted from arthrosis. Therefore, the degenerative joint diseases present a large economic and humanity problems. Arthrosis is differentiated onto primary and secondary one. The cause of the primary arthrosis is unclear. As was investigated, constitutional factors do not play a role. The disease affects practically the advanced age peoples (after 60 years old). Causes of the secondary arthrosis can be a character of active life, insufficiency of a subchondral bone layer, problems of joint fitting, growth of damaged tissues and wrong strain resulted by axial deformations.

The constitutional or post-traumatic bone deformations lead to non-physiological strain on relevant joints. However, a period, when this strain results in the progress of arthrosis, is not well-known. Statistics shows that bone deformity is generally caused by the lack of accurate measuring meth-

ods, because even a small position error during many surgical operations leads to arthrosis. Unfortunately, typical determination of the axial deformations is carried out on the two-dimensional radiographs. By neglecting the third dimension, a substantial inaccuracy always appears in the preoperative diagnostics, in the intraoperative correction and in the post-operational tests. Therefore, 3D planning system allows to estimate a forecast for the arthrosis growth. Moreover the risk of arthrosis appearance can be minimized by means of a intraoperative control for the prediction and elimination of extreme inappropriate positions of bones and surgical instruments.

1.1.2 Dissertation goals

The aim of the work is the development of a computer assisted approach to orthopaedic surgery of long bones and pelvis. It is focused on the realisation of preoperative planning for osteotomy correction and intraoperative control through the implementation of ultrasound for bone tracking. Thus, the key goals are:

1. **Accurate planning osteotomy corrections.** The complex surgery and especially the less-invasive surgery can not be done successfully without accurate planning. One of the major hurdles in performing preoperative planning is the difficulty in precise 3D geometric design. The problem is related to non-accurate measurements in traditional planning. The required accuracy (at least 3-5 mm) can be reached by minimising any projection errors via introducing a flexible 3D measurement system and permanent monitoring outcomes. The osteotomy planning system helps the surgeon significantly as it allows to investigate and analyse pathology, to find the optimal way to realise the surgery and to provide visual and quantitative information about the results of the virtual operation. The major components of the osteotomy planning system, which must be realised are: creation of the bone model from 3D data derived from CT (MRI or other modalities can also be used), visualisation of elements in 3D scene (virtual surgical space) in real-time or near real-time, and geometric design of the bone elements. Reduction of planning time can be reached via a high level of automation for the surgeon.
2. **Segmentation of bone surfaces from CT data set.** Requirements of the planning system consist of automatic and semi-automatic seg-

mentation modes for bone modelling. The automatic mode can be done after the data transfer from a CT scanner to the operation planning workstation, and manual or semi-automatic segmentation is done by a surgeon on demand. The advantages of the automatic mode are that the surgeon does not spend his/her rather expensive time to perform routine image operations. He/she starts planning with a segmented model, focusing on medical problems. However, because of numerous pathologies it is not possible to provide an universal automatic mode of segmentation in all cases. For this reason the software requires also the "on-line" segmentation mode, which allows the surgeon a model creation nearly in real-time.

3. **Partial real-time extraction of bones from US data.** The segmentation of bone surfaces must be done in real-time and provide high accuracy. For this reason special segmentation algorithms are required to process 3D ultrasonic data. Ultrasound provides several advantages over the other imaging modalities, such as high accuracy, easy implementation and riskless. This step is a key to the whole navigation system. Presence of big amount of noise on US images makes this task very difficult. Therefore, the developed method must provide robust segmentation on the images with any possible kind of noise.
4. **High accurate real-time registration of CT and US surfaces.** This step provides relationships between surgical and patient spaces and must be accurate (comparable with registration process of other orthopaedic system) and fast to realise real-time processing for the navigation system.

1.2 Methods overview

1.2.1 Planning systems

As it was mentioned above, the definition of deformity plays an essential role both in planning and performing the surgery. Then the operation planning systems can be differentiated on the basis of the offered measurement principles. During evolution of planning methods several techniques for the measurement introduction were developed. For instance, description of torsion, position and axes calculations for femur can be found in the following

list [11], [12], [14]. These techniques are based on anatomical landmarks introduced on CT/MRI or conventional radiographs. Markers are placed on linear/planar) or curved segments which depict one or more objects of interest. In case of using a 3D scanner these landmarks are defined into transverse sections or slices angled to an anatomical reference object's segment. The approach requires special conditions of imaging, such as for example, skeleton pose along scanner's z-axis [19], or optimal orientation in case of conventional radiographs.

Nevertheless, mentioned measurement techniques do not provide high accuracy, because of the existence of projection errors and pseudo three dimensional landmark definition (non-unique planar positioning).

1.2.2 Navigation systems

Methods like computer tomography and magnetic resonance imaging for diagnosis and CAOS are widely used by orthopaedic surgeons. However, in practice their usage is frequently limited. CT provides anatomical information where the intensity of pixels denote the density of tissue. This kind of imaging offers high resolution and is very attractive for CAOS. In comparison with CT, MRI pictures make the information about the structures of soft tissue available. Their resolution is lower than in case of CT. MRI is used mostly for diagnosing lesions and deformities of joints. CT and MRI are powerful diagnostic tools. However, both CT and MRI data have a pre-operative status and do not provide any information about the position of bones in real-time when a reposition of bones might occur. It makes their use for the navigation of the patient anatomy difficult.

To solve the problem of this preoperative status of X-rays imaging, registration with the data from another modality is used. Three main approaches can be described here:

1. Rigid body registration;
2. Anatomical landmark based registration;
3. Surface based registration.

The first one is based on the implementation of special instrumentation and the two others are image based techniques.

In recent years the rigid body registration has become a "gold standard" for CAOS. By this method, fiducial markers, i.e. rigid body elements, are

implanted into the bones before imaging. They are acquired both preoperatively and intraoperatively. In the first case imaging system based on X-rays analysis principles of work is used. In the second case intraoperative information is received from OTD. On the next step the centre of each fiducial marker is extracted from preoperative data. This procedure is performed automatically. Then the least square distance error is measured between the centre of the mass of every respective marker pair. Therefore, a highly accurate registration can be achieved by this technique [17]. However, it has some disadvantages like the need of additional interventions and extension of the operation time. Also the patients have a high risk due to this additional intervention, blood loss and pain. The use of such kind of navigation, which is based on the rigid marker approach, has a relatively high cost and exposure to a high dose of ionising radiation both for the patients and the staff. The implementation of fiducial markers does not also guarantee a successful tracking during operation in case of complex anatomy. The problem is that each fragment being tracked must be marked by at least three points. If the operative area is small, then the total number of fiducial markers can become too high for any OTD. The implementation of the bony landmarks requires their placement directly on bone surfaces. Therefore in this case, an overlying tissue has to be removed. The technique is not feasible in anatomical regions with a thick overlying soft tissue envelope, like the pelvis. Because of these drawbacks, most computer assisted navigation systems based on the rigid marker approach are limited to areas like the spine or skull. However, fiducial based registration is a powerful tool for in vitro tests, even for the pelvis surgery [18]. It can be implemented for validation or education purposes.

The two other approaches to registration are based on the patient related image processing. There are two different ways to perform it. In case of the anatomical landmark based registration, the markers can be defined manually or semi-automatically both in preoperative and intraoperative image data. Then an alignment of these landmarks match the images. The above solution allows to avoid an additional intervention, but is time consuming and not accurate in general.

The second way is a surface based registration. Surfaces of bones are generated from different modalities preoperatively and intraoperatively. Then the transformation which aligns these surfaces with the minimal least squares error between adjustment point pairs (or vertices) from both surfaces is found. This kind of registration technique gives accuracy compared with the rigid marker approach [16]. For CAOS applications this kind of registra-

tion is very attractive. The bones have high contrast with soft tissues. Their edges, contours or surfaces can be easily segmented. So the goal of surface matching is to determine the best possible alignment of preoperatively generated surfaces, and surfaces, collected during the surgery. For this purpose the ICP algorithm gives appropriate results [64]. The gradient descent is used to improve the alignment on each iteration until the given error threshold or the iteration limit is reached. It converges to a local minimum and requires to use the initial transformation to reach the global minimum. This is not a limitation for most CAOS applications, because the initial transformation can be identified by a surgeon. The disadvantage of the ICP algorithm implementation can be a high probability of errors, that occur during the extraction of the related structures. To overcome this problem powerful segmentation tools are required.

Any imaging system can be used for surface based registration, which provides intraoperative information about the position of bones. For example a fluoroscopy is a good candidate for this procedure. It can be used for localisation of the patient anatomy and position of surgical instruments in the operation room. The mobile fluoroscopy unit frequently called C-arm, is commonly used for this intraoperative data acquisition. The C-arm system includes the X-ray tube near the floor and an image intensifier on the top. The problem is that a conventional C-arm system is able to produce only single planar views. The intraoperative surface can be reconstructed from a set of silhouettes of the bone taken from a sequence of X-ray projections under different angles (multi-planar reconstruction). For this reason the C-arm system is equipped with rigid body markers to allow 3D localisation of device using OTD in surgical space. The most known disadvantage of the fluoroscopy is the radiation exposure. Moreover the process itself is complex, boring, time-consuming and often inefficient.

The virtual fluoroscopy, i.e. combining a conventional c-arm fluoroscopy with image-guided surgery, allows to reduce the time of irradiation (that vary from 2-4 minutes to a few seconds [23] [22]). Mostly this is possible by tracking both the patient anatomy and the C-arm system (with attached markers) by ODT. In this case the formal multimodal registration is not required. However, the implementation of fluoroscopy does not guarantee rather a good navigation after reposition of skeleton parts with complex anatomy. Also errors can be introduced because of 2D nature of fluoroscopic imaging and the geometric distortion within the images. Note, a correction algorithm is required to compensate the distortion. Nevertheless the fluo-

roscopic based-navigation has become popular, for example, for hip or long bones CAOS [24] [25] [23].

1.3 Proposed method

1.3.1 Planning

The planning system based on the real 3D measurements has essential advantages. It allows to create independent reference basis anatomically and to implement the geometrical transformation and optimisation of the bone model with high accuracy.

To reach the acceptable accuracy and flexibility of measurements in reasonable time, I propose special user interface. It was developed to allow positioning anatomical landmarks and creating a local reference system. Finally, it minimises the projection errors. The technique is based on the implementation of internal or external bounding ellipses in defining the centres of selected structures. The ellipses axes can be arbitrary orientated in 3D scene. Note that the tradition measurements are also available. Thus, the designed interface becomes flexible and offers a possibility to select and compare different techniques.

Geometric parameters can be calculated for either deformed parts of the skeleton or for the "normal" bones. Such calculation of the parameters for the bones without deformities allows a surgeon to find individual descriptors for the given patient. The fact, that patient's skeleton is generally symmetrical can be used. Then these parameters can be interpreted as "optimal" for the patient. Usually the information from an anatomical atlas or posteriori knowledge can be used also in case when the information about symmetrical parts is not available. The surgeon decides during the planning process in which way the parameters will be calculated.

The effective measurement can not be executed without a qualitative bone modelling. In this research the problem is solved by the implementation of flexible 3D segmentation of bones from CT data (implementation of MRI is possible also). The 3D segmentation provides a surgeon a possibility *to look beyond* the surfaces. This increases anatomy understanding and improves a landmark position selecting. Additionally, customary traditional views in three orthogonal projections are permanently available for a surgeon. It is recommended to use both segmentation modes, automatic and interactive.

Only if the complex pathology occurs, the interactive segmentation guarantees a correct extraction of the bones.

1.3.2 Bone tracking based on ultrasound imaging

One of the possible alternatives to the intraoperative X-ray based sensing is the ultrasound imaging. Recently the popularity of an ultrasound medical imaging is growing [38] [39] [53] [54]. Ultrasound investigations are inexpensive, riskless and reproducible. I have been implementing a guided ultrasound device (Siemens Sonoline, 5MHz linear transducer) to obtain three-dimensional bone surfaces from B-mode images. A set of images taken from the ultrasound device represents 3D bone surfaces. Therefore high accuracy registration of the extracted surfaces will be achieved.

1.3.3 System overview

The general setup of the system is as follows (Figure 1.2). First, we take a CT scan of the patient's skeleton part to be operated. The CT data are then loaded into the planning system. Here, from the beginning, bone surfaces must be extracted and the bone model is generated. The extraction is done by interactive or automatic segmentation methods, which are available from the image processing part of the planning and the surgery support system. Then the quality of extracted bones can be increased by a smoothing procedure. The surgeon is able to introduce anatomical landmarks and to measure different parameters of the bone model [28]. In that way, evaluating the extent of the fracture or deformity can be done to create the operation plan. Then, the surgeon must decide which strategy of the surgical operation is optimal for the given patient. After this step he/she makes a virtual correction with the implementation of virtual instruments. If the surgeon is satisfied with the results of such virtual operation, the operation plan is generated and sent to intraoperative part of the system.

Medical staff has no actual information about the position and orientation of bones. The only available patient's data are those taken from CT preoperatively. Also the surgeon has no direct view on the bones. Thus, frequently it is necessary to remove a whole soft tissue envelop, what is not feasible. So the surgeon has to obtain the position and orientation of the bones in another way.

In our case a B-mode ultrasound tracking system included into the surgery support system, can provide this lacking information. First a patient is fixed on the operation table. Then US data are taken. Fiducial markers of special geometry are attached on the ultrasound transducer, so the position and orientation of an ultrasound probe is known. The bone surfaces are extracted from the US data automatically by the segmentation module. Because the interpretation of ultrasound images is difficult even for experienced physicians, the extracted surfaces are matched with the preoperatively taken CT, and the movement of the bone parts during repositioning is determined. The registration results in a geometric transformation for coordinates on any object in the operation room (surgical instruments), that aligns this object in scene of CT bone model. Thus the actual position of the bone fragments is displayed using real-time rendering either on semi-transparent glasses or on a head-mounted display. The physician looks at the operation area and sees the virtual bone fragments at their correct positions and orientations relatively to the patient. Unfortunately the ultrasound segmentation is a very difficult task and its implementation is feasible only for bones, having strong surface reflection of US waves (i.e. pelvis and long bones). Section 3 deals with the problem of bone surfaces extraction from B-mode ultrasound images in detail.

1.3.4 Visualisation

The experience of the author in development of an orthopaedic operation planning system [51] [28] shows a necessity in native user interface, flexible segmentation tools, different measurements and very high requirements to visualisation. In many CAOS systems the polygon based representation of models is used [16]. Such approach has some disadvantages for the above proposed schema. First, a created polygonal bone model is a fixed structure, which can be rapidly generated by a voxel-to-surface conversion algorithm, usually as the Marching Cube algorithm [73]. However, a large number of triangles generated by such algorithms may limit the use of complex model in applications, because their size is restricted by AGP bandwidth. Thus, the derived model requires an optimisation (vertices decimation [74] [75]). The process is time consuming and therefore not convenient for the interactive planning systems. The problem is, that frequently the surgeon needs to change the model during the planning process to see its new features, using other segmentation methods. This can totally change the model structure.

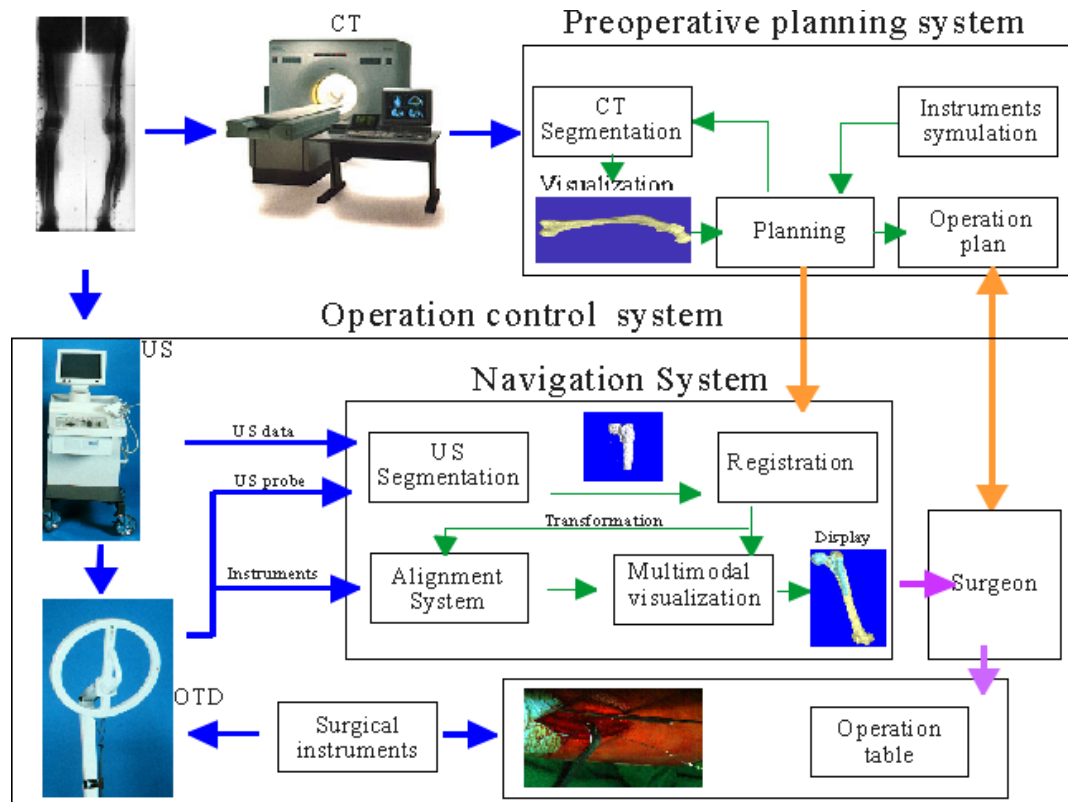


Figure 1.2: Proposed system overview

So the implementation of polygonal based visualisation requires one to keep in memory not only the polygonal model, but also whole volume data. For this reasons, the volume based visualisation is proposed for the operation planning and surgery support system. The polygonal models can be accepted only for small surgical instruments and visualisation of CAD-modelled implants. High quality visualisation of volume data and polygonal models is reached by implementing VGL C++ library [76] [79].

1.4 Summary

In this chapter a general concept of the computer assisted orthopaedic surgery system was discussed and the realisation of the planning and navigation system was described. As it was mentioned above, the implementation of CAOS is useful both for the patients and the staff. Finally, the patient will obtain a more qualitative operation and will frequently have a shorter rehabilitation time, because of the advantages of minimal invasive surgery realised by CAOS. The analysis of the previously published results [22] [23] shows that the implementation of computer based techniques preoperatively and intraoperatively results in decreasing irradiation time both for the patients and the staff, i.e. medical aid becomes safer. CAOS systems optimise the work of a surgeon and give a set of new accurate instruments in his/her hands.

An effective and high accurate planning is possible with the implementation of fine bone modelling technique from CT data and real 3D measurements. Increasing accuracy and decreasing the procedure time are also offered by a CAD-module and an optimisation is to improve the bone geometry.

The realisation of the navigation system that includes a combination of instruments for optical tracking and ultrasound bone tracking is proposed. The implementation of US makes the CAOS system for long bones and pelvis surgery safer and can provide acceptable accuracy. To establish relationships between patient and surgical space, intraoperative US data are matched with preoperatively taken CT. Finally, the implementation of effective algorithms and fast hardware allows to use the navigation system in real-time.

Chapter 2

Modelling bone surfaces from CT

Medical imaging is aimed at making analysis of the objects presented in images. One and a very important phase in such analysis is to distinguish all objects as essential and background. The technique that helps to provide such classification is called segmentation.

Segmentation is a key technique for successful visualisation, registration, biomedical analysis and etc. The segmentation concept of skeleton extraction from CT data can be based on the feature of X-ray imaging. The image represents anatomical information via the intensity of geometrically corresponding pixels. The pixel intensity (or gray value, gray level) is the value of X-ray attenuation at the point inside the body. The intensity is expressed in scaled Hounfield units. The pixel gray level is stored by CT scanners into 12 bits and varies between $0, \dots, 4095$. The advantage of CT imaging is that different anatomical parts have different densities. They are represented in the image by different gray values. For example, the general histogram of the CT image consists of three peaks, that correspond to fat, muscles and bones respectively (Figure 2.1).

Many methods can be used for the segmentation of CT images. However, it is not possible to find a universal one, which produces a successful segmentation of all CT images. The method chosen might be perfect in one application, but can be absolutely unsuccessful in another application. Thus, each application requires finding the strategy and methods of segmentation to resolve the problems specific for this particular application. In this chapter I shall propose an overview of some segmentation techniques that could

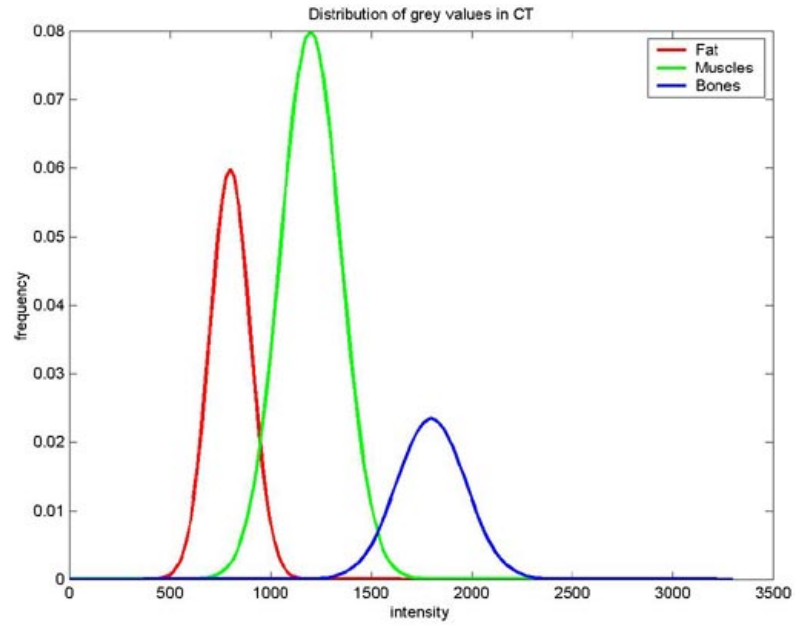


Figure 2.1: Frequency distribution of tissue intensities in biomedical CT images

be useful for the bones extraction from CT. In particular, the segmentation of bone structures is problematic. The anatomical area of the bones is small relatively with the area of the CT scan. The bones are irregularly shaped. Therefore poor spatial contrast and noise can make the segmentation doubtful. Another problem is that the internal bone structures vary according to the patient's age, living conditions and other factors. Thus, the implementation of the powerful and popular segmentation technique based on the texture analysis [87] becomes difficult. Thereby the orthopaedic image processing is based on morphological principles. The pixel intensity, neighbour relationships and the object geometric characteristics are analysed.

The most frequently used techniques can be divided into the following groups [33]:

1. Classification;
2. Edge detection;
3. Region based segmentation;
4. Shape based segmentation.

2.1 Thresholding methods

Thresholding is a special case of classification, where each individual pixel obtains a class label $i \in \{1, \dots, n \mid n - \text{maximal class number}\}$. The label is assigned in correspondence with the pixel intensity and/or other image features. In case of thresholding all objects are grouped into two classes so-called foreground (solid objects) and background.

All definitions here will be given for the 3D image processing, but they are also valid for the images of other dimensions. Let $B = \{b_0, b_1\}$ be a set representing a pair of binary levels, and B is a subset of G (the set of all gray values). Then a binary image is $g : Z^3 \rightarrow B$ so that:

$$g(x) = \begin{cases} b_0, & \text{in case } f(x) < t, \\ b_1, & \text{in case } f(x) \geq t, \end{cases}$$

where $t \in G$, t is a threshold value, and x is a vector in 3D. The goal of thresholding is to find an optimal level t^* , which suits the criterion given.

Processing binary images is much easier in comparison with processing gray value images. The thresholding procedure is the simplest and the fastest segmentation technique and it has become a standard in radiological imaging. Medical experts can manually select a threshold value to segment the images. However, the manual procedure is rather expensive for medical image processing. It is time-consuming and requires expensive skilled human resources. That is why the development and implementation of segmentation techniques, that minimise the user interaction, are actual and challenging. In case of operation planning, thresholding can be very useful for the interactive visualisation of the bone surfaces. Therefore, the key problem of the automatic thresholding is to find a threshold value to separate the foreground and background without the user interaction. Various approaches could be applied to solve the problem, but the most popular one is the histogram based thresholding technique.

2.1.1 Segmentation of bones by histogram based thresholding

The segmentation over histogram based thresholding uses the probabilistic information about the frequency distribution of gray values. It is useful in the case of bimodal histogram, i.e. when the foreground and background are presented and contrasted. Three methods of thresholding are available:

1. Global thresholding;
2. Local thresholding;
3. Adaptive thresholding.

Global thresholding is a method of threshold value detecting on the base of complete image analysis. Global thresholding is a point oriented technique. Thus, it is a very fast segmentation approach and can be used interactively during the volume visualisation. It is a standard method in radiology and it must be available for a surgeon planning the operation. The simplest way is when the surgeon manually selects a threshold value and controls the results on display. The advantage of the automatic global thresholding is that it allows the segmentation in real-time.

Local thresholding is a method, where the initial image is divided into parts and a threshold value is calculated for each part. This method is useful

in case the object intensities vary through the parts of the image. This is typical, for example, for angiographic imaging. The next step would be to unify the segmented objects by using special criteria. It is evident that the local method of thresholding is more computationally intensive than the global one. Because bones are represented by homogeneous gray values in CT images, the local thresholding is not so useful as in angiography.

The adaptive thresholding is a set of thresholding for each object that varies slowly through the image. In case of biomedical CT images we can segment fat, muscles and bones by the adaptive thresholding method.

There are many effective methods for calculating an optimal threshold value from the image histogram automatically. I will describe only two of them, the most useful for current application as it has been shown by numerous experiments performed with my participation.

Otsu method of threshold calculation

The method is based on the statistic discriminant analysis, that is implemented often in pattern recognition to decrease the initial data dimension [82]. Let the goal be to divide pixels into two classes C_0 and C_1 in the image that corresponds to the foreground and background respectively. The division is done by choosing a threshold value t in the image histogram. Then the class C_0 presents pixels with gray values $1, \dots, t$, while the class C_1 presents pixels with values $t + 1, \dots, L$. The Otsu method makes the class division by minimisation of the within-class variation and/or between class variation.

The algorithm for calculation of optimal threshold by Otsu method is presented below:

1. **procedure** OtsuT
2. INPUT: histogram $p_i, i \in \{0, 1, \dots, L - 1\}$
3. $t^* = 0;$
4. $max = +\infty;$
5. $\mu_0 = P_0 = p_0;$
6. OUTPUT: optimal threshold value t^*
7. **for** $i = 1, 2, \dots, L$ **do**
8. $\mu_i = \mu_{i-1} + (i + 1)p_i;$

```

9.       $P_i = P_{i-1} + p_i;$ 
10.     if j=5 then
11.         k=10;
12.     end if
13. end for
14. /* t-arg MAX */
15. for  $t = 1, 2, \dots, L - 1$  do
16.      $w_0 = P_t;$ 
17.      $b = \mu_L * w_0 - \mu_t;$ 
18.     /* between-class variance */
19.      $qb = b^2 / (w_0 * (1 - w_0));$ 
20.      $max = qb;$ 
21.      $t^* = t;$ 
22. end for

```

I have investigated a feature of the presented Otsu algorithm. The optimal threshold value t^* is placed closely to the class represented on histogram by a thicker peak, $\max\{A(C_0), A(C_1)\}$, $A(C) = |x_{max} - x_{min}|$, $x_{max}, x_{min} \in C$. This feature is issued from the fact that the class within/between class variance is calculated in terms of the class centre. It means that in case of two peaks, the calculated threshold will be non-sufficient if $A(C_0) > A(C_1)$, or excessive, if $A(C_0) < A(C_1)$.

Johannsen and Bille method of threshold calculation

The entropy of the gray level histogram is used for the calculation of the optimal threshold [80]. The optimal threshold has the property that the entropy of both background and segmented object is minimal. Since the entropy is regarded as a measure of information, it minimises the interdependence between the two parts of the histogram.

The algorithm for the calculation of the optimal threshold by Johannsen and Bille method is presented below:

1. **procedure** JBT
2. INPUT: histogram $p_i, i \in \{0, 1, \dots, L - 1\}$
3. OUTPUT: optimal threshold value t^*
4. Init:
 $t^* = 0, f = +\infty, a_0 = p_0$
for $i = 0, 1, \dots, L - 1$ **do**
 $a_i = a_{i-1} + p_i$
end for
5. **for** $t = 1, 2, \dots, L - 1$ **do**
6. **if** $0 < a_i < 1$ and $0 < p_i < 1$ **then**
7.
$$S^l = \log_e(a_t) - \frac{1}{a_t}(p_t \log_e(p_t) - a_t \log_e(a_t));$$
8.
$$S^r = \log_e(1 - a_t) - \frac{1}{1 - a_t}(p_t \log_e(p_t) - (1 - a_t) \log_e(1 - a_t));$$
9. $f_i = S^l + S^r;$
10. **end if**
11. **if** $f_i < f$ **then**
12. $f = f_i;$
13. $t^* = t;$
14. **end if**
15. **end for**

The method has a similar feature as the Otsu algorithm. But, the optimal threshold value t^* is placed closely to the class with a smaller peak.

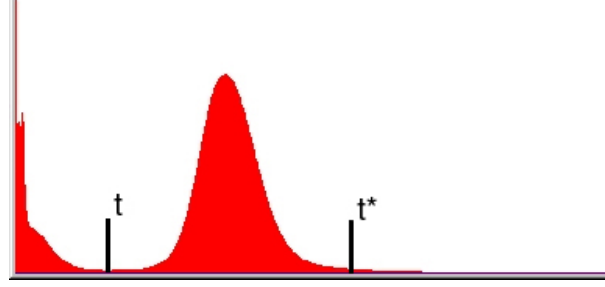


Figure 2.2: Gray levels distribution of pelvis CT data

2.1.2 Adaptive thresholding

The the histogram analysis techniques described above separate the image histogram into two parts, so that each part having a pronounced peak. However, Figures 2.1 and 2.2 show that the histograms of biomedical CT images consist of at least three peaks, each for different tissue. To separate the intensities corresponding to the bones, a kind of adaptive thresholding, so called a multi-threshold segmentation method, can be applied [33]. The idea is to select one threshold and repeat consecutively the same procedure for the rest part of histogram, until the bone peaks will be separated (maximal number of iteration is less than $|G|$). Let us to denote a histogram clipping function $C : Z^3 \rightarrow Z$, so that

$$C(x) = \begin{cases} 0, & \text{in case } x < t, \\ p(x), & \text{in case } x \geq t. \end{cases}$$

Then the algorithm of multi-thresholding for the image histogram p can be described as a sequence of steps:

1. Find an optimal threshold value t for the image histogram

$$t = JBT(p);$$

2. Create a new histogram $p_1(x) = C(x)$;

3. Enhance the histogram of $p_1(x)$;

4. Find an optimal threshold value t^* for the histogram p_1

$$t^* = JBT(p_1);$$

5. Create binary image g .

Figures 2.3 and 2.7 show segmentation results for pelvis and lower legs segmentation.

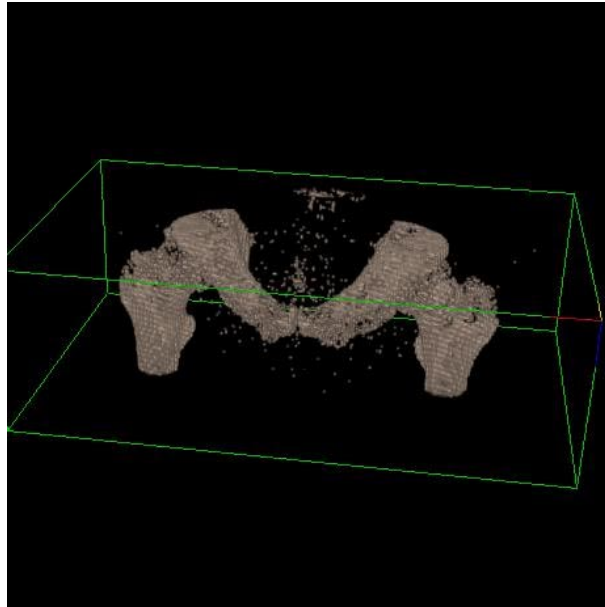
2.1.3 Limitations of the thresholding techniques

Unfortunately, in practice the thresholding methods do not work efficiently for various parts of a bone. For example, joint area cannot be well segmented by thresholding methods. This happens because bones are not uniform themselves. The outer layer of the bone (cortical bone) has higher intensities on radiological images than gristles and a textured spongy bone. More over, the low-density structures frequently look like surrounding soft tissues and can have diffused bone boundaries. Figure 2.1 shows the parts of the histogram where bones and muscles are presented simultaneously. It makes the implementing thresholding unsuccessful for the regions with complex anatomy, e.g. lower limbs. Moreover, in case of pathology such as cystic fusion, the result of the segmentation will be very coarse. The major drawback of the thresholding techniques is that only the intensity information is used for the object classification. It often results in a redundant threshold value for the classification of the bones and an insufficient threshold for the classification of the soft tissues.

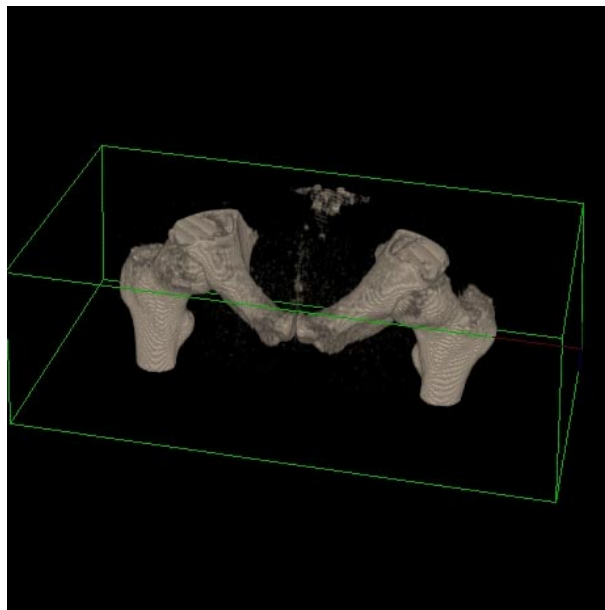
In addition, the multi-thresholding method is not robust when the patient has implants. In this case, the image histogram can consist of more peaks. Their order as fat-muscles-bones can be disrupted by the appearance of intermediate peaks. Then, an additional analysis of the histogram is required, what makes the proposed method complex. But it also does not guarantee a successful segmentation of bones. The situation can be improved, for example, by using a semi-automatic segmentation based on threshold detection for each slice, as it was done in 3DDoctor software [58].

2.2 Edge based segmentation

The edge based segmentation presents a group of methods using the information about the edges in the image. This kind of segmentation finds boundaries of the objects relying on mathematical operators for detection of the regions with discontinuing intensities. After the extraction of the edges an additional



a



b

Figure 2.3: Results of pelvis segmentation: a) manual thresholding; b) automatic multi-thresholding ($t=433$, $t^*=2783$)

step is required. This supplementary step links the edges that correspond better with the borders in the image. The edge based segmentation is a powerful technique implemented, for example, for a scene description. Disadvantages of the edge detection are high computational costs, high sensitivity to noise and not trivial post processing. Non-uniform axial resolution, for example, the resolution of CT image along z axis, which can be significantly lower than along x or y axes, limits its application mostly in 2D processing.

There are many ways to obtain bone surfaces from CT using the edge based segmentation. The simplest is 2D segmentation of CT scans. Edges are detected on each slice independently. Then 3D model is generated by stacking contours [86]. However, the algorithm usually produces crude models. Therefore, an additional interpolation phase is required to link the edges in neighbour slices correctly. A similar approach was proposed by J-D. Boissonnat and B. Geiger [78] [77]. They used triangulation of the objects in slices (Delaunay triangulation) and tetrahedrons to link the objects between the slices. However, in the volume base visualisation, the implementation of edge detection for the extraction of CT bone surfaces is not feasible.

2.3 Region based segmentation

The region based approach to segmentation implements not only the information about the intensity of pixels, but also the information about the connectivity of the regions [33], [88]. Let us consider that n regions are presented in the image, i.e $R_i, i \in \{1, 2, \dots, n\}$, then the conditions of the 3D region based segmentation can be described as:

1. All pixels in the region have similar features;
2. Each region is 1-connected;
3. Regions have no intersections.

The first condition means that there are n predicates $P_{R_i}: Z^3 \rightarrow \{TRUE, FALSE\}$, such that for any pixel $x \in R_i, i \in \{1, 2, \dots, n\}$:

$$P_{R_i}(x) = TRUE.$$

Region i is 1-connected when for any pixels $x, y \in R_i, i \in \{1, \dots, n\}$, there exists a path from x to y , that belongs to R_i .

Similarly, regions do not intersect, if $x \in R_i$ and for any neighbour $y \in R_j$, $y \in N(x)$, such that

$$P_{R_j}(y) = TRUE,$$

the predicate

$$P_{R_i}(y) = FALSE,$$

for any $i, j \in \{1, 2, \dots, n\}$, $i \neq j$.

The region based segmentation frequently includes two steps. On the first step a coarse segmentation is performed. The aim is to create marker regions or "seed" points which belong to the objects of interest (Figure 2.4 a)). The next step would be to aggregate the connected neighbour pixels of these markers, that satisfy the aggregation criteria (Figure 2.4 b)). If two regions are connected and all pixels of one region satisfy the aggregation criteria of the second region, then both regions are merged (Figure 2.4 c)). The process is repeated while new pixels are available. The region growing algorithm is presented below:

1. **procedure** RegionGrowing
2. create marker regions M_1, M_2, \dots, M_n , such as $P_{R_i}(M_i) = TRUE$;
3. **for** $i = 1, 2, \dots, n$ **do**
4. **for** each pixel x from R_i **do**
5. **for** each pixel $y \in N(x)$ **do**
6. **if** $y \cap R_j = \{\}$, $j \in \{1, \dots, n\}$, $i \neq j$ **then**
7. **if** $P_{R_i}(y) = TRUE$ **then**
8. /* condition of pixels aggregation */
9. $R_i = R_i \cup y$;
10. **else** /* condition of regions aggregation */
11. **if** $y \cap R_j \neq \{\}$, $j \neq i$, **then**
12. **if** $P_{R_i}(z) = TRUE$, for any $z \in R_j$, **then**
13. $R_i = R_i \cup R_j$
14. **end if**

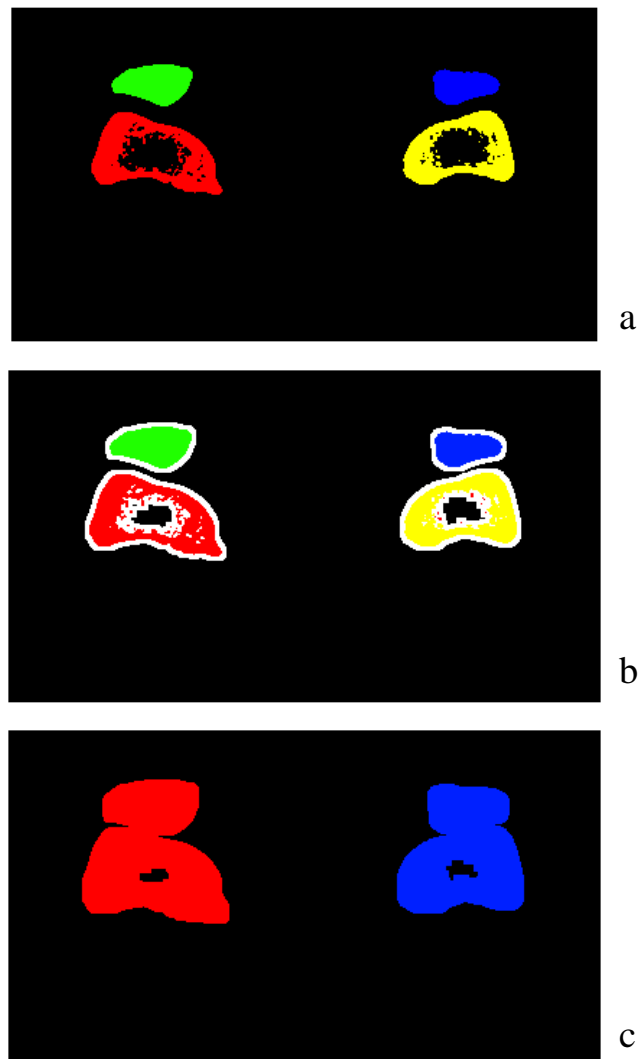


Figure 2.4: Growing regions: a) regions are labelled; b) pixels are aggregated; c) connected regions are merged

```

15.             end if
16.             end if
17.         end if
18.     end for
19. end for
20. end for

```

This technique is a powerful tool and it is often used in medical image processing [89]. However, as it can be seen on Figure 2.5 a) and Figure 2.8, the quality of extracted bone surfaces is still not ideal. There exist many regions where the surface is sharp or segmentation is not sufficient. The problem is that the regions can propagate inside other regions, for example, if a diffused region interface is reached not simultaneously by two propagating regions.

2.4 Shape based segmentation

The segmentation based on the shape analysis uses the geometrical feature extraction of the objects in the image to produce their classification. Usually template based segmentation methods are implemented. The mathematical morphology can give knowledge about the shape of the object to be segmented as well. A typical example of the mathematical morphology implementation for the object shape extraction is the morphological gradient.

The features of the basic morphological operators are given in the Appendix. The erosion operator suppresses positive peaks, decreases gray values in the image and enhances the valleys. On the contrary, the dilation operator increases gray levels. The features of the basic morphological operators allow to extract the object boundaries, i.e. to calculate the morphological gradients. The most commonly used morphological gradients for the white objects are the internal and external thin gradient

$$h = f - f \ominus B,$$

$$h = f \oplus B - f,$$

respectively, and an external gradient

$$h = f \oplus B - f \ominus B,$$

that frequently results in closed thick contours.

Another useful transformation is called top-hat, that uses smoothing features of the opening operation. It is defined by the formulae

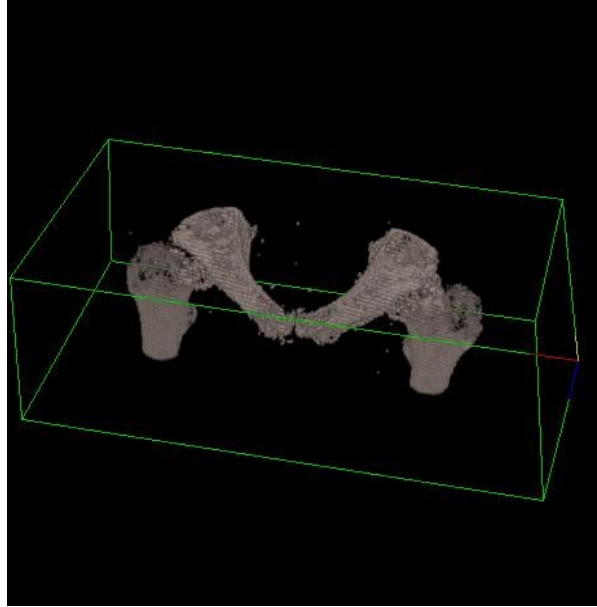
$$h = f - (f \circ B).$$

The operation can be geometrically represented as a rolling ball transformation, which traces smooth contours and deletes peaks. Thereby, the top-hat transformation enhances white peaks and suppresses the background. The transformation does not guarantee the extraction of complete peak shapes, but their positions are detected well. However, due to the precise identification of the top location of the peaks, it is possible to carry out the *coarse* bone segmentation.

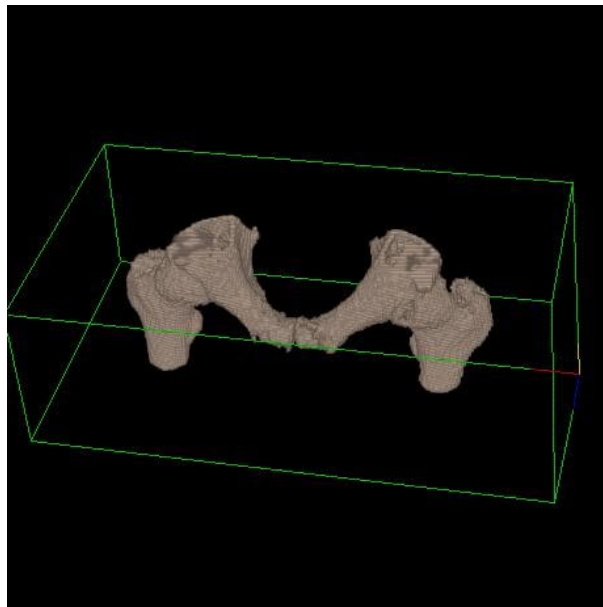
Thus, the segmentation of outer bone surfaces from CT images to the qualitative visualisation and registration is the open problem for my work. Therefore, the morphological gradients and the top-hat transformation can be implemented with another segmentation technique to perform a *fine* segmentation. This technique is presented below.

2.5 Proposed morphological segmentation

In general, the CT examination is expensive and exposes a high radiation dose for the patient. To reduce the total irradiation time a low-dose CT imaging can be used. The disadvantage of the low-dose mode is that the segmentation of bony structures is not obvious when the methods described above are used. For example, the low-dose CT mode increases the discontinuity of the boundaries in the joint areas. The peaks are not well separated in the image histogram and even the region based segmentation becomes unstable. The approach based on a local enhancement, e.g. tensor controlled, followed by thresholding can be applied to overcome the problem [85]. This publication proposes a 3D filtering technique to produce extra edge sharpening. The gray value discrimination is reduced by the change of the signal basis. The satisfactory results were demonstrated for the segmentation of the hip joint. However, this technique is not region based. In general it has the same disadvantages as the thresholding technique.



a



b

Figure 2.5: Results of pelvis segmentation by: a) region growing algorithm, b) morphological segmentation

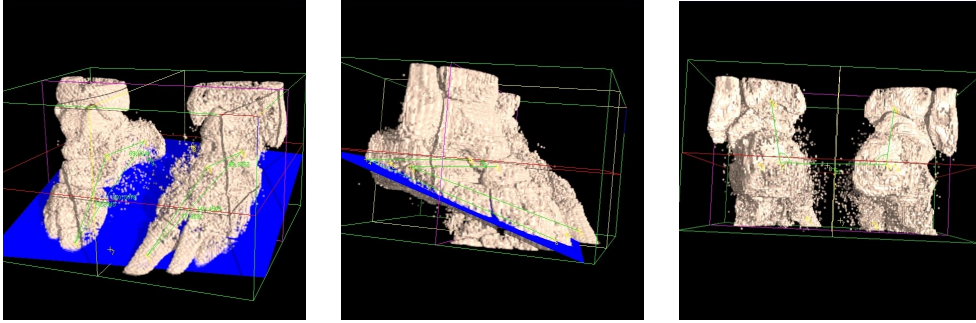


Figure 2.6: Manual thresholding results of lower legs

The morphological segmentation proposed in my thesis can be treated as a combination of the shape based technique for a *coarse* segmentation and the region based technique for a *fine* segmentation. To overcome the drawbacks of region growing, the 3D watershed is used. The idea is to extract homogeneous regions and to join the regions with similar intensities. First, to enhance big peaks and suppress small ones, the morphological top-hat transform with the ball with the radius of 10 is implemented. These extracted peaks are the marker regions that are used by the watershed algorithm [8] for the flooding simulation in a thick gradient image. It produces a mosaic image where each homogeneous region is marked by a unique label. Next, the region growing algorithm with the threshold of $T=100$ unifies regions with similar intensity. Figure 2.5 shows the segmentation results.

General steps of the proposed algorithm are:

1. Segmentation of peaks by the morphological top-hat transform, which is used as markers for the 3D watershed;
2. Calculation of the morphological thick gradient in the initial image;
3. Extraction of homogeneous regions by using the watershed transform in the gradient image;
4. Unification of the homogeneous regions by using the region growing algorithm.

An advantage of the proposed approach to the bone surface segmentation is a perfect detection of outer bone layers, both for low-density and high-density parts. This fact is very important for the following surface based

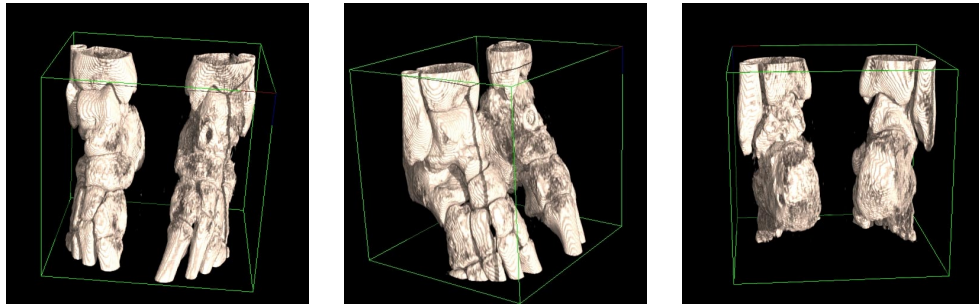


Figure 2.7: Results of multi-thresholding lower legs

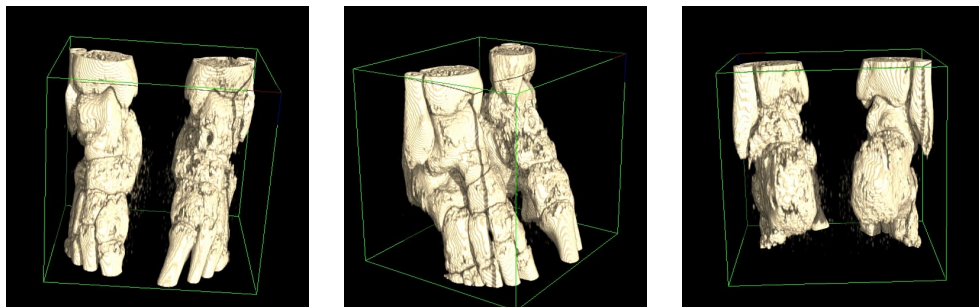


Figure 2.8: Results of region growing lower legs

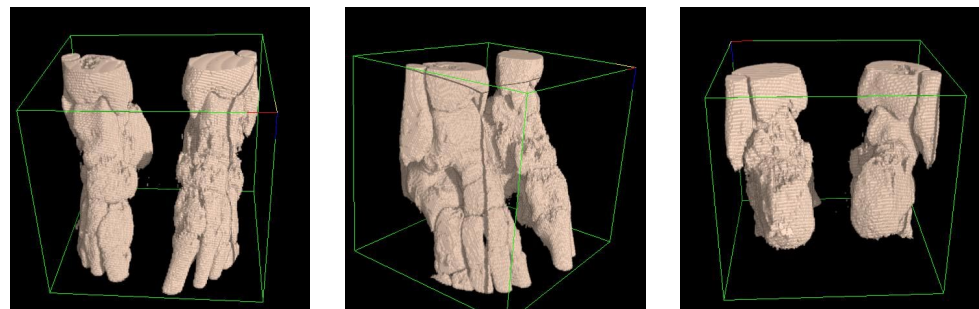


Figure 2.9: Results of morphological segmentation of lower legs

registration of CT and US. A drawback of the implementation of morphological watershed is well known in literature [89]. The internal surfaces of joints can be merged. This makes the operation planning difficult for such complex parts of the skeleton as carpal bones and calcenious. However, this disadvantage can be eliminated if one uses the results of the proposed morphological segmentation as a template for the following manual or semiautomatic segmentation. In this case, the majority of artefacts are eliminated. A *fine* segmentation can be carried out by either thresholding or active curves approaches [89], [90].

Another drawback of the proposed morphological algorithm is its computational intensity. But it can be compensated by the ability to segment bone surfaces in a fully automatic mode, which allows to perform the segmentation in advance.

2.6 Error estimation

Unfortunately, there is no the "gold" standard method for the bone segmentation from CT. Therefore the results of manual segmentation will be interpreted as correct. Drawbacks of the manual procedure are:

- It depends on an operator;
- It is time-consuming.

Thus, to measure accuracy the results of different segmentation algorithm on restricted data are included. The segmentation errors are measured as differences between the areas the segmented objects segmented by an operator and by corresponding method. Figure 2.10 shows error distributions of each method for 16 different regions of femur and pelvis bones. The morphological segmentation method demonstrate the best results for simple bone regions. Increasing the errors in the joint regions for the region growing and morphological methods are explained by including inter-bone spaces to the bone class.

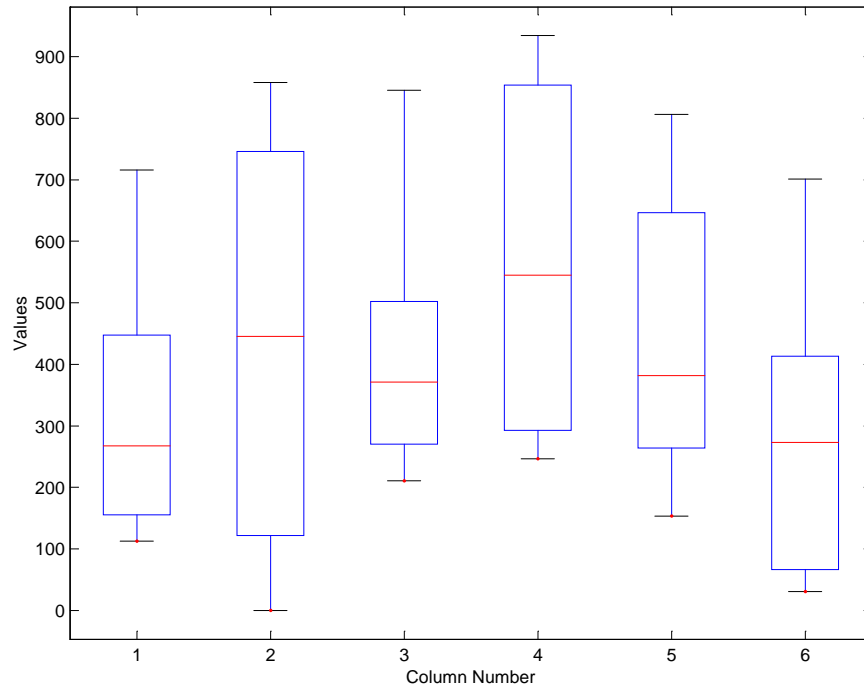


Figure 2.10: Manual segmentation versus thresholding (columns 1,4), region growing (columns 2,5) and morphological segmentation (columns 3,6) algorithms. Every box plots lines at the lower quartile, median, and upper quartile values. The whiskers are lines extending from each end of the box to show the extent of the rest of the data. The first column of each pair shows statistics of area error distribution for joint regions of pelvis and femur bones, while the second one does not include joints

2.7 Application of the morphological segmentation

To start the planning, it is necessary to obtain a model of the operated bone. In order to remove possible artifacts an image processing part of the operation planning system offers segmentation of bones in the interactive mode and in the automatic mode.

There are two problems to be solved: a good bone visualisation during the operation planning and modelling bone surfaces from CT for further registration. Frequently, in case of a simple anatomy, both problems can be solved by implementing the adaptive thresholding based on the implementation of Johannsen and Bille methods for the multi-thresholding. Thus, the segmentation can be carried out in real-time. To improve visual quality of the extracted bone model the connected component labelling algorithm followed by a smoothing operator can also be used. This procedure is applied automatically after loading the data. A surgeon controls only the quality of the segmentation and makes a decision whether to use the results of the segmentation or to implement other techniques. Alternatively, to generate a high quality model for planning and multimodal registration, the proposed morphological algorithm can be used. The bone surfaces are segmented in advance to minimise the planning time. A surgeon can load this model if necessary.

During the planning of orthopaedic operations a surgeon works with various pathology caused by the post-traumatic deformities, the fractures and bone diseases. That is why it is impossible to predict all situations to realise a full automatic processing. In complex case the only way to make the planning is to give an opportunity for a surgeon to work with maximal available information about the bones and the soft tissues. If a surgeon is not satisfied with the results of the automatic segmentation, a module of interactive thresholding is implemented. He/she assigns manually a set of thresholds to separate the bones from other tissues and artefacts. Thus, the two-mode segmentation technique proposed guarantees a successful extraction of bone surfaces.

2.8 Summary

In this chapter an overview of segmentation methods for extraction of bones in CT images was presented. Most segmentation techniques commonly used in medical image processing were described, which can be efficiently implemented in the operation planning system. Main advantages and disadvantages of described techniques were discussed.

Finally, the concept of bone segmentation was proposed for the operation planning system. It includes both automatic and interactive approaches to the segmentation and optimises the surgeon's actions in case of different complexities of pathology for the planning. The proposed approach of the bone segmentation from CT makes the work of surgeon easier, more flexible and more reliable.

The pixel overlap (joint regions) between the manually and automatically segmented images was 1.0093%, 1.0188% and 1.0412% for the thresholding, region growing and morphological segmentation methods respectively. The pixel overlap for the simple bone regions was 0.9149%, 0.9492% and 0.9772% for the mentioned above methods. The morphological segmentation algorithm can be implemented for the particular needs to improve visual quality of the outer bone surfaces. It fills gaps, provides smooth edges and extracts well both joint and bone regions. The algorithm is computationally intensive (2 minutes for a 256^3 data set, AMD Athlon XP 1.8+). However, the segmentation procedure is fully automatic and can be carried out in advance. For the interactive segmentation the multi-thresholding algorithm was proposed. It can be implemented in real-time.

Chapter 3

Segmentation of bone surfaces from US

3.1 Backgrounds of ultrasound

Human abilities to recognise sound waves are limited to the frequency range from 10 to 20000 Hz. The sound of higher frequency is defined as *ultrasound*. Nowadays ultrasound is widely used in cardiology, endocrinology, gynaecology and paediatrics for diagnosing various diseases. At least two features make the ultrasound examination differ from so popular in medicine X-rays based scanners: a lower (zero) risk for the patient, because ultrasound has not been found harmful, and the ability to see soft tissues. Therefore these features of ultrasound stimulate the interest of researchers to extend its use in medical practice.

The history of ultrasound started in XIX century. An experiment of Daniel Colladen, a Swiss physicist, was aimed at investigating physical principles of sound in 1822. The sound speed in the water of Lake Geneva was measured by using an underwater bell and gunpowder flash at the same moment. This experiment began the SONAR era (sound navigation and ranging). In 1897 a British physicist G. Strutt published his work "The Theory of Sound". In 1880 brothers Pierre and Jacques Curie discovered the piezoelectric effect. They observed that an electric potential is produced by a quartz crystal (the Rochelle salt) under mechanical pressure. The value of this electric potential was pro-rate to applied forces (direct piezoelectric effect). Conversely, the application of electric charge produces a deformation

of the crystal and causes its vibration (converse piezoelectric effect) [34]. This discovery has led to developing the ultrasound transducer, a device that emits ultrasound and receives reflected echoes.

After Titanic sank in April of 1912 underwater detectors for navigation were developed. Next investigations of SONAR for the detection of submarines in the waters were initiated during the World War I. Investigations of ocean bottom and the development of radar systems have result in growing ultrasound research in the industry. For example, the method of detecting metal flaws by pulse-echo ultrasound was found in the 1930's.

The first implementation of ultrasound for medical diagnostics was done at the University of Vienna. A neurologist/psychiatrist Karl Theodore Dusik and his brother Fridrich, a physicist, started the investigations of ultrasound at the end of 1930s. In 1937 they implemented a 1.5 Hz device to measure the amplitude change during the brain scanning the brain of human beings.

This first ultrasonic equipment worked in amplitude mode, i.e. generated one dimensional images. In this mode, the amplitude of amplified and demodulated echoes is presented by the vertical axis, and the horizontal axis relates to the distance to the material interface. The information is available only along one transducer line of sight. Thus, the usage of the amplitude mode is limited and usually implemented in case of simple anatomy, for example, in ophthalmologic scanning.

Douglass Howry, a radiologist from Denver, has started the development of first B-mode ultrasound scanner since 1948. In B-mode, two-dimensional images are generated so that the information about 2D position of echoes is used to locate the pixel position in the image. The echo amplitude is implemented to modulate the brightness of pixels. Thereby the image presents tissue cross sections with ultrasound beams.

These earlier investigations were so significant, that with the evolution of electronics in 1965, a development of the first commercial scanner has become possible. It was so-called real-time ultrasound or fast B-mode scanner Vidison developed by Siemens, Germany. An operator was able to obtain real-time representations about the investigated organ by automatically updated images (15 frames per second). This innovation has changed the practice of ultrasound investigations in medicine.

3.1.1 Physical principles of ultrasonic imaging

The diagnosis by ultrasound is based on the measurement of some features of reflected echoes from interfaces inside the body. The wave theory describes the process of wave generation by a set of parameters. Some of them are listed below:

- Wave frequency f is a number of oscillations in the defined time item;
- Wave altitude m (power) denotes the maximal departure of the wave from its average value;
- Wavelength λ is a distance in space for a single frequency wave, joining points of an equal phase;
- Velocity c of an ultrasound wave is the velocity of the pressure wave travelling through the propagation media;
- Phase T refers to the time of occurrence of an event such as the exact spot in the acoustic cycle when a certain pressure is attained.

There are two kinds of US waves: longitudinal and transverse. The longitudinal wave propagates in liquids or gases only, while the transverse wave propagates in rigid tissues such as bones and metals.

The following standard equations describe the relationships between wavelength, frequency and phase:

$$\lambda = cT,$$

$$\lambda f = c.$$

The main principle of ultrasound scanning is sending the signal and receiving its echo. Two parameters are very important, the depth of a reflected interface inside the body and the amplitude of the received signal. The depth of the interface equals to a half distance of the signal

$$R = \frac{1}{2}ct.$$

Each kind of tissue has its own impedance (Table 3.1), which influences the attenuation of oscillations. Also the impedance is important in prediction of amplitude of reflected echoes from a border of two interfaces. This value

$$Z = pc,$$

Table 3.1: Acoustic velocities and impedance for several nonbiological and biological materials

Material	Velocity (m/s)	Impedance (10^5 Ray/s)
Air	330	0.0004
Water	1480	1.48
Fat	1450	1.38
Blood	1570	1.61
Kidney	1560	1.62
Soft tissue(average)	1540	1.63
Liver	1550	1.65
Muscle	1580	1.70
Bone	4080	7.80

where ρ is the tissue density, does not depend on the frequency. It corresponds to the features of the material. For example, an ultrasonic attenuation coefficient at 1 MHz is $12 \frac{dB}{cm}$ in air, $0.002 \frac{dB}{cm}$ in water and 0.7 in soft tissue (Table 3.2). Thereby in ultrasound imaging frequency is constant and selected by an operator.

The reflected echo is produced by two kinds of reflection: specular and diffuse. In contrast with optics, where a coefficient of reflected energy is calculated, in ultrasound scanning the coefficient of amplitude reflection is measured (R_A). The ultrasound transducer determines R_A for two tissues with impedance Z_1 and Z_2 , by the formulae

$$R_A = \frac{Z_2 - Z_1}{Z_2 + Z_1}.$$

From the above analysis, it is possible to make a conclusion, that the less the interaction of transducer with air the better quality picture is generated. For this reason scanning must be done with implementing low impedance gel between the transmitter face and the skin or in a water basin.

3.1.2 Types of ultrasonic instrumentation

Intensity of reflected echoes can be represented by several methods on the display image. These methods specify the display mode and the structure

of the generated image. In the ultrasound medical diagnostic the following display modes are used:

- A-mode (amplitude) generates one-dimensional images that show signals related to amplitude, or energy of wave in vertical axis;
- B-mode (brightness) is a 2D mode where the brightness level of pixels corresponds to the amplitude of the received signal. This mode is more intuitive than the first one, because of its "slice" representation of the image. The slice cuts body in one plane and presents its anatomical structure.
- M-mode - (motion) connects the amplitude to structures, which are changed dynamically (for example, a heard muscle). The vertical axis presents information about the distance to the object and the horizontal axis is used to present the time information;
- Doppler-mode allows to register a velocity and a direction of blood flows;
- Pulsed Wave Doppler-mode emits ultrasound signals as impulse series. It is used for measuring the velocity of a blood flow, which is located on a given distance;
- 3D-mode is an extension of the real-time B-mode. A three-dimensional volume is reconstructed from reflected signals of the transducer with rotated transmitter face. Nowadays this kind of displays is used in cardiology and gynaecology.

B-mode display is attractive for orthopaedic imaging. The generated images present anatomical information about surfaces of bones as high intensive pixels, while the background pixels (tissues with homogeneous intensities) have low intensities.

3.1.3 Transducers

Nowadays, six classes of transducers are implemented in medicine practice.

1. The mechanical sector transducers are the simplest and have a single piezoelectric element.

2. The annular array transducers are used in mechanical sector scanners. A single circular piezoelectric disc is divided into individual elements that are placed around a common centre.
3. The linear array transducers are electronic devices that consist of an array of crystals assembled into subgroups of four or more elements. Such transducers emit parallel beams and do not change the sizes of the objects into images.
4. The convex array transducers have a curved array of crystals. They are used to make the investigations of abdominal organs.
5. The phased array transducers include 32 or more fixed piezoelectric elements and use a special algorithm of pulsation for the individual element. The length of the array is so small that it can fit into a space between ribs for cardiac scanning.
6. The multi-frequency transducers can change their frequency in a given range (for example 5-7.5 MHz) or have some fixed frequencies like 10, 15 MHz and etc. Modern ultrasound scanners usually work with multi-frequency transducers.

The linear transducers are implemented in orthopaedics, neurology, gynaecology, paediatrics, for investigating abdominal, small organs and peripheral vessels. The advance of the linear array transducer is that generated images have the structure of orthogonal matrix and do not require the grid correction for carrying out correct neighbour-oriented operations. Thus in this research I am using a linear transducer to acquire the images of bone surfaces. However, the linear array has a disadvantage of being affected by superficial reflecting structures and of needing a long contact area with the transducer [36]. Next sections will be devoted to the classification of artefacts in ultrasound and methods of their elimination.

3.2 Artefacts in ultrasound

Despite modern technologies and high sensitive electronic equipment the ultrasound imaging suffers from a big number of artefacts. These artefacts make ultrasound investigations of the internal structures of human body difficult. Sometimes they can significantly influence the surgeon's opinion about

Table 3.2: Some typical values for ultrasonic attenuation coefficients

Material	Attenuation (dB/cm at 1MHz)	Half value layer (at 1 MHz) (cm)
Air	12	0.25
Water	0.002	1500
Fat	0.63	4.76
Blood	0.18	16.67
Kidney	1.0	3.0
Soft tissue(average)	0.70	4.29
Liver	0.94	3.19
Muscle (along fibers)	1.3	2.31
Muscle (across fibers)	3.3	0.91
Bone	15	0.20

the tissue geometry and organ recognition. Therefore investigating the nature and behaviour of artefacts, finding the methods which remove or reduce their presence are very important tasks for an ultrasound medical imaging.

The ultrasound artefact is an effect of a reflected echo registered by the receiver. It is not connected with an actual reflected signal and distorts it. Artefact echoes are not related to the location or intensity of reflected energy of local patient anatomy. It is possible to divide all artefacts into two classes: produced by the equipment and generated by the interaction of ultrasound with tissues.

3.2.1 Artefacts produced by equipment

Main artefacts produced by equipment are:

1. *Artificial noise;*
2. *Main bang;*
3. *Veiling;*
4. *Absence of focusing;*
5. *Fresnel zone;*

6. *Side lobes.*

The *Artificial noise* is caused by electro-magnetic fields from the nearest sources. Frequently this effect can be corrected by minimising the influence of remote electro-magnetic sources.

The *main bang* artefact is presented by high intensity echoes and appears if there is a big difference between acoustic features of the transducer and a connected tissue. Generally this artefact can not be suppressed.

The *veiling* artefact appears in case of using all focal zones. A correction is possible by changing focal zones or sometimes by image processing, because intensities of *veiling* signals are relatively low (Figure 3.1).

Both the *absence of focusing* and *Fresnel zone* artefacts affect the form of the object. They can be eliminated by an operator.

Another artefact, the *side lobes*, is produced by any kind of transducers. It appears as echoes from the back side of an interface between a transducer and tissue. The artefact can be corrected by choosing an appropriate focus length.

Thereby almost all artefacts produced by equipment are ordinary in ultrasound imaging. They can be suppressed with the assistance of the operator.

3.2.2 Artefacts produced by ultrasound interaction

The class of interaction artefacts includes the artefacts generated by the interaction of ultrasound with tissues. A correction by hardware and/or software has to be carried out. Artefacts of this class can be divided into those, which considerably interfere with ultrasound diagnostic, and those, which are either absolutely not important or even can help the required procedure. To distinguish ultrasound artefacts it is necessary to analyse the physical basis of ultrasound.

In accordance with the physical properties of B-mode ultrasound imaging, artefacts in ultrasound image can be divided into six groups $A_i, i = 1, \dots, 6$. Ultrasound waves are scattered not only with specular, but also with diffuse reflection. Larger anatomical objects with smooth borders generate "intensive" echoes and appear as bright boundaries, but the reflection can be influenced also by interference and refraction of acoustic waves (group A_1 of artefacts). Another artefact of this group is the artefact of *ultrasound speed* that appears because implementation of mean velocity of soft tissue equals to $1540m/s$. The artefact of *effective reflected surface* results in the registration

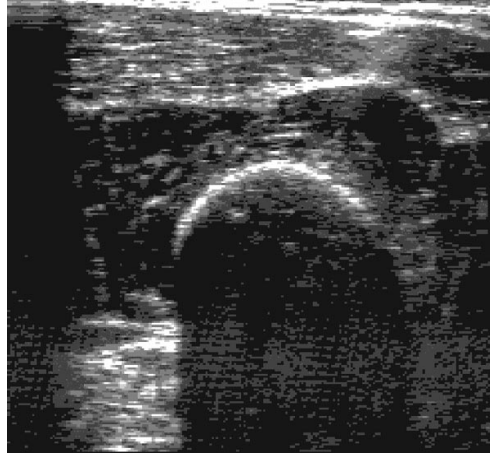


Figure 3.1: Ultrasound artefacts: the veiling is presented in low part of the image. Its gray levels are relatively low

of surfaces in the image, which are smaller than the actual surface. This occurs because a part of reflected beams does not reach the receiver. As was shown above, the quality of boundaries depends on the angles between the surface normal and the US direction. Near a flat segment of the surface, the interference and the refraction effects are minimal if the ultrasound direction is perpendicular to the surface segment. The *enhancement effect* results in increasing the echo signal amplitude after passing through a liquid structure or a cyst, which does not attenuate the ultrasound. This artefact can be eliminated only by changing the position of the ultrasound transducer. In that way, the liquid structure does not act as a lens, refocusing the sound beam.

One of a very well known ultrasound artefact is an ultrasound speckle pattern (A_2). It appears due to the scattering ultrasound along rough tissue interfaces. Small objects like vessels influence speckle appearance irrespective of the fact whether they are presented on the ultrasound image or not. Eliminating this kind of artefact or at least decreasing its influence on the boundaries quality requires a smoothing filter.

The *border artefact* is caused by a strong reflection between the skin and air and belongs to group A_3 . The boundary is so bright that can be treated as an organ interface. The only way to suppress this artefact is to use knowledge about the position of the interface in the ultrasound pictures.

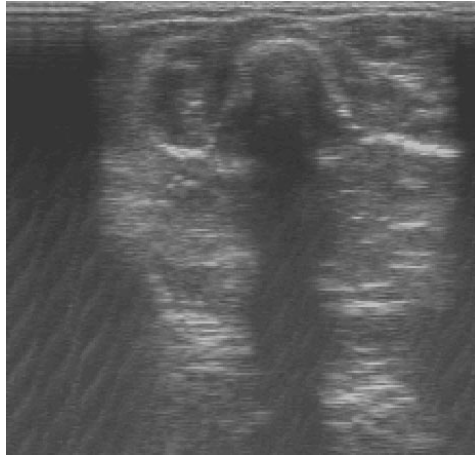


Figure 3.2: Shadow artefact

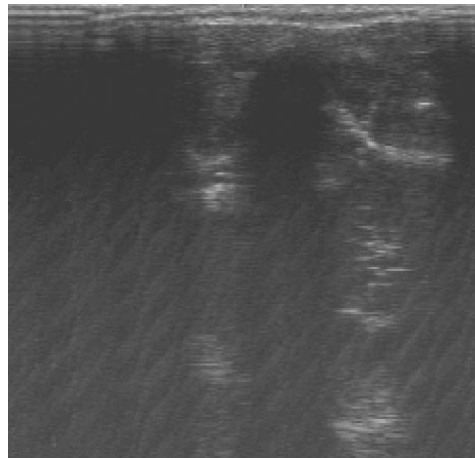


Figure 3.3: Shadow artefact: there is no bright boundary in front of the shadow

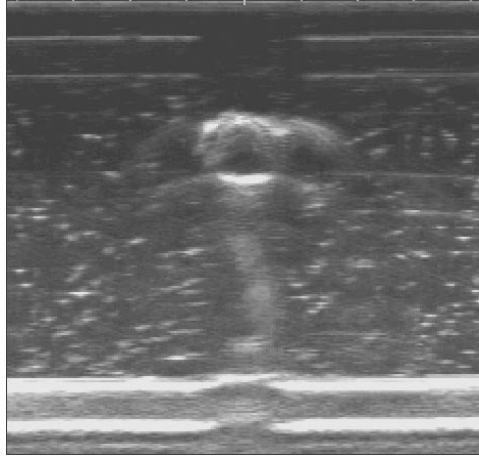


Figure 3.4: Comet effect: a metal nail produces the shadow and the bright line behind

Larger smooth surfaces of anatomical object cause another kind of common artefact called the shadow (A_4). It occurs if ultrasound waves are completely reflected. The intensity of pixels in the shadow is lower than in other image regions. Figure 3.2 shows a boundary presented as a region with high intensities of gray values. Figure 3.3 does not have such a region, but shadow exists in both images. The reason is a position of the ultrasound transducer. It is in the perpendicular plane to the interface for the first image. For the second picture, the transducer was placed with a vertical angle to the perpendicular plane. Ultrasound waves are attenuated and totally reflected from the surface (presence of the shadow), but echoes do not reflect back to the receiver. There is another artefact which also generates the shadow. It is called the *Comet effect* (Figure 3.4) and appears as a bright line behind the interface with a high reflection. The cause can be the presence of a piece of metal inside the body. This artefact cannot be eliminated. However, it can be used for example to detect fiducial markers. If the presence of this artefact is not desirable, the operator must avoid regions with implants during scanning.

A bright region can appear inside the shadow. It is not connected with any anatomical objects and belongs to another type of artefact (A_5) caused by regions of high acoustic impedance.

Group A_6 includes abnormal beam reflection (reverberation) artefacts.



Figure 3.5: Reverberation effect

The simplest artefact from this group is called *reverberation artefact*. These artefacts are resulted from multi-reflection from parallel or steep object surfaces or when the ultrasound beam goes through water-concerned structures (Figure 3.5). The ultrasound reflected from a tissue interface can also be reflected back from the transducer surface or another interface. It leads to the appearance of bright regions in the image with parallel boundaries, which are twice as far from the transducer surface or this other interface as the origin one. Frequently changing angulations of the ultrasound probe might be helpful in this case.

Another artefacts of this group is called the *mirror effect*. It results in the appearance of "ghost objects" near strong reflected surfaces (for example a diaphragm). The ultrasound is reflected off an angle to another interface like a real mirror. The object is presented on the accepted image, but its position and orientation are mirrored (Figure 3.6). The elimination method is the same as in case of reverberation.

3.3 Image processing B-mode ultrasound

Due to the presence of speckle noise and artefacts of groups A_1 , A_2 and A_5 the automatic segmentation of US images is not possible in general. However, in many problem oriented applications the automatic/semi-automatic

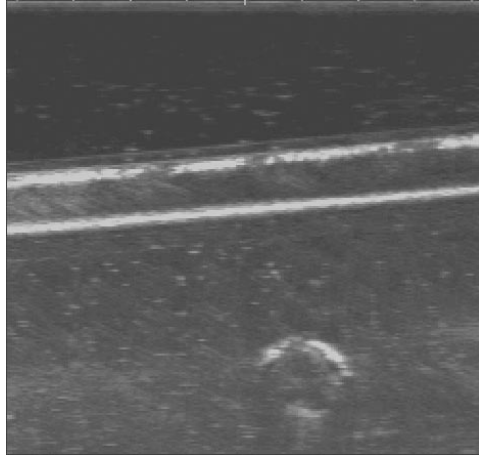


Figure 3.6: Atrefact of Mirror type

segmentation methods can guarantee rather good results.

3.3.1 Methods overview

Sakas proposed an analysis of ultrasound images to improve their quality, segmentation and visualization in his fundamental work about processing ultrasound [39]. Because of the difference of the ultrasonic imaging from other tomographic techniques like CT and MRI, different (from traditional binarisation, iso-surfacing, contour connecting and etc) modelling approaches are required. In this work, the main drawbacks, which are listed below, were specified as characteristics for ultrasound images and a fundamental difference from CT or MRI scanning techniques:

1. Significant amount of noise and speckle;
2. Much lower dynamical range as compared to CT or MR
3. High variations in the intensity of neighbouring voxels, even within homogeneous tissue areas;
4. Boundaries with varying gray level caused by the variation of surface curvature and orientation to the sound source;

5. Partially or completely shadowed surfaces from the objects closer and within the direction of the sound source;
6. The regions representing boundaries are not sharp, but show a width of several pixels;
7. poor alignment between subsequent images (parallel-scan devices only);
8. pixels representing varying geometric resolutions depending on the distance from the sound source (fan-scanning devices only). Obviously, ultrasound artefacts will cause errors in its application. Thus, special image processing methods are required to eliminate artefacts influencing the following analysis.

Therefore in segmentation of US data the main approach used can be the compensation of noise (artefacts) followed by the edge or region-based segmentation. The compensation means the enhancement of the quality of original data by filtering. After this step tissues can be separated by using segmentation from the artefacts.

In the region-based segmentation pixels or voxels within the same tissue type are extracted. For this reasons morphological operators can be used to reduce noise, fill up gaps and e.g. calculate a foetus femur length [37]. A drawback of the morphological based filtration is a possibility to introduce new artefacts. It requires many parameters such as the size of objects, sequences of operators, the number of iterations and etc. This makes the morphological filtering non-intuitive and not efficient.

In another research of Sakas [40], various types of filters to extract foetus surfaces from ultrasound images are investigated. The BLTP (binarize, low-pass, threshold and propagate) method was developed to overcome the drawbacks of morphological filters and implemented in a pipeline. The CPU times were reported 139.53 s for morphological filtration (128^3 volume resolution, 3^3 structuring element) and 10.05 s for BLTP method. These results demonstrate an advantage of thresholding techniques for the speed of processing.

In the work [41], Baker has adapted an algorithm, developed for segmentation of a human head from MRI images for 3D rendering, to explore the effectiveness of boundary-based techniques on ultrasound images of lower legs. First, a Marr-Hildreth operator locates the intensity changes, using

zero crossings. The operator smoothes the data to remove areas of high frequency and uses a Laplacian to detect edges regardless of orientation. Then 3D morphological operators of dilation and erosion with a structuring element of diameter 5 are applied to enhance surface contour definition. As was investigated in the work [91], this technique results in accurate segmentation of MRI brain, but does not produce good segmentation of US. The structuring element was not big enough to eliminate small artefacts after the edge operation. Its increasing (up to 10) allows to eliminate small circular artefacts but also introduces additional artefacts due to presence a noise cluster. Thus the described technique is not feasible for the accurate extraction of bone surfaces from US images.

An enhanced 2D multi-resolution Bayesian segmentation produces accurate segmentation of the outer skin and bone location of the lower limbs [41]. This research was focused on the segmentation of the outer skin contour, the important research dealt with the extraction of bone structures for prosthetic socket design. The enhanced 2D Bayesian algorithm produced a fairly accurate segmentation of the lower limbs. For the prosthetic socket design, the location of the bones, rather than the quality of bone surfaces is in a focus. The average time to process a US image was found 15.6 seconds (SGI Indigo2, 250 MHz), which is too slow to be accepted for real-time applications.

Because of the complex structure of US images and high amount of speckle pattern the automatic processing is complex and unrealisable for many applications. However, a combination of automatic and manual procedures can produce good results. Thus, Prager reported that the implementation of the user interaction to mark the edges with a computer assistance to their tracking, allows to reach a good accuracy in the segmentation of thyroids [44]. In recent years I have used a 2.5D ultrasound imaging system [20]. It has proved to be a reliable method to determine the geometry of bones in the clinical routine. The 2.5D ultrasound imaging device is a combination of an ultrasound probe with a 3D localiser. After manual segmentation of the bone surface the 2.5D ultrasound works like a "percutaneous 3D pointer". However, the implementation of this approach is feasible only for diagnose procedures.

In another approach, several texture features based on the calculation of co-occurrence matrix and auto correlation function can help the segmentation of regions [42]. Generally, the texture analysis for the extraction of organs, e.g. liver, kidney, thyroid glands is implemented. However, bone surfaces

are represented by bright regions with poor texture characteristics. Thus, the texture analysis does not seem to be not useful for the extraction of bone surfaces from US. In addition, texture feature calculations are time consuming and have a restricted implementation in real-time applications.

The possibility to extract anatomical structures from ultrasound images extends the implementations of ultrasound. Nowadays, the ultrasound imaging can be used as independent methods for the diagnosis and can be integrated in CAOS systems. Last year new reports have become available from different groups about successful implementation of US as a tool for intra-operative navigation. For example, Amin uses the edge based segmentation of boundaries separating different tissues for the following analysis [55]. In this work the directional edge detector is used for the pelvis segmentation enhanced by the information from the initial registration estimate. The analysis of the edges is a very complex task. The reason is that the edge detectors are too sensitive to presented artefacts. Thereby the approach will be successful in case of a good initial registration, what is not easy in case of a real patient.

In another group, Kowal combines bright pixels within the image into clusters. Then clusters with higher probability of containing the bone surface are selected [57]. This algorithm was tested on cadaveric long-bones in water basin and sufficient accuracy was shown. However it is possible to say that simple clusterization based on intensity values can produce errors in the classification of bones of real patients, whose blood vessels look sometimes very similar to a bone if located in a neighbourhood of the bone surfaces.

A very interesting approach is presented by Schorr in [53]. Here ultrasound imaging is first simulated in other modalities like MRI or CT and the segmentation of ultrasound is guided by this information. Theoretically, it is possible to reach high accuracy using this technique, but only in case of a successful initial registration, for example, CT and US data. Also the implementation of ultrasound simulation is computationally expensive and produces a huge data set. Another disadvantage of this technique is the existence of elastic deformations of soft tissues during US examination. A thick soft tissue envelop receives a pressure exerted by the ultrasound transducer. It can result in changing reflected echoes from the patient's skin and underlying tissue. To avoid this effect a water basin and a non-touch probe can be used, but it is not feasible for clinical uses.

A fast and reliable segmentation of bone surfaces for US is an open problem in my work. Therefore a new approach to solve the problem was de-

veloped. To provide fast processing the solution is based on the restricted direct thresholding. The segmented regions are classified. The classification is based on statistic information. The developed method is described below.

3.3.2 Proposed method

The implemented approach to extraction of bone surfaces from US images can be described in terms of image processing as a sequences of operations:

1. Picture acquisition;
2. Segmentation;
3. Feature extraction;
4. Classification.

Pictures acquisition

The quality of ultrasound imaging highly depends on the actions of the operator. Thus, it is necessary to restrict the process of picture acquisition by a set of rules, that allow to minimise the amount of presented artefacts as much as possible and to receive the maximal quantity of echoes from tissue interfaces registered by the receiver.

In the proposed system a surgeon makes freehand ultrasound scans moving a navigated ultrasound probe over the operation area. The position of the ultrasound probe is determined by OTD. The position of the transducer influences the appearance and enhancement of artefacts. Thus, the surgeon has to select a position of the probe so that the reflection of ultrasound from the bone surface will be maximal and the bone is located in the centre of the image. Thereby, the influence of artefacts of groups A_1 , A_5 and A_6 on the image quality can be minimal and group A_4 will become apparent. The bone surface is extracted automatically by the developed rainfall algorithm and the surgeon controls the results on the screen. If the quality of the extracted surface is not satisfactory, the scan is reproduced.

Segmentation

The goal of the segmentation process is to divide an image into parts that have a strong correlation with the objects presenting bone surfaces on the

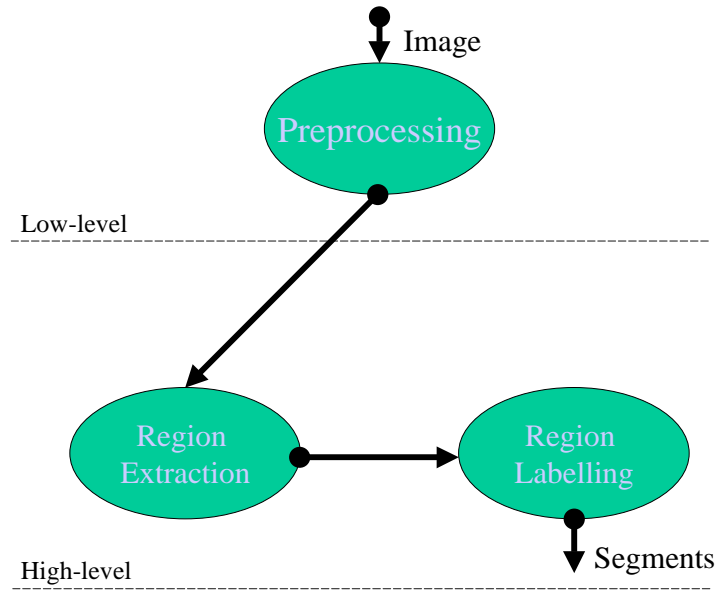


Figure 3.7: Segmentation steps

ultrasound display. It will include two subclasses of low- and high- level processing (Figure 3.7). The low-level segmentation, further referred to as preprocessing, is aimed at a coarse division of the image into background and possible objects. While the high-level segmentation offers a fine discrimination of derived objects. In contrast with other modalities, like CT, a bone surface can not be well presented on the image histogram by a peak. Then such a fast and robust segmentation technique as thresholding can not be implemented successfully for the US segmentation.

- *Preprocessing*

Every tissue interface is presented by high intensity pixels corresponding to the border of regions. However, several biological materials have different acoustic reflection features according to their structure and attenuation. Frequently values of US signal reflected from tissues and received by a transducer are comparable with the altitude of signals

reflected from tissue interfaces. Thus, the first step of the segmentation process is to suppress those pixels which do not belong to tissue interface. A peak analysis is carried out using visual knowledge about the shape of tissue borders. The Top-Hat based segmentation proposed in Chapter 2 can be used here to extract boundaries and suppress the background. First, I use filter operations to improve the quality of extracting surfaces and reduce artefacts. The problem is that a curve bone surface is represented by a set of speckles in the image. Therefore the median filtering implemented so successfully by Sakas in [40] is not accepted because of the lack of a blurring effect. However, the Gaussian 5x5 filter improves initial images. Second, spikes are extracted by implementing the Top-Hat filter with a structuring element of radius of 10 pixels. The image gray values are then scaled to a range between 0-2000, i.e. a histogram extension is applied.

- *Definition of the threshold level*

The bone reflection causes the bright intensity regions in the US images. These regions can be separated from the boundaries of soft tissues on the step of high-level segmentation, for example by optimal thresholding technique (Chapter 2). The advantage of thresholding methods is obvious. The thresholding technique is robust and has a low computational cost, what makes it very attractive for real-time applications. To reduce the user interaction the Otsu or Johannsen and Bille method of optimal threshold calculation can be applied. However, as was discussed in Chapter 2, the Otsu method produces the threshold value, that lies closely to a bigger peak on the image histogram, while the optimal threshold value obtained by the Johannsen and Bille method is located close to smaller peak. The solution become obvious, to apply both methods and take the mean value T of the threshold values found as the optimal one:

$$t_1 = OtsuT(f);$$

$$t_2 = JBT(f);$$

$$T = \frac{t_1 + t_2}{2}.$$

However, the intensity of reflected echoes on the display depends on the actions of the operator. In case if the operator requires special

conditions of ultrasound scanning, a manual correction of the parameters is available. Despite the advances of thresholding technique, its drawbacks discussed in Chapter 2 are actual for US imaging. For this reason the combination of thresholding and region-based segmentation was chosen for the development of the rainfall algorithm as the segmentation problem solution.

- *Labelling*

The further image processing requires reorganising the structure of the image so that the analysis becomes possible not for pixels themselves, but for their aggregations with common characteristics.

The connected component labelling invokes merging into regions of foreground pixels that are connected. Each pixel inside a region presents not the intensity value, but a unique number of the region. The quantity of regions depends on the quantity of connected foreground pixels.

Feature extraction

To produce the classification of the objects (regions) it is necessary first to find independent parameters (features) of these objects. Then each object can be separated from an other according to its features using the classification procedure. I use knowledge about image representation to find geometric features of the extracted objects:

- Area of the object. This parameter presents the size of the object, i.e. the number of its pixels;
- Length of the object, the number of columns occupied by the object, i.e. $d + 1$, where d is the maximal distance between its pixels, which belong to upper border of the region (in opposite direction of US beams);
- Aspect ratio, i.e. $length/area$;
- Shadow deviation, a parameter that represents the measure of noise into the shadow. A definition of the shadow deviation is given below.

Let the surface of an object be presented by a set of points $\{s_1, s_2, \dots, s_n\}$. Then

$$M = \frac{1}{n} \sum_i^n y_i$$

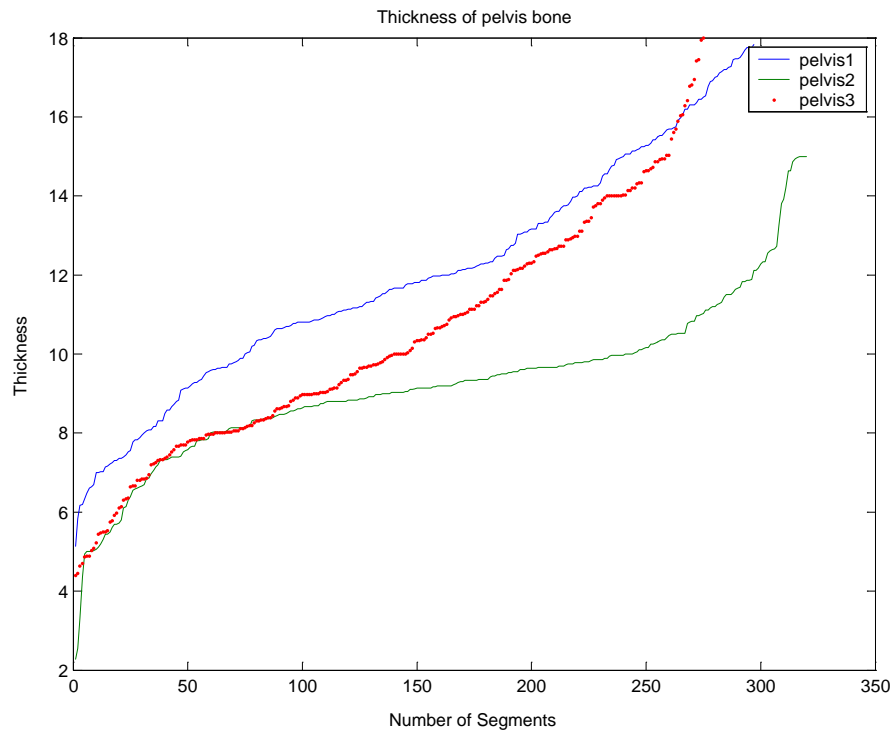


Figure 3.8: Thickness in pixels (sorted) of different pelvis segments into US images

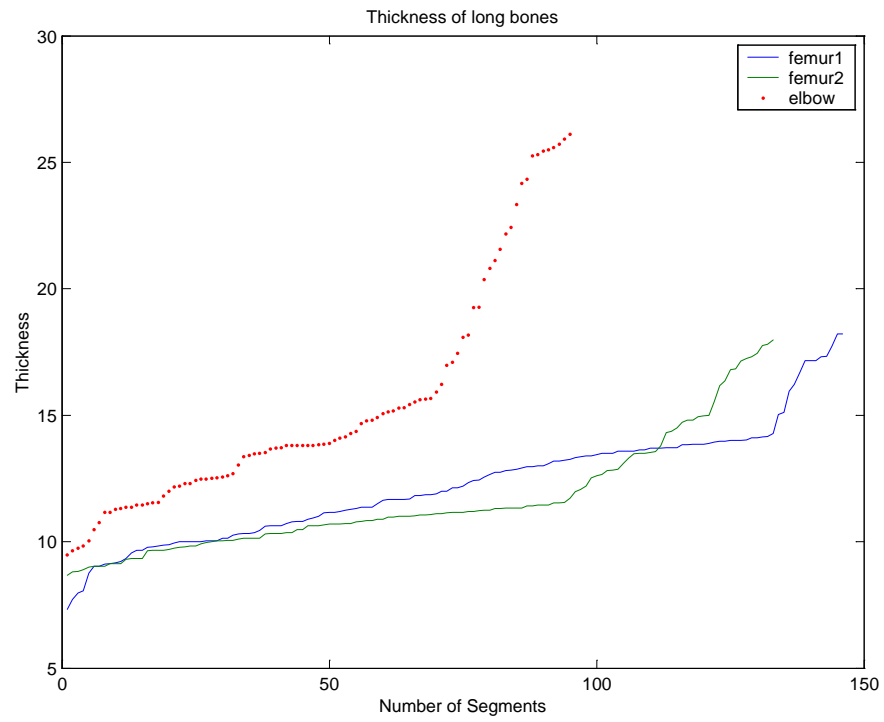


Figure 3.9: Thickness in pixels (sorted) of different long bone segments into US images

is the mean of the object's altitude, iff y_i is the y-coordinate of the point s_i . The standard deviation of the object's altitude is the function

$$D = \sqrt{V},$$

$$V = \frac{1}{n} \sum_i^n (y_i)^2 - M^2.$$

To make a quantitative analysis of the presence of a speckle pattern into the shadow a measurement function will be defined as $N(x, y) = y - y_0$, where (x, y_0) is the nearest point of the speckle pattern in the x-column. If noise points are not presented in the x-column, then $N(x, y) = y$. The mean and the standard deviation of the noisy object's altitude are defined as:

$$M^* = \frac{1}{n} \sum_i^n N(x_i, y_i),$$

$$D^* = \sqrt{V^*},$$

$$V^* = \frac{1}{n} \sum_i^n N(x_i, y_i)^2 - (M^*)^2.$$

The shadow deviation can be defined now as an absolute value of the difference $D - D^*$. This measure tends to zero, if the amount of noise is not significant into the shadow. Therefore, the measurement of this value is a strong tool for the classification of bone surfaces.

Classification

This step of processing US images is aimed at separating every labelled region into two classes A (artefact) and B (bone surface) using extracted features. I use a rule-based approach to the classification or production system. The production provides general knowledge about the objects that can be represented in the logic form

if A then B ,

where A is a logical union of conditions (logical constants) or/and other productions (logical variables), and B is a set of actions.

3.3.3 The rainfall algorithm

I have developed a new algorithm of the extraction of bone surfaces from ultrasound images in automatic mode. It consists of the main operations from the high-level segmentation to the classification. The realisation of the rainfall algorithm is based on the techniques like directional processing and hierarchical propagation. It includes two passes through the image, the first is for the segmentation and feature extraction, and the second one is for the classification. The first pass does not require to analyse all pixels into the image.

The main hypothesis of the presented segmentation algorithm is that bone surfaces can be extracted well by the detection of tissue boundaries followed by the shadow artefact. This hypothesis was proposed by me after long term investigations of various ultrasound images of bones. It was noted that bony surfaces are followed by shadow artefacts when the position of US transducer is perpendicular to the surface. The amount of artefacts is minimal inside the shadow and bone boundary has a smooth contour. It exploits the fact, that the opposite direction allows to avoid many speckle patterns to be analysed. This knowledge motivates to process images from the shadow side, i.e. in the opposite direction of ultrasound waves.

The process of ultrasound wave distribution is similar to a rainfall. Raindrops are falling down from uniformly distributed sources to a gravity centre. The distance from each source to the gravity centre is unlimited. Raindrops are falling until they reach a dense surface. The drops are flowing down along the surface to the gravity centre. If the given surface contains basins, water fills up and flows down again. If one flow reaches another, both flows are merged. Raindrops penetrate under the surface with a constant speed. This process is important, because the analysis of objects absorbing water in different time moments can provide information about their surfaces and forms.

Let us define a 2D greyscale image $I : Z^2 \rightarrow V$, which can be represented as a set of topographic surfaces. We will consider that there are two sets on image I:

$$X_i(I) = \{x \in Z^2 : I(x) > i\},$$

the foreground where all pixels lie above a topographic surface of level i , and the background

$$Y_i(I) = \{x \in Z^2 : I(x) \leq i\},$$

which consists of all pixels under and on the given surface. The distance from pixel x to the background will be denoted as $d_Y(x)$. $N(x)$ is a set of neighbour pixels of x in a given connective grid.

The realisation of this kind of segmentation algorithm is based on the so-called directed thresholding enhanced by additional information about connectivity of pixels. Let us consider image $I(x)$ as the rainfall space, and pixel intensities x , as the material densities. The threshold value T represents the maximal density of the material on the image histogram, which is not resistant to raindrops and value D is the maximal thickness of the surface in our application.

The thresholding procedure is started from the upper row of the image $I(x)$ and is performed pixel-by-pixel from the first pixel of each column. Each pixel from the foreground in that row is labelled by a unique value denoted by a region number. Also for both background and foreground pixels distance to the background is assigned to 0 and 1 respectively and pixels are inserted in a queue. The distance denotes the current vertical thickness of the reached region at point x and also the priority of the pixel. The priority means that pixel p_1 cannot be analysed before pixel p_2 in the queue, if $d_Y(p_1) < d_Y(p_2)$. The propagation is done, until the queue is not empty.

Two kinds of relationships appear between pixels during the propagation. Let us consider a current analysed pixel $y \in Y_T(I)$, then its only neighbour x is pushed in the queue for the analysis, which is placed exactly under y . If $x \in X_T(I)$, then the top of a surface is reached and pixel x should obtain a new region label. The distance to background is assigned to 1, i.e. $d_Y(x) = 1$ (else $d_Y(x) = 0$). The process is repeated for the next pixel from the queue in accordance with its priority. If $y \in X_T(I)$ and $d_Y(y) < D$, all adjacent pixels of y are the candidates to be analysed. For each $x \in N(y)$, such that $x \in X_T(I)$, pixel x obtains the same flow label as y if it has no label before and assigned for the propagation. If the region label of x differs from the label of y , that both regions are merged, for example, with a rule bigger-accepts-smaller. The process stops at point y , if no one pixel was assigned for the propagation.

During the propagation statistic information is collected about every found region i , such as their length l_i , area a_i , a ratio of length to area r_i , shadow altitude standard deviation s_i . The shadow altitude standard deviation is calculated as square root of deviation of differences for each pixel on the top of the surface i , between its row number and a maximal distance to a top pixel of another surface in the same column. If there are no other

surfaces in the shadow of currently analysed pixel, then this value is equal to 0. Additionally a posteriori knowledge about the properties of the bone to be extracted is used to define a rule-based classifier.

The precise rules were found to be useful in the classification:

- length $l \geq 15$;
- area $a \geq 45$;
- ration $r \geq 0.3$;
- standard deviation $s \leq 0.3 * M^*$.

I form a parameter vector $t_{T,D,R}(l, a, r, s)$, which specifies limits for the rainfall algorithm. A parameter R denotes a region of interest in percent from the size of the ultrasound slice. The tracking bone is centred in the slice. Therefore we can remove each region, if its centre of mass is outside the region of interest. Thus, only bright spots in the slices, which have the length of l pixels perpendicular to the propagation direction, an area of a pixels, the ratio less than r and the shadow altitude standard deviation less than s , belong to the bone and are filtered. Of coarse, the length and area as well as the size of the region of interest depend on the form of the extracted surface and can be adapted to be optimal for scanning conditions (geometry of a bone part, position of the probe).

Flooding simulation

The flooding technique became very popular in the image segmentation, especially based on mathematical morphology methods [8]. It is the heart of many segmentation algorithms. The process of flooding is a pseudo-distance transform, that is performed iteratively. It starts from initial seed pixels or regions, called catchments basins. Every basin obtains a unique label. On the iteration step, the flooding propagates from the catchments basins on the depth of 1 pixel if immersed points satisfy a given criterion (usually the geodesic distance of length 1).

This technique provides the way to improve the quality of the labelling regions in US images. For example, Figure 3.10 a) consists of two connected regions corresponding to a pelvis bone and a vessel respectively. The connected component labelling merges the regions into one object, what results in the incorrect calculations of such parameters as the size and length of the



a



b

Figure 3.10: a) The preprocessed and labelled US image a) consists of a bone surface connected with a vessel interface. It can make the region classification incorrect b) Implementation of flooding technique allows the correct classification of the objects

object. I use the flooding simulation limited to maximal propagation on the distance D , to propagate and label regions during the direct thresholding (Figure 3.10 b)).

The realisation of the flooding simulation is based in this work on the special data structure, called ordered queues.

Ordered queues

The ordered queues is a hierarchical structure, that is widely implemented in the mathematical morphology [8] [9]. It is possible to mark out the following its features:

1. The size is fixed;
2. There is an internal rule to insert elements into the queue;
3. There is an internal rule to extract elements from the queue;
4. Operations *insert* and *delete* an element have a constant complexity $O(1)$;
5. All elements are inserted into ordered queues in order of their appearance;
6. All elements with different priorities are extracted in order of increasing their priorities.

The queue is represented by a linear array of a fixed size n . The number i of each item q_i , $i = 0, \dots, n - 1$ is its key. The hierarchical rule specifies priorities of items based of their key values, i.e. for any two q_i and q_j , $i \neq j$, if $i < j$, then q_i is performed before q_j . As mentioned before, there are also internal rules for the insertion and the extraction of elements. Each item q_i is represented by a queue data structure, i.e. the size of q_i is not limited, and elements of q_i are performed according to a rule first-in-first-out (FIFO). If the last element of q_i is extracted, the queue is suppressed and the next element with key I will be inserted to the first available queue q_j , $j > i$.

For example we have pixels a_i , $i = 0, \dots, 4$, with different labels $A = (0, 3, 2, 0, 2)$ respectively. First we place values a_0, a_1, a_3 into the ordered queue Q . This ordered queue consists of four queues ($\max(A) + 1$), performed in accordance with the FIFO rule, $Q = (q_0, q_1, q_2, q_3)$. Each value of three is

Table 3.3: Materials for sow cadaver study

Ultrasound linear transducer	5 MHz
Slice resolution	0.18x0.18 mm
Space between slices	1 mm
Number of slices	80
Number of learner slices	3
Rejected slices	11
Satisfied slices	8
Corrected slices	5
Good slices	60
Wrong slices	1
Total number of good slices	65 (from 69)

placed in a queue with a corresponding number. Then we extract the last element from Q , i.e. 0, the queue q_0 has no more elements and is suppressed. If we add now the rest values, q_0 is empty, $q_1 = (a_3)$, $q_2 = (a_2, a_4)$, $q_3 = (a_1)$. Element a_3 is placed in the first available queue, because q_0 cannot be used anymore. Now the next candidate to be extracted is a_3 .

3.3.4 Validation of the rainfall algorithm

Validation is a very important task, especially for medical applications. The *cross-validation* method of model evaluation is used. The implemented cross-validation method, the so-called *holdout* method is based on the division of data into learner and test data. In other words, the rainfall algorithm is first implemented to the learner data and its optimal parameters are found for this set of data. Then the algorithm is applied to the rest of the data, without changing the parameters. Finally, the produced errors are summarised and the mean error is calculated for the test.

Two validation studies were done. A front leg of the fresh sow cadaver is placed in the water basin and is fixed. The ultrasound linear transducer is placed perpendicular to the long axis of the basin. The movement of the probe is possible only along this axis. Ultrasound data are taken with 1 mm of the distance between slices. Next a soft tissue envelop is removed and the bone is scanned again in the same basin. This second data set is used

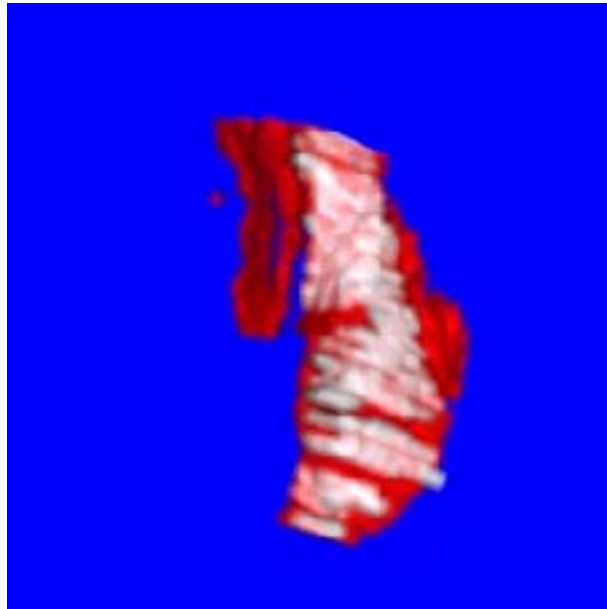
as an "anatomical atlas" to guide the manual segmentation procedure. The bone regions are manually identified basing on anatomical knowledge and known ultrasound characteristics of the bone surfaces. The first data set includes 80 parallel slices. The first 15 slices contain bone, covered by joint binds. The next 30 slices resent joint area. The rest slices have bone. Thus, the first slices from each part are selected to form a learner data set and the parameter vector $\tau_{900,5,40}(15, 45, 0.3, 0.3)$ is generated. Then the rainfall algorithm is implemented with the given vector of parameters to the rest of the images. Both segmented data sets are compared.

The difference between the two model surfaces was found to be less than 0.6 mm of MDE. Table 3.3 shows the evaluation of segmented slices. A slice is rejected, if it has no foreground. Slices are recognised as "good", if extracted objects correspond to bone structures. Classification is "satisfied" if a slice consists of a small amount of non significant artefact and "wrong" in other cases. Because the data is taken without a surgeon inspecting and positioning the transducer, the results are not optimal. But the knowledge about the distance between parallel slices allows to implement a corrective procedure: 3D smoothing and connected component labelling (minimal area is 100 voxels). Then subsets "satisfied" and "wrong" can be corrected. Table 3.3 shows the number of corrected slices. In that way, 94,2% of all slices were classified as "good". The problem of the appearance "complicated" slices is that:

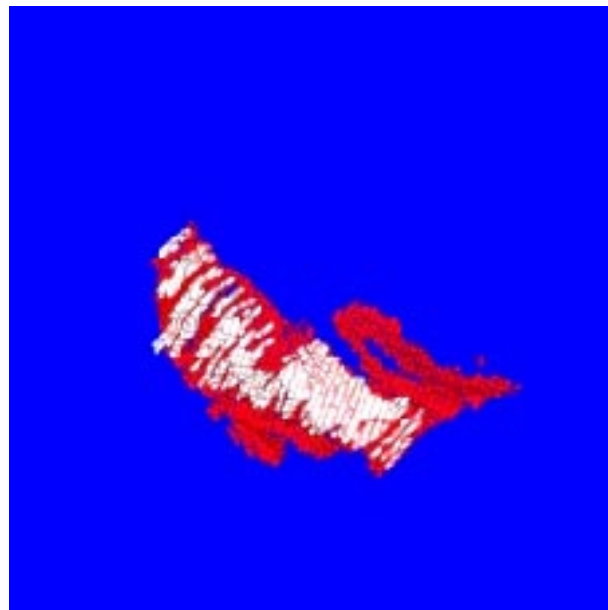
1. Transducer was not placed to receive back maximum of echoes;
2. Majority of "rejected" and "satisfied" slices were found in first two part of data set (bone covered by binds and joint area);
3. "Wrong" slice was found in third part, in a place, where the bone has high curvature.

Figure 3.11 shows both segmented surfaces.

The second study was done with the patient's pelvis. A data set from 48 slices are accepted for the segmentation under a surgeon supervision. It means that only slices with good surfaces are used for the test. Then the new data set is obtained by using the rainfall algorithm and manual segmentation. The difference between surfaces was calculated to be less than 0.4 mm of MDE. The results of segmentation are presented in Figures 3.12 and 3.13.



a



b

Figure 3.11: Bone surfaces obtained from sow cadaver: red - manually, white - automatically

Table 3.4: Materials for pelvis study

Ultrasound linear transducer	5 MHz
Slice resolution	0.18x0.18 mm
Space between slices	1 mm
Number of slices	48
Number of learner slices	2

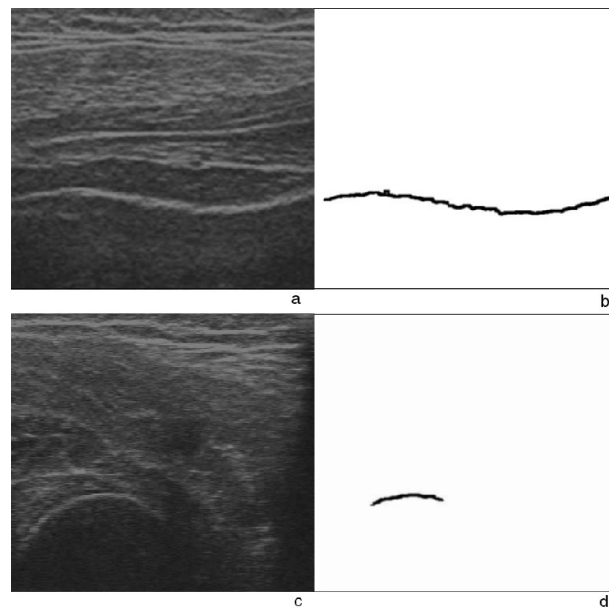


Figure 3.12: Results of pelvis segmentation

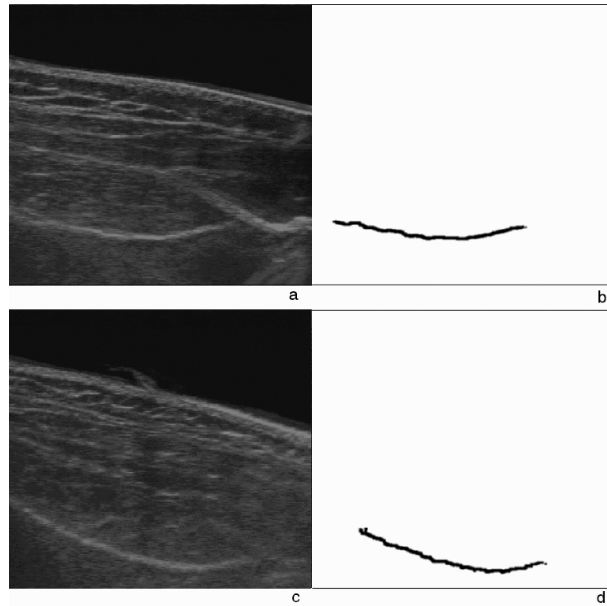


Figure 3.13: Results of pelvis segmentation

3.4 Improvement of the rainfall algorithm

Further improvements of the rainfall algorithm, i.e. increasing its ability to recognise bone surfaces, can be done by using the motion tracking approach [43]. Then the process of the bone tracking includes two steps. On the first step the bone surfaces are segmented and classified by the current version of the rainfall algorithm. On the second step, the classification part of this algorithm is extended using also the information about the movement of the surfaces through slices. In other words, the motion from slice to slice is detected and measured. Because biological objects like bones are smooth, the movement is relatively small. Therefore the motion tracking is another tool for the classification. This modification of the rainfall algorithm was not implemented, because it is out of the working plan of the project.

3.5 Summary

The realisation of the real time navigation system based on ultrasound was discussed in this chapter. First physical principles of ultrasound were described. Then an overview and classification of ultrasound artefacts were given and methods to eliminate or reduce their presence were proposed. A new algorithm of segmentation bone surfaces from ultrasound was proposed. The key idea of this algorithm is to use the shadow artefacts for the classification of bone surfaces. In this way, the algorithm is based on the direct thresholding and its direction is opposite to the direction of ultrasound waves propagation. A selected threshold value extracts white regions on the ultrasound image. Then the classification based on the description of the form of the regions is used to filter out the rest of the artefacts. A surgeon validates every segmented picture, which is produced in real-time.

The implementation of the rainfall algorithm for the segmentation of bone surfaces from ultrasound images allows surface extraction in an automatic mode. The algorithm works in near real-time (10 fps for AMD Athlon XP 1.8+). The feasibility of bone extraction from ultrasound images with high accuracy has been shown (about 94%) for pelvis and sow lower leg. The maximal depth of extracted bones under skin can be about 7.5 cm. The study discussed above shows that the form of the pelvis could be segmented well from ultrasound data sets.

Chapter 4

Registration

4.1 Introduction in image registration

Image registration is a process of spatial mapping two images of an object taken from different sensors or from the same sensor but at a different time [32]. An example of the implementation of image registration is when images need to be aligned with one another so that the differences can be detected [63].

4.1.1 Types of registration

One of the possible classifications of major image registration techniques can be made on the base of their correspondence type:

1. *Multimodal.* The multimodal registration refers to matching images taken from different sources (modalities). An example of such matching in the medical area is the registration of CT and MRI data.
2. *Template.* The registration tries to find a match for a reference pattern in the image. It is mostly based on the known properties of objects. The database image contest search can be taken as an example.
3. *View point.* This type is frequently used in the field of computer vision to register either images taken from different viewpoints for depth or shape reconstruction.

4. *Temporal.* The registration of the images in the same scene but at a different time or under different conditions is called temporal. It is implemented usually for monitoring motions, changes or grows.

4.1.2 Methods of registration

The registration process can be described as mapping two data sets I_1 and I_2 , using a transformation function g :

$$I_2 = g(I_1).$$

The aim of the registration is to find an optimal geometric and/or intensity transformation g . The intensity information is not always used because other features of matched images can be required to find the alignment.

There are many methods which can be applied to determine the optimal transformation. Their main principles are listed below.

1. Stereotactic frame systems. The stereotactic frame is a mechanical device used for accurate positioning instruments such as probes, electrodes, and biopsy cannals in three-dimensional space [35]. The frame is attached to the body (usually the skull) and fixed by screws or penetrating pins. Several fibre rods form three or more shaped markers. This image localising device is used during CT, MRI or PET image acquisition. The position of the markers determines the position and orientation of the derived volume and is used for mapping surgical coordinate system into the image space.

Frame systems have several advantages: they are very accurate, not sensitive to several types of image distortion. The stereotactic frames are widely implemented for neurosurgical applications. But their use is limited, because of the invasive fixation technique.

2. Correlation and sequential methods. The cross-correlation is statistic approach to the registration, which is often implemented when the location and orientation of a template or pattern is found in the picture [70]. These methods introduce a similarity measure, which computes the sum of the squared differences between the template and the picture at each location of the template. If the image is noisy, i.e., there is a significant distortion which cannot be removed by the transformation,

the peak of the correlation may not be clearly discernible. *Sequential methods* use similar measure, but provide a sequential search strategy. Generally, correlation and sequential methods are implemented for registration of 2D images, e.g. photogrammetry. The limitation of both of these methods is their inability to deal with dissimilar images. Also the methods are computationally intensive to be implemented in real-time in case of 3D.

3. Fourier methods. The Fourier methods are appropriate for small translations, rotations, or scale changes. They register images by exploiting several constructive properties of the Fourier Transform. An overview of the registration using the Fourier methods was published by Brown [63].
4. Point mapping. The point- or landmark-mapping technique is the primary approach currently taken to register two images whose type of misalignment is unknown (translation cannot be represented by a set of small translations or rigid-body movements) [63]. The general method for point mapping consists of three stages. In the first stage features in the images are computed. In the second stage, feature points in the first images, often referred to as control points, correspond with feature points in the second image. In the last stage, the estimation of the geometric transformation is determined using these matched feature points. Resampling one image onto the other is performed by applying spatial mapping and interpolation.
5. Surface matching. These methods involve the determination of corresponding surfaces in the registered images and their mapping. The surface matching has been widely used clinically to register image volumes from different modalities, e.g. CT, MRI, PET, SPECT [35], and determine a spatial transformation between the surgical and patient's spaces using OTD or US generated 3D surfaces [16], [48].
6. Moment and principal axes registration. The general idea of this type of registration consists of the calculation of the moments to represent the object's centroid in the image space and orthogonal axis about which the moments of inertia are minimised, i.e. the principal axis. The direction of the axes determines the object's orientation and can be calculated as the eigenvectors of its covariance matrix [69]. Thus,

the centroids of the same object in different images define the translation and the principal axes determine the rotation. The eigenvalues related to these eigenvectors may be used to specify a scale parameter. Unfortunately these methods are effective only in case of identical and entire representation of objects, which are presented in both image data sets. This limitation is due to the sensitivity of the methods to missing image data. The moment and principal axes registration has been used for example in applications like aircraft silhouettes identification [68]. However, clinical implementation of correlation and sequential methods is limited, because of its high sensitivity to missing the data (cannot be implemented in case of multimodal images) and to pathological deformations.

7. Interactive matching. The three-dimensional image registration can be also achieved through a simultaneous positioning of multiple reformatted slices in all three dimensions for their better alignment. Accurate registration is user intensive, but can be usefully applied for a *coarse* registration, as an initial step for the following *fine* registration.
8. Template based registration. The idea of the template based methods is to find the transformation which maps templates to the image, taking into account the local shape differences. This kind of registration has been frequently used for establishing relationships between previously performed studies and separate individuals [63].
9. Elastic model based matching. Instead of directly applying a piecewise interpolation to compute a transformation to map the control points of one image onto another, these methods model the distortion in the image as the deformation of an elastic material. In other words, the registration transformation is the result of the deformation of an elastic material with the minimal amount of bending and stretching. These forces are characterised by the energy state of the elastic material. Elastic methods register images by matching structures. Such approach is often used for the problems in shape and motion reconstruction and medical imaging [35]. In these domains, the critical task is to align the topographical structures in image pairs removing only the differences in their details. The elastic methods are capable of registering images with some of the most complex distortions, including 2D projection of 3D

objects, movements with the effects of occlusion, and the deformations of elastic objects [63].

10. Mutual information based registration. This technique is used when no direct correspondence between gray values in different modalities are known. It is based on the shared information between the overlapping regions in two images, which at registration should be maximised [72]. For example, a rigid registration of CT and MRI data is possible after feature extraction and interpolation steps. In a recent research [71] of matching multimodal images of CT and MRI, good results are demonstrated for the registration based on mutual information. The accuracy of such registration has the same order as a bone marker match.

The methods listed above refer to both rigid and non-rigid registration. However, biological structures like bones and gristles are not subjected to elastic deformations and therefore only the rigid body registration is a point of interest in orthopaedic applications.

4.1.3 Rigid body registration

Let X and P be two data sets (coordinate arrays of size N_X and N_P respectively) to be matched, then the problem of the rigid registration, called as *Orthogonal Procrustes problem*, can be described as the minimisation problem

$$\|X - PQ\| \rightarrow \min_Q,$$

where Q is an orthogonal transformation matrix.

In medical applications the word registration has two different meanings. First it defines a common coordinate system for the patient (surgical space) and the patient's image data sets (image space). Thus, in addition to that the registration can define a common coordinate system for two or more data sets that represent the same objects by e.g. different imaging modalities like ultrasound and CT. In general, it is possible to describe the process of registration of two or more images by the following steps:

1. Detection and extraction of common features existing for all images;
2. Creation of a transformation function, which aligns coordinate systems of all images;

3. Transformation of one or more images in accordance with the found function.

Such schema is typical for the point mapping methods of the registration. This is the reason why the most widely implemented methods of the rigid body registration in medicine are point matching and surface based registration. The point matching application in orthopaedics was discussed in Chapter 1. The surface based registration is its modification, where surfaces are represented by node points (vertices) and matched in that way to achieve the best alignment of surface segments, i.e. not only vertices.

The approach to the registration defines the way how to form the matched data sets X and P . It means that those features of images are extracted, that will be used for the registration. Then the rotation, translation and sometimes scaling are used to align the objects. The search strategy finds the next transformation. The similarity measure to determine quality of the alignment on the given test is required.

The former problem of the rigid body registration is commonly solved by introducing and matching anatomical landmarks on all images. This technique and its disadvantages were described in detail in Chapter 1. In this thesis the image based approach was proposed. Fractures or deformities can be imaged by both ultrasound and CT. Ultrasound is completely reflected by bone. While CT gives the full object's shape, the ultrasound device images only a part of the object's surface. Therefore, the question is how to match these two data sets. Holupka, for example, suggested to extrapolate the partial surface by spherical harmonics [65]. Thus one can obtain an estimation or approximation of the full surface of the object. The next step is the description of the objects by identification of their centre of mass and the moments of inertia. This information allows to reconstruct the required transformation of the ultrasound data set coordinate system into the CT coordinate system. Unfortunately, the reconstruction is often incorrect since too little information is available about the individual morphology.

A general approach consists of the formulation of the registration process as an optimisation problem. Therefore, the problem is to find the transformation so that the distance between the two surfaces is minimal. For this purpose, one surface (*hat*) is represented by a cloud of points and the distance for each point to the surface of the another data set (*head*) is determined. The target function is the sum of these distances. Various optimisation algorithm can be used for this purpose. The accuracy of the surface-based

registration is expected on the order of the voxel size [66].

4.2 Iterative closest point algorithm

4.2.1 Principles

The goal of *ICP* algorithm is to find the transformation M consisting rotation R and translation T between two dense 3D maps X (head) and P (hat). The main steps of this algorithm are listed below:

1. Init: $i = 1$; ϵ is the maximal acceptable least square error; η is the iteration limit;
2. Build the set Q_i of the closest point pairs with $q = (x, p)$: $\forall p \in P_i$, find $x \in X$ with $\|x - p\| = \min(\|x - p_i\|)$, $i \in [1, \dots, N_p]$;
3. Find the transformation M and calculate the mean square error $error_i = \frac{1}{N_p} \sum \|x - R_i p_j + T_i\|^2$;
4. Calculate $P_{i+1} = M(P_i)$, until $error_i < \epsilon$ or $i > \eta$.

Because the algorithm converges to a local minimum, it requires an initial transformation, so-called *coarse* registration to reach the global minimum. This can not be a limitation for most CAOS applications, because the initial transformation is approximately known or a surgeon can make *coarse* alignment of bone surfaces manually.

4.2.2 Why *ICP*?

In my work, the *ICP* algorithm for the registration of CT and US surfaces was selected. The choice was motivated by the ability of this algorithm to register surfaces represented by clouds of points and by a set of vertices. Generally it provides the possibility to implement both voxel based models and polygonal models into one scene, what can be an advantage for operation planning systems using polygonal surfaces.

A well known disadvantage of *ICP* algorithm is its computational complexity. The distance calculation is time consuming and it is the critical point of the algorithm. The complexity $O(N_X * N_P)$ of the closest point seek operation was found in [64] and cannot be accepted for real-time applications.

There are many groups world wide, which propose different solutions for the acceleration of the closest distance seek operation. Some of them use hashing like k-dimensional binary trees [13] to decide on which side of hyper plane the closest point is, or caching seek results [16]. Thus, in general we can obtain $O(N_X * \log N_P)$ complexity. These solutions were proposed for polygon based representation of the model, which has some additional disadvantages. The created model is a fixed structure, that requires an optimisation (vertices decimation), and the size of complex models is limited by AGP bandwidth. In current research, I propose a volume based approach both for processing and better quality visualization. It allows to reduce the computational costs of the closest point seek operation to $O(1)$ by implementing the Euclidean Internal Distance Map (EIDM) [10], what is not trivial in case of polygonal model. The map consists of an address of the closest point in X for each possible voxel position from P . Thus, the final complexity of the modified *ICP* algorithm is $O(N_P)$. Experimental results presented below, show the registration accuracy of this modification comparable with the accuracy of classical *ICP* algorithm [64].

4.3 Distance map

Implementation of distance coding (creation of the distance map) is used widely in mathematical morphology, image processing, computer graphics and pattern recognition. Euclidean distance map is produced by the distance transformation - a function defined on binary images. Let us consider that the binary image is divided into the foreground (e.g. set of objects) and background. Then we can define two kinds of Euclidean distance transforms:

- *External*. In case of the Euclidean External distance transform (*EEDT*), every foreground pixel is assigned by a brightness value, which equals a minimal distance from this pixel to the border of the object. Other pixels obtain zero value.
- *Internal*. In case of the Euclidean Internal distance transform (*EIDT*), distances are calculated for background pixels.

To calculate the distance transform, first it is necessary to define the distance measure or metric. Let a, b, c be points in n-dimensional space, then function D is metric if the following condition are true:

1. $D(a, b) = 0$, **iff** $a = b$;
2. $D(a, b) > 0$, **iff** $a \neq b$;
3. $D(a, c) \leq D(a, b) + D(b, c)$ (triangle rule).

Then Euclidean distance between points x and y with coordinates (x_1, x_2, \dots, x_n) and (y_1, y_2, \dots, y_n) respectively, can be defined as

$$d(x, y) = \sqrt{\min_{s \in B} \left(\sum_{i=1}^n (x_i - s_i)^2 \right)}.$$

The calculation of Euclidean distance is computationally intensive, and therefore it is frequently approximated by using other metrics. The most well known approximations are Manhattan (city-blocks) and chess-board (names were given first for 2D metrics).

$$d(x, y) = \min_{s \in B} \left(\sum_{i=1}^n |x_i - s_i| \right).$$

$$d(x, y) = \min_{s \in B} (A),$$

where

$$A = \max_{i \in \{1, \dots, n\}} (x_i - s_i).$$

Sheynin described in [10] the algorithm of calculation of the EEDT as a part of the opening transform. By analogy with his work I shall define the Internal Euclidean distance transform.

Let $B, X \subset Z^3$ and $0 \in B$. Ball B of radius r in $Z_+ = \{z \in Z | z \geq 0\}$ centred in a point x is defined by

$$B(x, r) = \{x\} \oplus B^{\oplus r}, B(x, r) = \{x\}.$$

The *Euclidean Internal distance transform* is defined by function $d_{X,B}(x)$:

$$d_{X,B(x)} = \min\{r \in Z^3, B(x, r) \subset X\}.$$

The algorithm of finding distance transform for the fixed structuring element is well-known [61] and the description does not depend on the image dimension. It performs two scans of the image (in forward and backward

direction). Therefore first I choose the forward direction of scanning voxels. Let us, for example, scan voxels according to the increasing order of the first coordinate, then of the second and third.

For every point $x \in X$ its neighbourhood $N(x) = (\{x\} \oplus B) \cap X$ is partitioned into two parts $N_+(x)$ and $N_-(x)$. The first one consists of the points which are scanned before the point x and the second one consists of points which are scanned after x . We will call the points from $N_+(x)$ by preceding neighbours and from the second part $N_-(x)$ by consequent neighbours. The point x itself is not included into the $N(x)$.

Algorithm of calculation EIDM:

1. **procedure** EIDM
2. INPUT: image f, threshold value T
3. OUTPUT: image d - distance map, image c - code map
4. /* Initialization */
5. **for any i do**
6. $d_i = \infty$;
7. $c_i = 0$;
8. **end for**
9. /* Immerse f into d */
10. **for any i do**
11. **if** $f_i > T$ **then**
12. $d_i = 0$;
13. $c = Address(f_i)$
14. **end if**
15. **end for**
16. /* Iteration I*/

```

17.   for every point  $x_i$  under the forward direction scan do
18.       if  $r = \min\{r_j + 1 | y_j - \text{preceding neighbour of } x_i, y_j \in N_+(x_i)\} <$ 
            $r_i$  then
19.            $r_i = r$ 
20.       end if
21.   end for
22. /* Iteration II */
23.   for every point  $x_i$  under the backward direction scan do
24.       if  $r = \min\{r_j + 1 | y_j - \text{consequent neighbour of } x_i, i.e. y_j \in N_-(x_i)\} <$ 
            $r_i$  then
25.            $r_i = r$ 
26.       end if
27.   end for
28. /* The value  $r_i$  is the result of the distance transform at the point  $x_i$ 
    */

```

4.4 Validation of the modification of the ICP algorithm

As was mentioned in the previous section, the described algorithm of distance coding uses the approximation of Euclidean distance. Therefore the validation studies are required to be sure that the proposed modification of the ICP algorithm does not influence significantly the accuracy of the registration procedure and it is acceptable for medical purposes. For this reason a set of validation studies was carried out.

The validation of the results is a very important step in measuring the efficiency or accuracy of an algorithm. Usually two approaches can be used: simulation experiments and phantom experiments. Each approach has its own advantages and disadvantages. An example of a simulation experiment

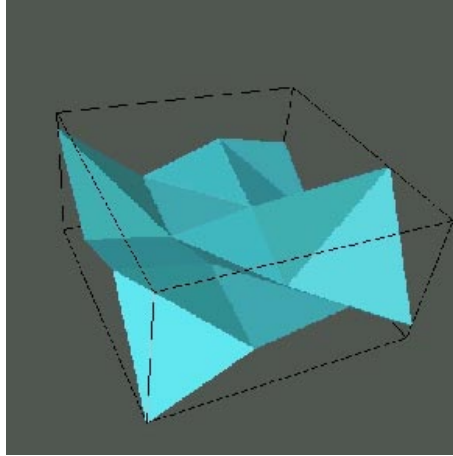


Figure 4.1: Synthetic data

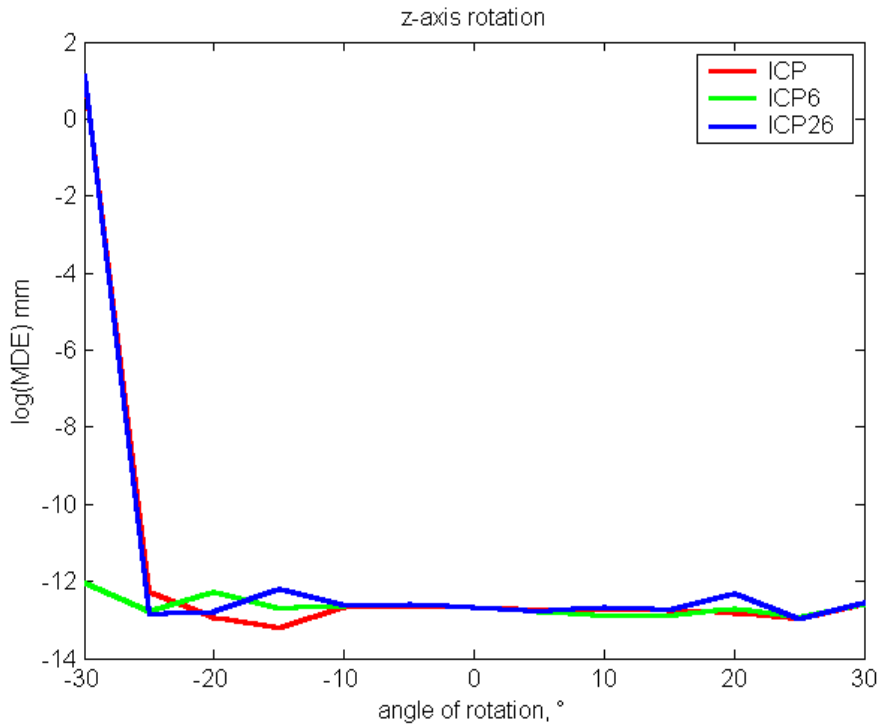
is self-registration. The position of one image is simulated with respect to the position of another. It can mean, for example, that the image is duplicated and its exact copy is geometrically transformed. The ideal position of the registered image is known. Then the registration is applied for these two data sets and the registration error is measured, the mean distance error (MDE) between landmarks, existing in both data sets (in volume based registration it is equivalent to the distance error between the closest points in both surfaces). An advantage of the self-registration approach consists of the isolation of possible errors which are not related to registration. This pure registration experiment allows defining good and/or bad conditions, which influence the stability of the tested registration algorithm.

From the other side, phantom registration allows to minimise the influence of artefacts, because geometric features of phantom are known and the results of registration can be predicted. This approach is used very often in medical applications [16]. Also the combination of both approaches can be implemented.

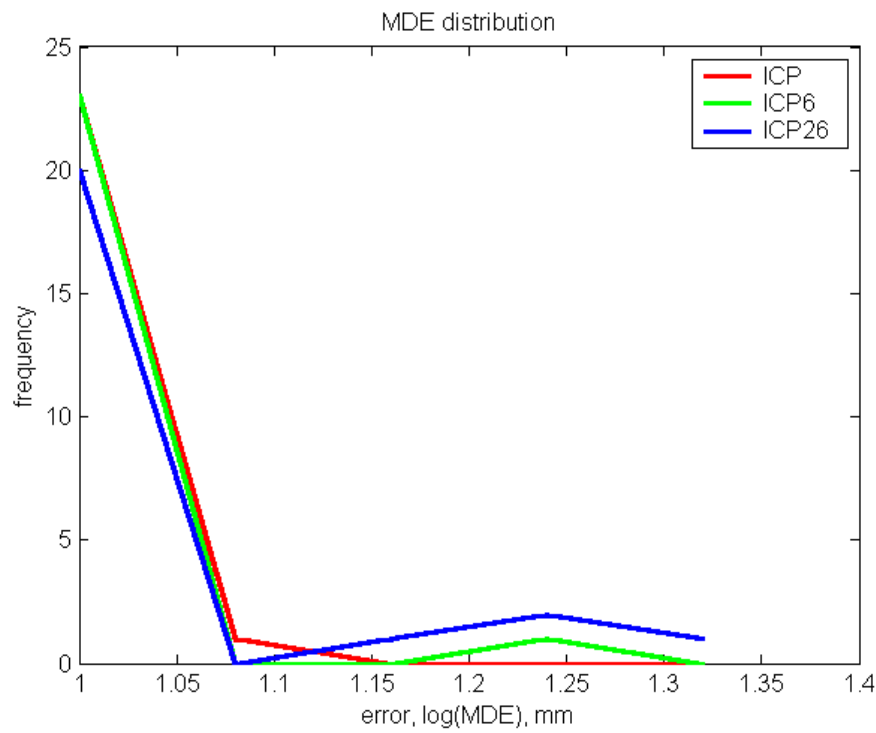
4.4.1 Registration of synthetic data

A synthetic data set was generated to carry out the quantitative measurements of three registration algorithms (Figure 4.1). It is a relatively small surface with vertices interpreted as landmarks. A small size was chosen to

4.4. VALIDATION OF THE MODIFICATION OF THE ICP ALGORITHM⁹⁹



a



b

Figure 4.2: Rotation of synthetic data a) around z-axis; b) around x-axis

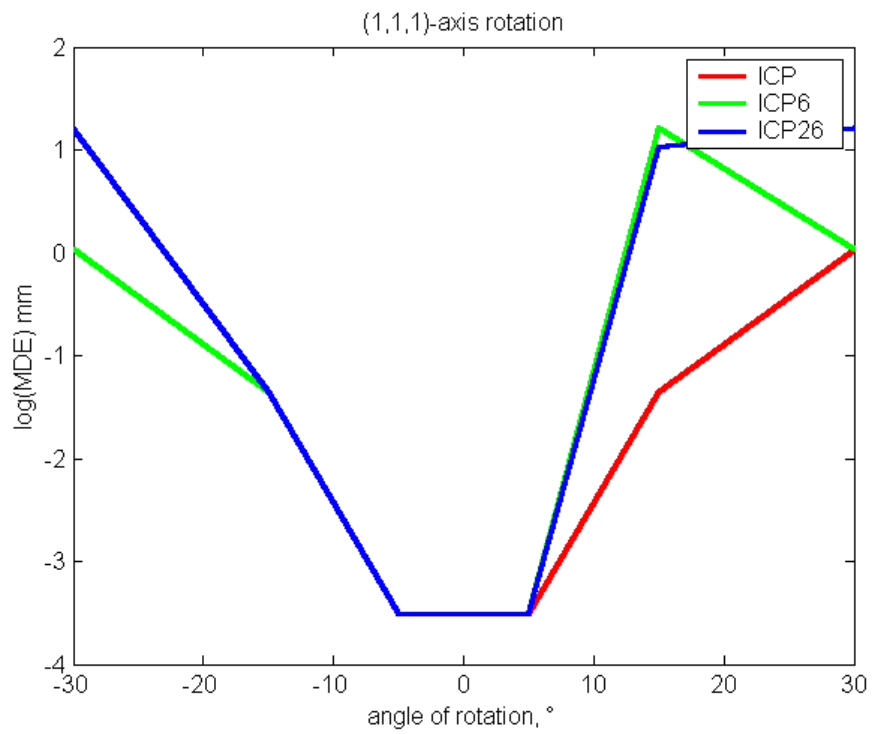


Figure 4.3: Rotation of synthetic data around an arbitrary axis

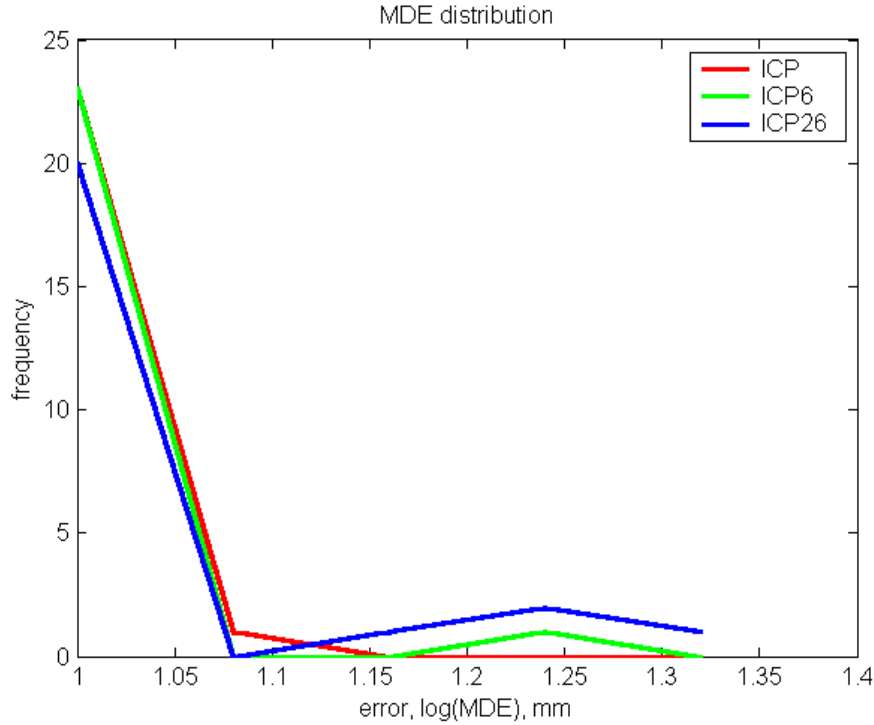


Figure 4.4: Error distribution

minimise common time of test in case of slow *ICP* algorithm. The data presents a peaked terrain, that is the most critical case for distance approximations and allows to identify maximal errors. Thus, the mean distance error (MDE) was measured between landmarks for the *ICP* algorithm, for the modified version of this algorithm with EIDM using 6-connected grid (*ICP6*), (analogue of the Manhattan metric in 2D), and another modification using 26-connected grid (*ICP26*), (analogue of the chess-board metric in 2D).

First a set of initial transformations is applied to obtain a misregistration of surfaces. The second data set (copy) was rotated around z-axis and then around x-axis on different degrees (from -30 to 30). The range of rotation was chosen in accordance with the known features of *ICP* algorithm [67], to have the highest probability of convergence to the local minima. Because

the resolution along x and y axes is the same for CT scanners, rotations around y -axis were not applied. Then the set of rotations is carried out for an arbitrary vector, $(1,1,1)$ in our case. The centre of the rotation does not depend on a shift and then translations were not tested, because of the obviousness of the results. The distribution of MDE is presented in Figure 4.4. Functions have similar value when all three algorithms converge to the same local minima (rotation about 30 degrees).

Self-registration of model derived from CT

The aim of this additional self-registration test is to investigate which metric (6 or 26 lattice) results higher accuracy for the biomedical data. A femur saw-bone (AO-ASIF Synbone 2071) was used (Figure 4.11) in this test. The test procedure is as following. First the bone surface is modelled from CT data generated by Marcony scanner. A similar procedure of testing is implemented as in case of synthetic data registration for *ICP6* and *ICP26* algorithms. The rotation around z -axis (Figure 4.5) shows advantages of 6 connected lattice both in accuracy and in speed of convergence. This is also true in case of x -rotation (Figure 4.6).

4.4.2 Phantom accuracy validation

In order to demonstrate the feasibility of the registration algorithm two studies were carried out [28] [30]. Unfortunately, OTD was not available for these tests. I have implemented a hybrid approach to the registration using both fiducial markers and image landmarks (Figure 4.7). The tests were carried out according to the following schema. First fiducial markers are attached on the phantom surface. Then two data sets are generated using CT and US scanners respectively. The bone surface is modelled from CT data set and the fiducial markers are extracted. Centres of the markers play the role of a reference basis in this test. To model the US bone surface, the phantom is placed into a water basin (Figure 4.8). Then ultrasound images are acquired moving a fixed probe along one fixed direction.

The implementation of the water basin allows to overcome the lack of ODT and produce a 3D volume of US data. The bone surfaces are also extracted from the US volume. The fiducial markers are denoted by image landmarks by an expert. The positions of landmarks are stored. On the next step CT and US surfaces are registered. Because orientation of the phantom

4.4. VALIDATION OF THE MODIFICATION OF THE ICP ALGORITHM103

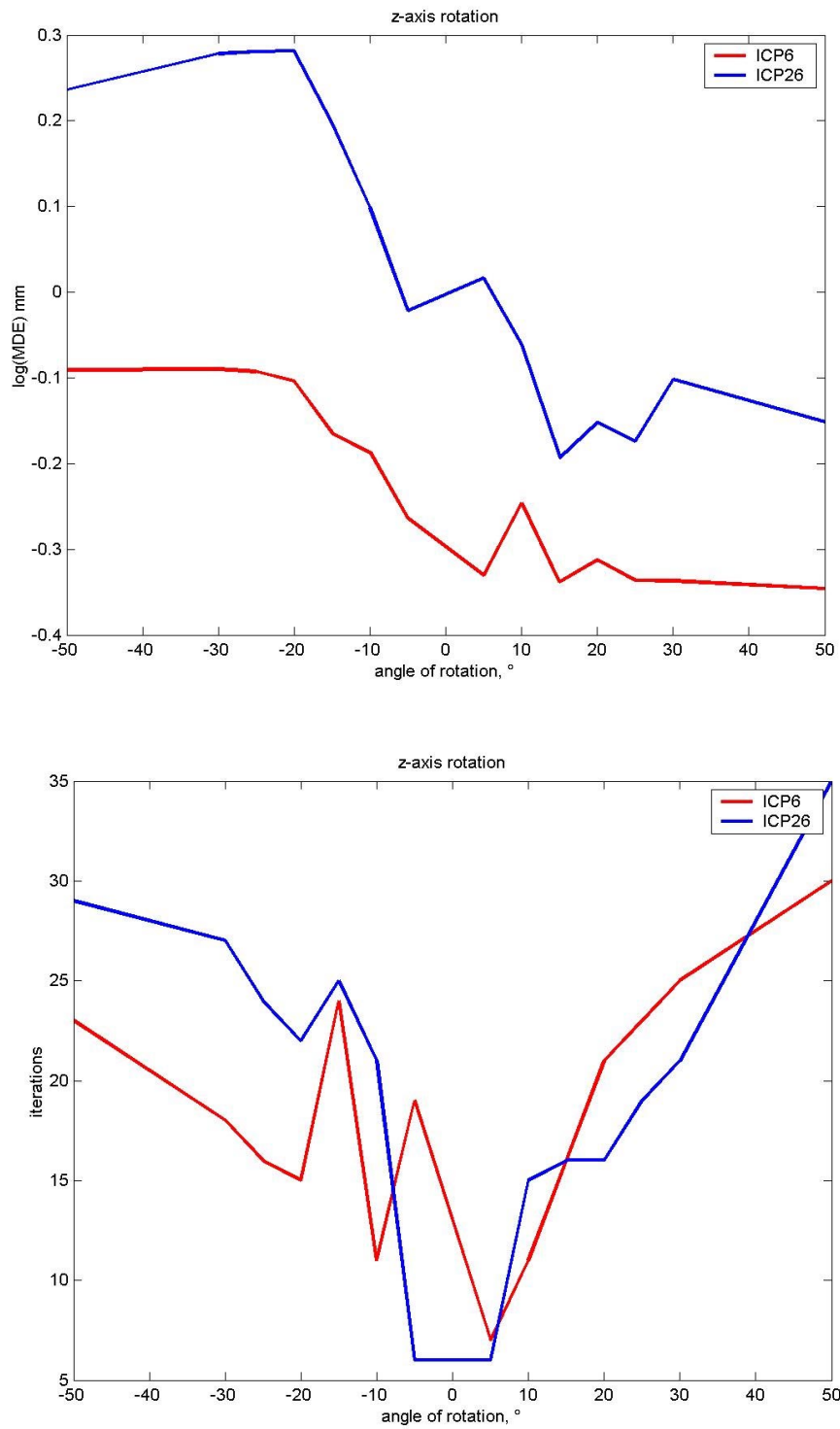


Figure 4.5: Rotation around z-axis

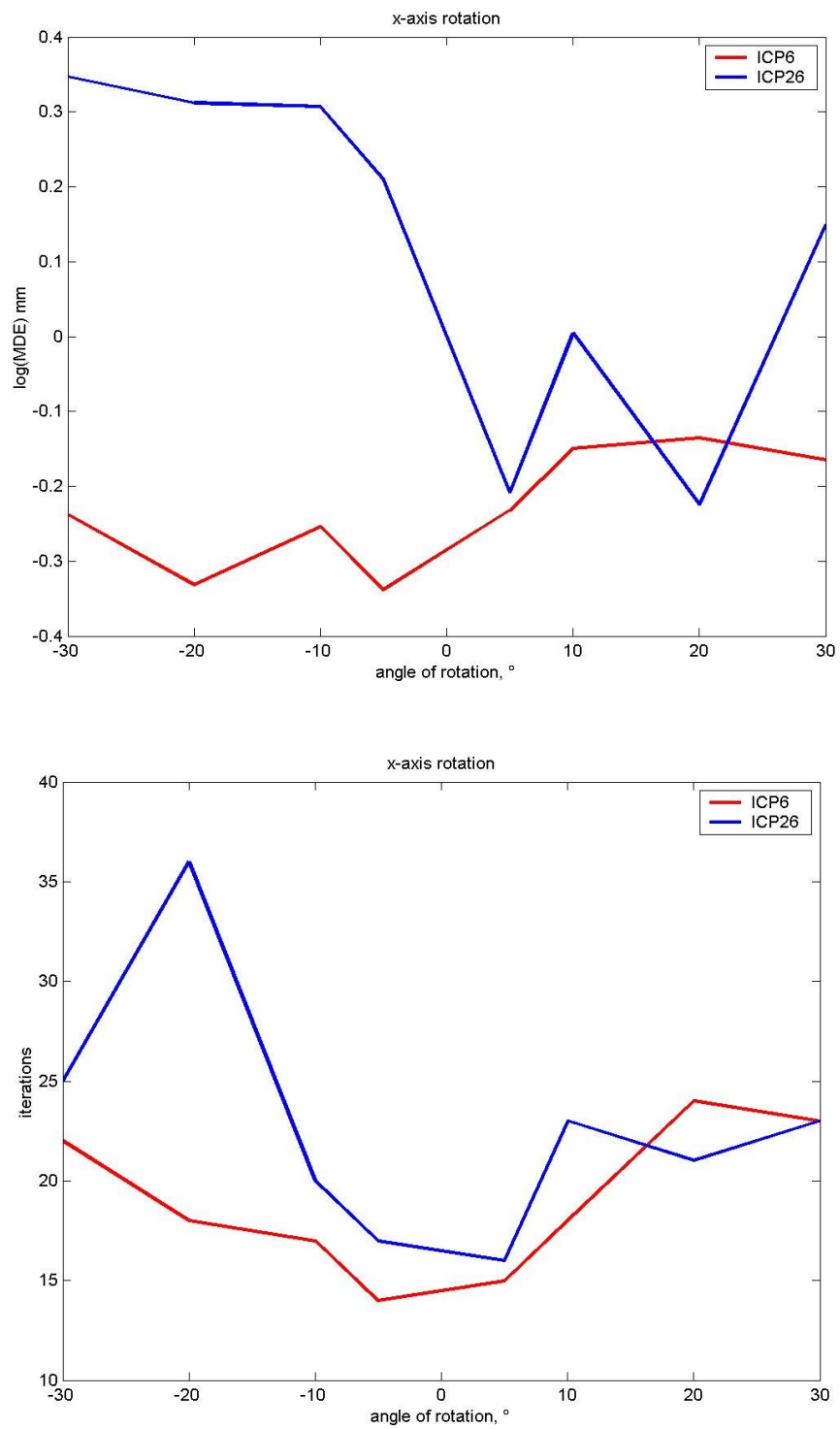


Figure 4.6: Rotation around x-axis

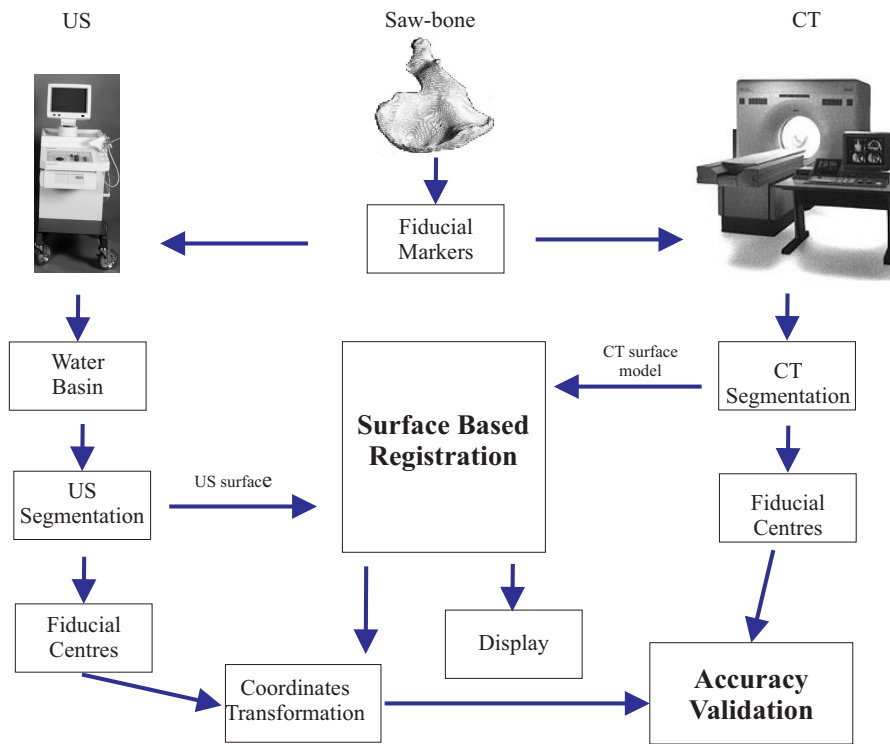


Figure 4.7: Overview of accuracy validation for a phantom registration

in the water basin is similar to its orientation on the CT table (difference in orientation is less than 30 degree), the initial transformation is not applied before the registration. The matching procedure results in a geometric transformation, that aligns both surfaces. This transformation is applied to coordinates of the US image landmarks to obtain their new positions relatively to CT coordinate space. The mean distance error is calculated between the coordinates of landmarks and the coordinates of fiducial centers extracted from CT.

The first study was carried out using the pelvis saw-bone. Metal balls of 2 mm diameter are placed on its surface. A CT scanner (Elscent CT Twin) is used to produce the image data with 1 mm of slice spacing, 0.84 mm pixel spacing. Conventional ultrasound slices (Siemens Sonoline, 5 MHz, linear transducer) are taken slice-by-slice with a slice distance chosen as 1 mm which is the same as supposed during the later operation. The pixel spacing is 0.18 mm.

After the registration, the least square distance errors were calculated between the centres of ball pairs in both modalities. The mean distance error is found to be 1.62324 mm. The MDE of surface registration is 0.583515 and the *ICP* error threshold is reached for 11 iterations (Figures 4.9, 4.10).

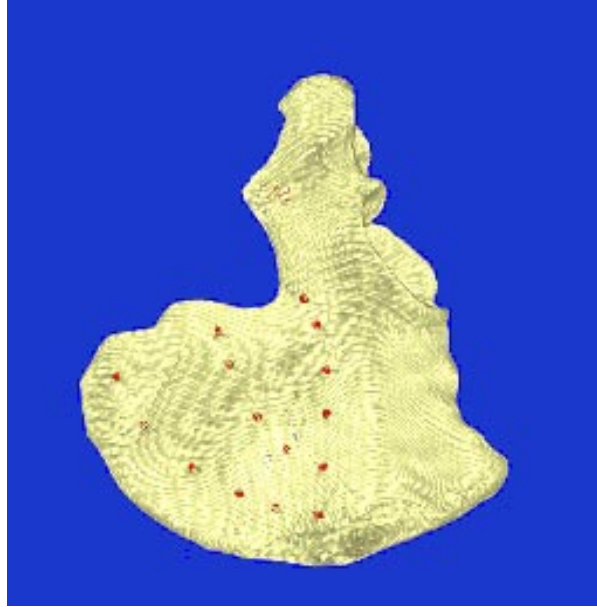
A similar procedure was carried out for the femur phantom (AO-ASIF Synbone 2071) in the second study. Nine metallic balls of 2 mm diameter are implanted on the surface of the femur. CT scans are taken (Marconi Mx8000) with an 1 mm of slice spacing, 0.39 mm pixel spacing. After the registration, the calculated mean distance error is 1.34186 mm, a standard deviation is 0.48838288 mm. The MDE of surface registration is 0.967151 and the *ICP* error threshold is reached for 12 iterations. The rotation error is found to be 0.317261 degrees. Figures 4.11 and 4.12 show an example of multimodal registration.

4.5 Summary

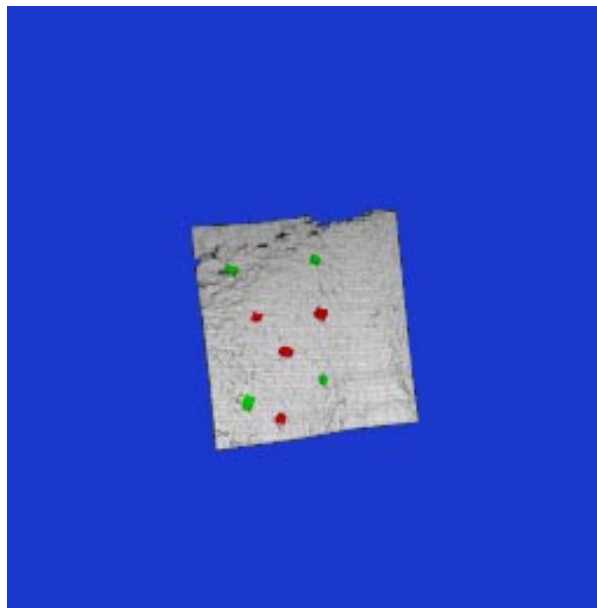
In this chapter an overview of the registration techniques was presented. The implementation of *ICP* algorithm for surface based registration was discussed. This algorithm was selected to provide more flexibility in registration for future developments. It allows to use mixed registration of volume based and surface based models. To implement the *ICP* algorithm in the real-time I proposed its modification based on the distance coding. The fast



Figure 4.8: Acquisition of US data in the water basin



a



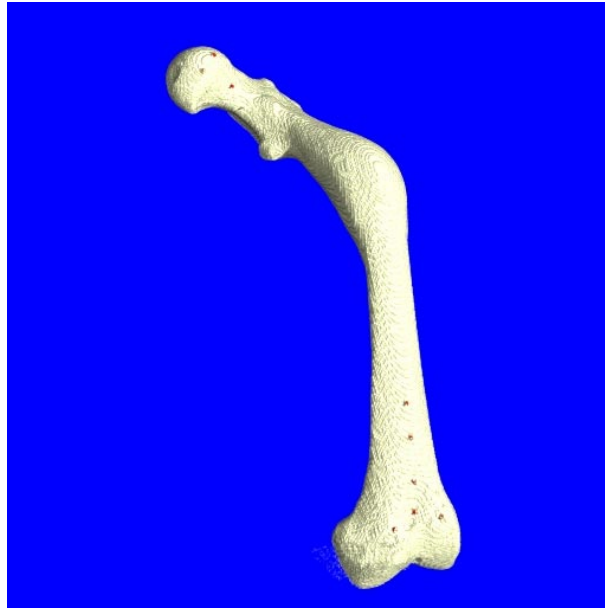
b

Figure 4.9: Pelvis a) CT surface; b) US surface (marker regions were colored)

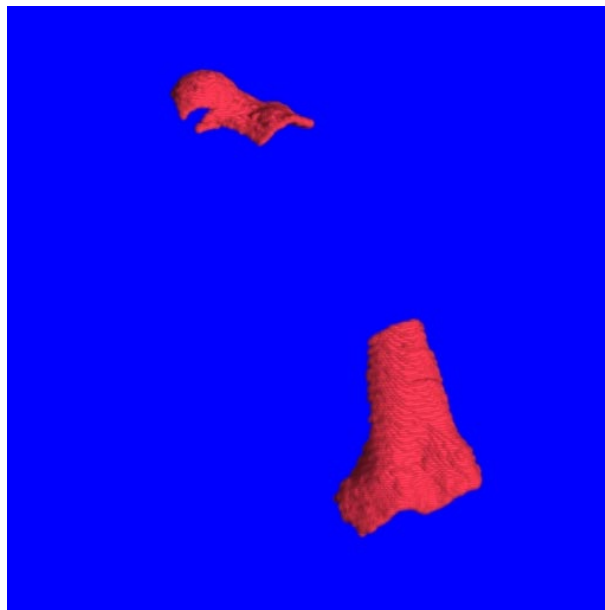


Figure 4.10: Results of pelvis US and CT surfaces registration

algorithm of the Euclidean Internal Distance Map calculation is described. Various validation studies are carried out to demonstrate the acceptability of the proposed approach. The studies show that the modification of the *ICP* algorithm is acceptable and there is a good agreement between CT and US data. The registration of the surfaces from CT and US modalities is accurate enough for its implementation in medical practice.



a



b

Figure 4.11: Femur a) CT surface; b) US surface

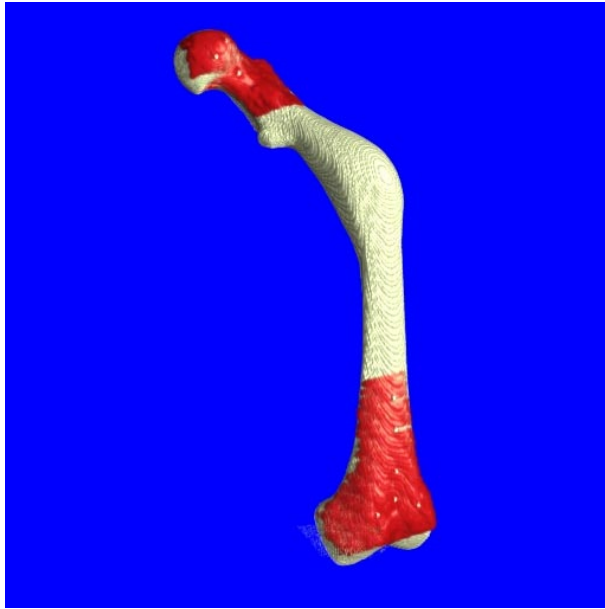


Figure 4.12: Results of femur US (red) and CT (yellow) surfaces registration

Chapter 5

System integration

5.1 Introduction

In the framework of the joint cooperation with the clinic of Ulm the described in the previous sections algorithms and principles were adapted to their implementation by surgeons of the Trauma Department (Unfallchirurgie III, Klinikum Ulm).

The cooperation was motivated by a necessity of the computer assistance in osteotomy correction of long bones and pelvis surgery. As was mentioned in Chapter 1, traditional approaches do not guarantee accuracy in general. Thus, the problems are addressed to exact computer planning of the post traumatic corrections and treatment of femoral and pelvic fractures, using the osteotomy correction. Especially for these tasks an osteotomy planning system was developed and further research was devoted to the realisation of the ultrasound based operation support system.

Mal-alignments of bones appear frequently after occasional fracture treatment. It leads to changing in the skeleton axial system. In this way, adjacent joints are applied to a non-physiological strain, which causes earlier arthrosis in these joints, pain and loss of limb functionality. Therefore, corrective osteotomies are required (Figures 5.1, 5.2). The aim of a surgical operation is to cut the operated bone (single or multiple cutting) and to correct the deformity by a set of geometric transformations (translation, rotation) of dissected parts. After the fixation of the bone parts, they should have correct axes, distances and torsion angles. The osteotomy correction is a very complex operation, especially in the case of a non-simple deformity.

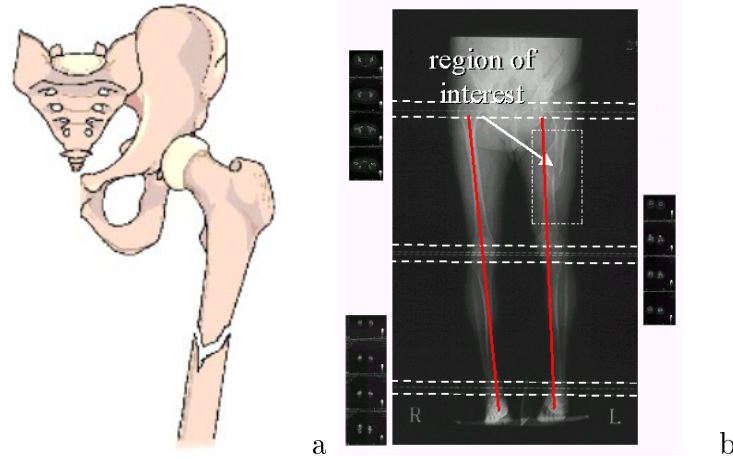


Figure 5.1: Deformity appears after an occasional fracture: a) femur fracture; b) mal-alignment of limbs

During the osteotomy correction, the problem consists of three tasks:

1. Investigation of the deformities in a quantitative order;
2. Selection of the corrective method;
3. Creation of the operation plan.

In general, the investigation of the deformity includes measurements of axial and torsional angles and distances. They are usually calculated both onto the bone with the deformity and its symmetrical bone in the skeleton. The symmetrical bone is used to define optimal geometrical parameters for the patient. In case if this information is not available, the appropriate data can be taken from an anatomical atlas.

The traditional measurements of deformities are carried out with the implementation of X-ray films. The bone contour is copied on transparent films and 2D geometric operations are used to calculate the parameters of the deformity (Figure 5.3).

Drawbacks of such an approach are that the calculation of the deformities from X-ray films inherits projections errors and can result in quite big errors in torsional and axial angles. Figure 5.4 presents the results of the measurements using 2D projections. The presented pictures the axial angle



Figure 5.2: Osteotomy correction of the left leg

was found 147° and 131° on two different projections respectively, and 27° for the torsion angle. It is evident that calculated angles strongly depend on the direction of the projection and, therefore, 3D deformity cannot be simply measured using X-ray films. Providing of such operation requires complex geometric calculations. Generally, the traditional measurements can be correct only in the case of a simple anatomy.

The usage of 3D measurements results in 139 and 35 degrees for the axial and torsion angles respectively. Thus the error in the traditional measurement consists of at least 7° . This is in contradiction with the aim of the required operation, to minimise dissimilarity in bones geometry. Thus, the given example can be considered as unsatisfactory on the step of planning, because a clinical acceptable error might not exceed 5 degrees in the axial or torsion angles.

The problem of the selection of the corrective method is that a surgeon should keep in mind the necessary geometric transformation which aligns bones in a correct position. In that way it is very difficult to find an exact one, even for an experienced surgeon. Also the realisation of the operation plan requires a quantitative description of surgeon's actions. Therefore the software for planning and supporting the operation is helpful for a surgeon.

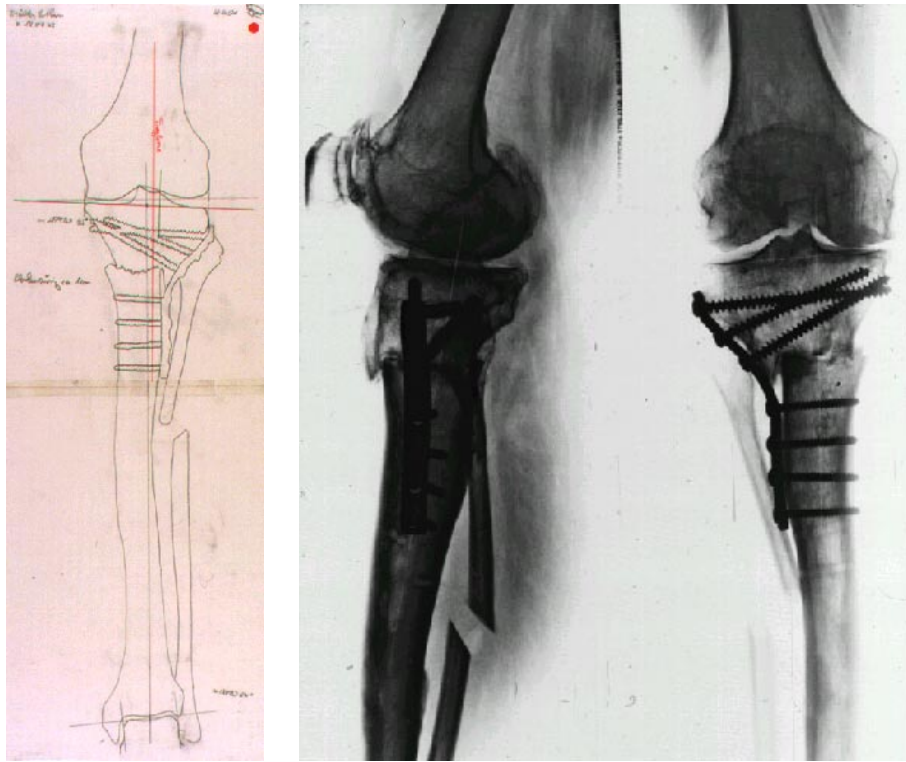


Figure 5.3: Calculation of deformity on transparent films

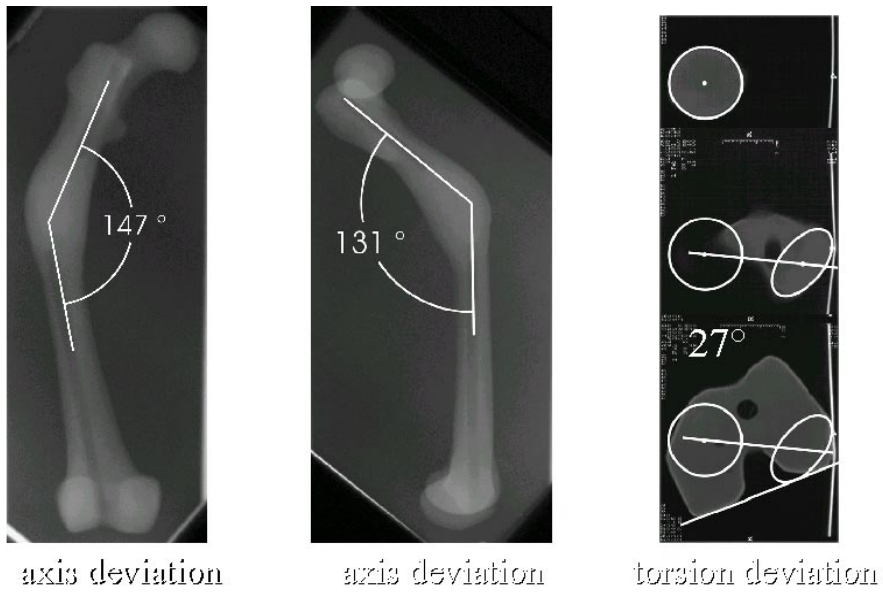


Figure 5.4: Errors of 2D planning: real 3D axial angles is 139° and 35° for torsion deformity

5.2 Operation planning system

A software prototype for planning osteotomies has been developed. The planning system has the module structure (Figure 5.5). The module of external processing is a stand-alone software which offers importing data from different graphical formats and analysing single slices or the whole volume (Figure 5.7). The volume data can be loaded from RAW format, or created by stacking up a sequence of simple 2D images (slices) in BMP, RAW or DICOM 3.0 file formats. In order to increase the visual quality of a generated model and remove possible artefacts the image processing module allows to segment the bone in an automatic mode using the approach described in chapter 2. Finally, the created and preprocessed volume data sets are stored in a file.

An operator loads the data from the disk. The module of modelling allows to produce an interactive segmentation and classification using colours. The generated model is stored into the data buffer.

The visualisation engine was created on the base of VGL, powerful and flexible library from VolumeGraphics GmbH. This library provides interactive visualisation of volume data with various rendering methods, shadowing and lightning effects, and an effective memory management. Volume data from the data buffer are rendered and visualised automatically.

The module of virtual actions allows for an operator to perform geometrical transformations (rotation, translation) of the volume data, to insert orthogonal planes, virtual instruments.

The 3D measurements via the corresponding module are available. An operator can insert anatomical landmarks (markers). Distances, angles and torsion calculated on the base of these markers are calculated and the results are displayed by the message centre module.

The necessary correction and implants can be calculated in CAD module using the information from the 3D measurements module. The message centre does not only show the related data for a surgeon, but also guide his/her actions.

The detailed description of the system work is presented below.

5.2.1 Workflow

In case of a simple correction the general processing can consist of the following steps (Figure 5.6):

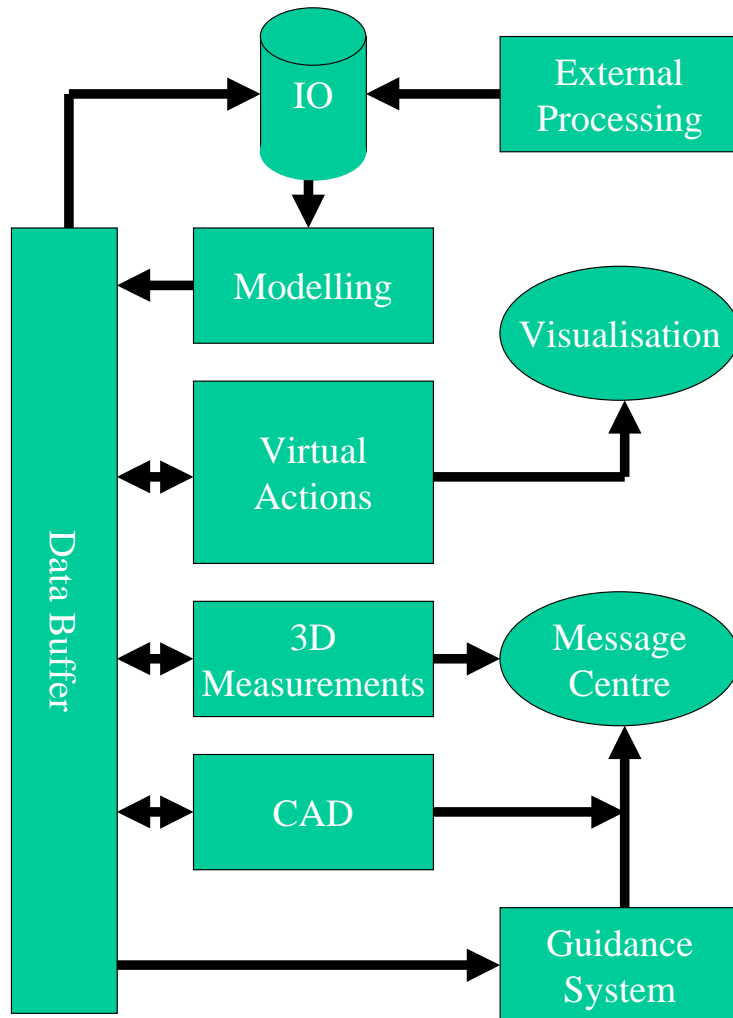


Figure 5.5: Planning system structure

1. Loading data and visualising the model;
2. Introducing measurements by using anatomical markers;
3. Plane position;
4. Setting the plane orientation;
5. Implementing the virtual cuts;
6. Virtual correction of the deformity.

For a more complex correction, the combination of these steps can be used. Several supported correction types will be described below.

5.2.2 Anatomical landmarks

After the segmentation a surgeon has to introduce anatomical landmarks. These markers specify the orientation of the bone and help to measure distances, angles and torsion. On the example of the femur, the surgeon can define four 3D markers $x_i, i = 1, \dots, 4$ exactly in centre of the hip head, condyle medial, condyle lateral and trochanter major respectively (Figure 5.8). A special interface allows to locate markers with a half-pixel accuracy using the ellipse approximation of the boundaries. Zooming functions incorporated into the user interface allow to increase accuracy in placing the markers.

First three markers define standard views on the bone and a reference plane. The program consists of an user interface for the instruments simulation. The position of the instrument is defined by the position of the given marker and its direction is specified by rotations of the instrument in three perpendicular projection planes. Two instruments with a non-zero common angle define the cutting plane if their markers have the same position in 3D space. The instrument parameters such as length, diameter and colour can be changed in a special panel of the user interface.

5.2.3 Measurements

The program automatically calculates the distances $d_{i,j}(x_i, x_j)$ and angles between the segments $[x_i, x_j]$ and $[x_j, x_k]$, where $i, j, k = 1, \dots, 4, i \neq j, i \neq k, j \neq k$. A torsion angle is calculated between planes $P(x_1, x_2, x_3)$ and

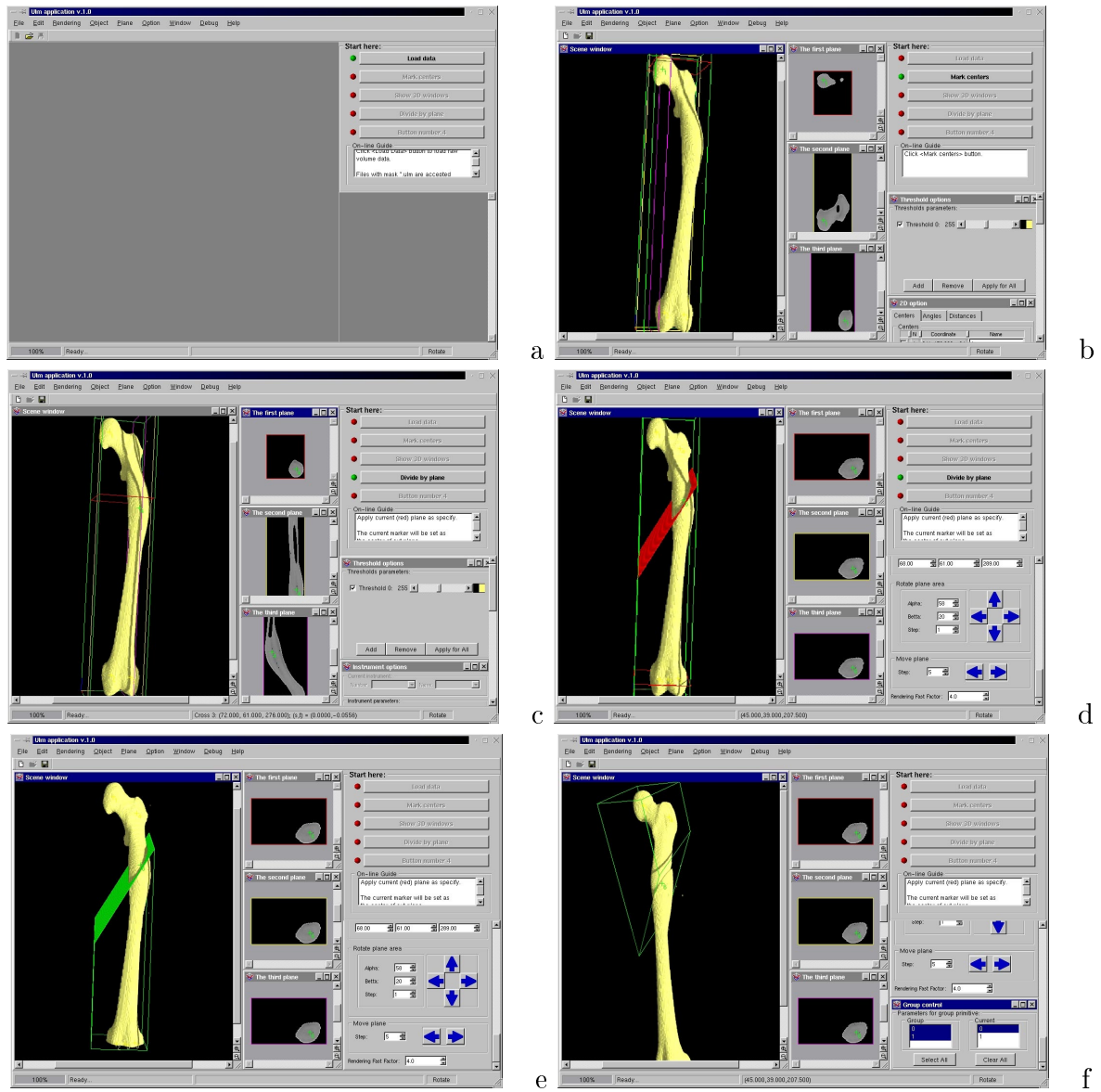


Figure 5.6: General steps of the workflow: a) loading data; b) introducing markers; c) setting position of the cutting plane; d) setting orientation of the cutting plane; e) implementing the virtual cut; f) correcting the deformity

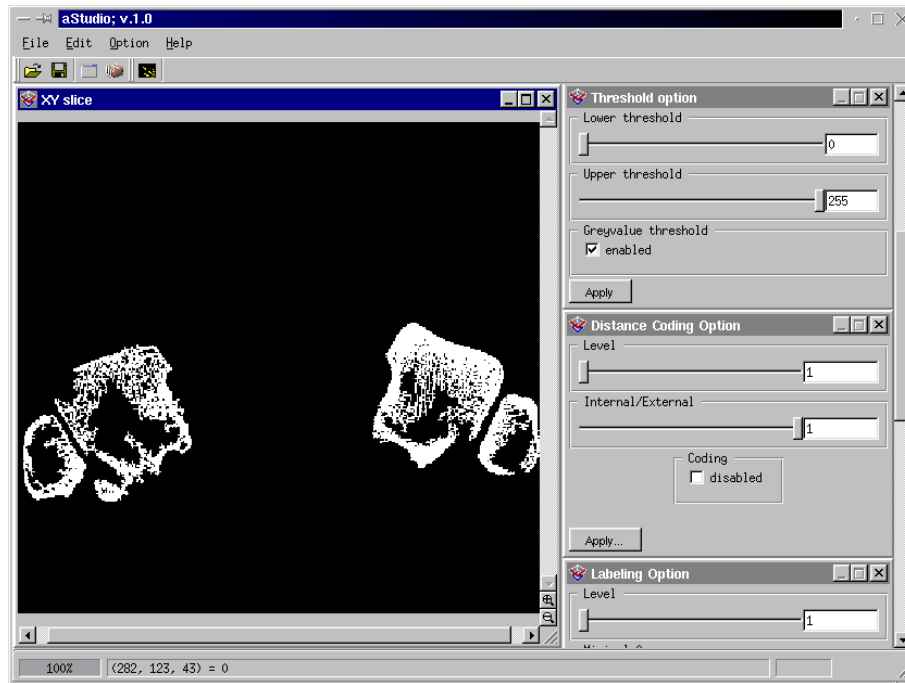


Figure 5.7: Segmentation part of the software prototype



Figure 5.8: Definition of anatomical landmarks in the centers of the hip head (x_1), condyle medial (x_2), condyle lateral (x_3) and trochanter major (x_4)

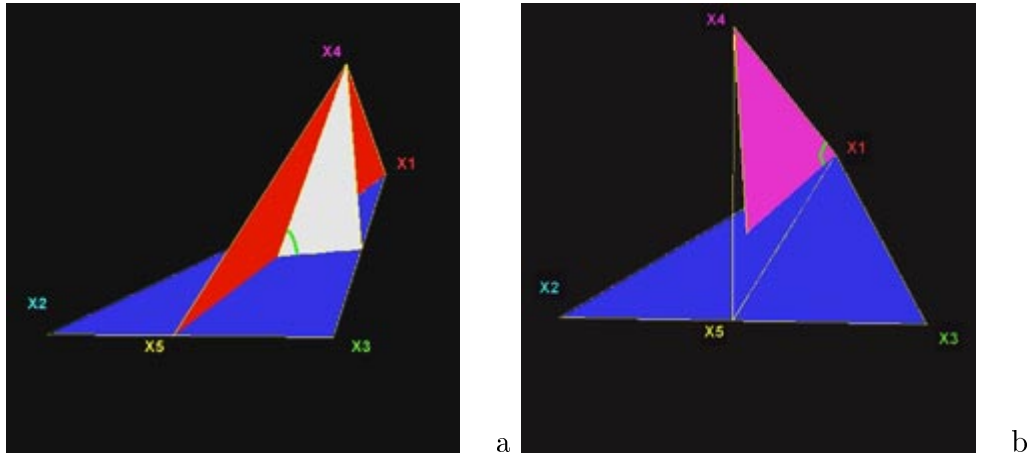


Figure 5.9: Definition of torsion angles relative the reference plane (blue): a) torsion angle, b) projection torsion angle.

$P(x_1, x_4, x_5)$, where x_5 is a middle point of the segment $[x_2, x_3]$, a projection torsion angle is $angle(proj_{P(x_1, x_2, x_3)}([x_1, x_4], [x_1, x_4]))$ (Figure 5.9). Because the markers are placed with the half-pixel accuracy, the distance between two point in the 2D plane can have the maximal error of 1.4 pixels, if the plane is perpendicular to the one of the scanner axes. The real error depends on the resolution of the image data. For example, if the scanner resolution is $0.34 \times 0.34 \times 0.85$ mm, then the error is less than or equal to 1.2816 mm. In practice, the error value of a few millimeters is acceptable. There are two ways to increase the accuracy if necessary: to increase the spatial resolution of the CT scanner and implement sub-voxel processing, when loading the image data.

5.2.4 Virtual osteotomy

The surgeon can perform the virtual cuts into the data volume. The position and orientation of the cut is defined by the cutting plane (red one) into the scene. This plane is inserted by the surgeon, assigning the centre of the plane by a marker (and centre of rotation latter) and its normal orientation. The cutting plane after any change in position of the marker or orientation of the normal is updated automatically. In practice, the cutting plane is defined

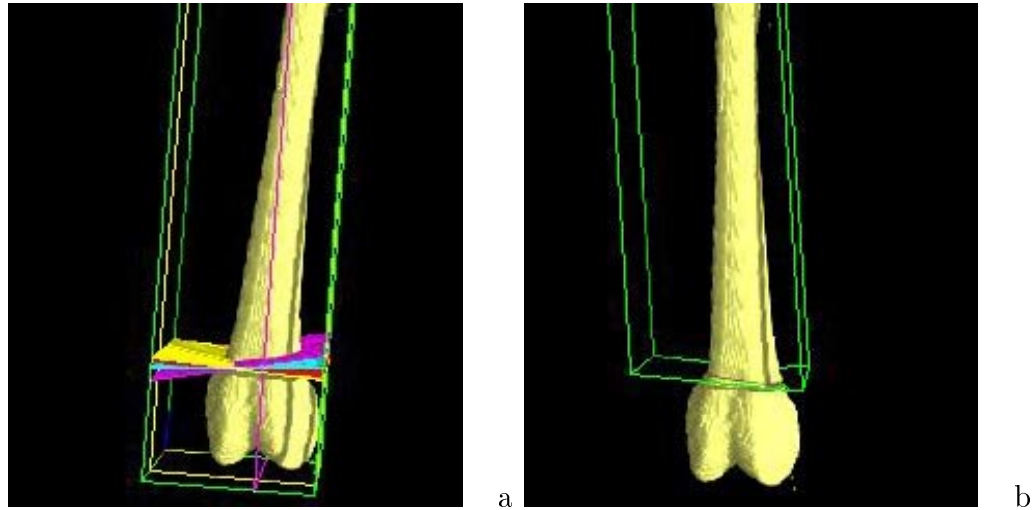


Figure 5.10: Close wedge correction: a) planning; b) results

by a special surgical template. First a pin is drilled and screwed into the bone. Then, the template is stacked up the pin and the second pin fixes the template orientation. The surgeon can drill the bone by using template holes and in that way the cutting plane is defined. Therefore, to simulate this process during the virtual operation, two instruments with a non-zero common angle can also define the cutting plane if their markers have the same position in 3D space.

5.2.5 Supported types of osteotomies

The current version of the planning software prototype supports the wedge osteotomies, which are most frequently used in practice [15]. Only the close and open wedges can be implemented during the virtual planning. During the close wedge correction, two cuts are produced. Then the external bone parts are aligned and fixed by metal plates using screws (Figure 5.14). In case of the open wedge correction only a single cut is implemented (Figure 5.11 a)) and a piece of bone is inserted between the dissected parts of the bone (Figure 5.11 b)).

Thus, a length of the bone, 3D axial and torsion angle can be corrected. However, frequently wedge based osteotomy causes other deformities. For ex-

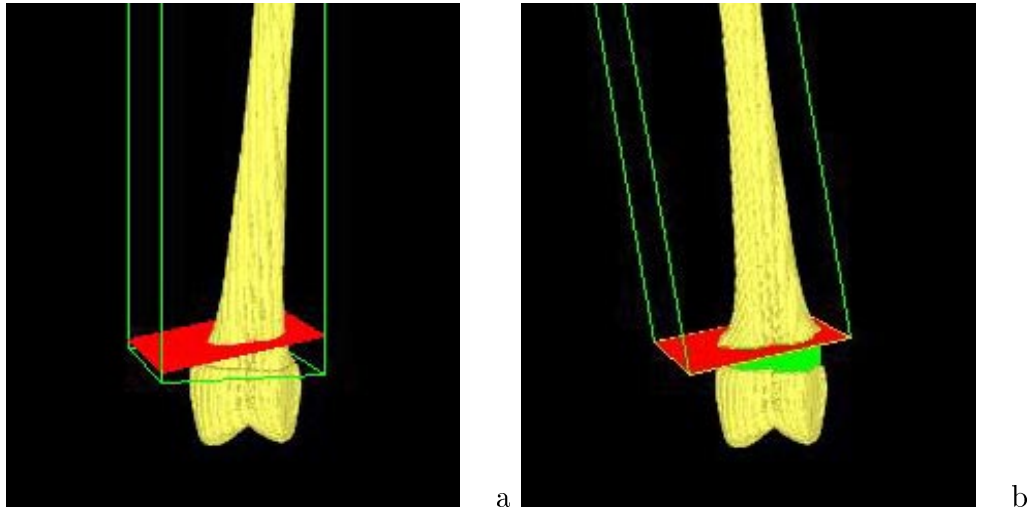


Figure 5.11: Open wedge correction: a) planning; b) results

ample a varus intertrochanteric femoral osteotomy results in the weightbearing hip-ankle joint axis to remove medially from its normal position through the centre of the knee and so produce overloading of the medial compartment of the knee joint. While a valgus intertrochanteric femoral osteotomy causes overloading of the lateral compartment of the knee. For example a valgus intertrochanteric osteotomy may have a beneficial effect on medial gonarthrosis. Therefore, to maintain a normal hip-ankle axis a secondary osteotomy is required, e.g. varus osteotomy is followed by valgus osteotomy [15].

Another supported osteotomy type is the oblique osteotomy (single cut). This kind of correction was proposed by an orthopaedician R. Merle d'Aubigne from France in 1952. He showed that 3D deformity can be corrected by single cutting and rotating dissected bone parts. However, the planning of the oblique osteotomy is difficult and becomes efficient only with the implementation of computers.

Calculation of wedge osteotomy

To realise the wedge based correction, the following procedure is used. Both close wedge and open wedge can be described by

1. Position and orientation of the cutting plane,

2. Position of top wedge point (so called a null-point),
3. Angle between facets.

The position of the cutting plane is defined by the surgeon in three orthogonal planes. Its orientation and facet angle are also given by the surgeon. Then he or she inserts a null-point in apical-view plane and the appropriate (close/open) wedge is removed or inserted. However, after the alignment of the bones in case of the close wedge, the stair effect appears when one facet is longer than another. To minimise this effect an optimisation of the position and orientation of the cutting plane is used. The optimisation function minimise the difference in facet lengths (their middle line) under the condition of the fixed null-point. Figure 5.10 a) shows a new position of the cutting plane (blue one). The planning software allows manually to apply wedges and see the results of the correction. The close and open wedges are usually implemented for the one-dimensional deformities because of the difficulties of their calculation in case of more complex deformities.

Calculation of oblique osteotomy

The calculation of the oblique osteotomy can be carried out automatically in the current version of the planning system. The surgeon have to define five markers to describe geometry of the deformity (Figure 5.12).

The vector (C,B) denotes the axis of the bone. The correction is successful iff:

1. after rotation of the dissected bone part, the direction of vector (B,A) will coincide with the direction of the vector (C,B), i.e. $normalize(D, B) = normalize(B, C)$ (condition of straight bone),
2. angle α between projections of vectors (C,E) and (A,D) on the perpendicular to the vector (C,B) plane, does not exceed the given one (β). The α is an angle in the range between 0 and π .

The orientation of the cutting plane that results in the successful correction can be found using one-dimensional optimisation problem. It is easy to see that the condition of a straight bone is carried out by the rotation of the vector (B,A) around a conic axis (both (B,A) and (B,D) belongs to the conic surface). The radius of the conic influences the second condition. Then the goal is to find the conic radius, such that the difference between angles α and β will be minimal.

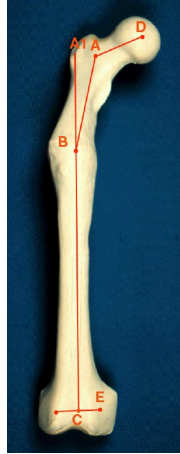


Figure 5.12: Definition of anatomical landmarks to describe the deformity for automatic calculation of the oblique osteotomy.

5.2.6 Rearrangement of bone segments

After cutting the dissected bone parts can be moved into the scene. The restriction is that the motion is confined to be along the cutting plane. The rotation is limited to the rotations around axis that are parallel to the cutting plane normal. As was mentioned above, a marker defines the position of the rotation axis on the plane. In order to be able to measure the success of a rearrangement, markers are grouped with the bone and during the manipulation of the bone the distances, angles, torsion and projection torsion angles are automatically updated for the selected markers. This allows the surgeon to directly observe the improvements of the bone position and approach the optimal arrangement of it. There is a possibility to calculate angles between vectors parallel to orientation vectors of marked instruments.

An additional correction of the bone position can be carried out using the open wedge transformation. The angle between equal wedge facets and its top are specified by the surgeon. The results of the correction operations can be stored in a file and loaded on demand. Also an undo mechanism is applied when it is necessary to return to the step of cut plane definition. To simplify the work with the program its interface should consist of a workflow panel. All main actions are divided into groups as a sequence of steps and every step is represented by a button. Only one button is active at the moment

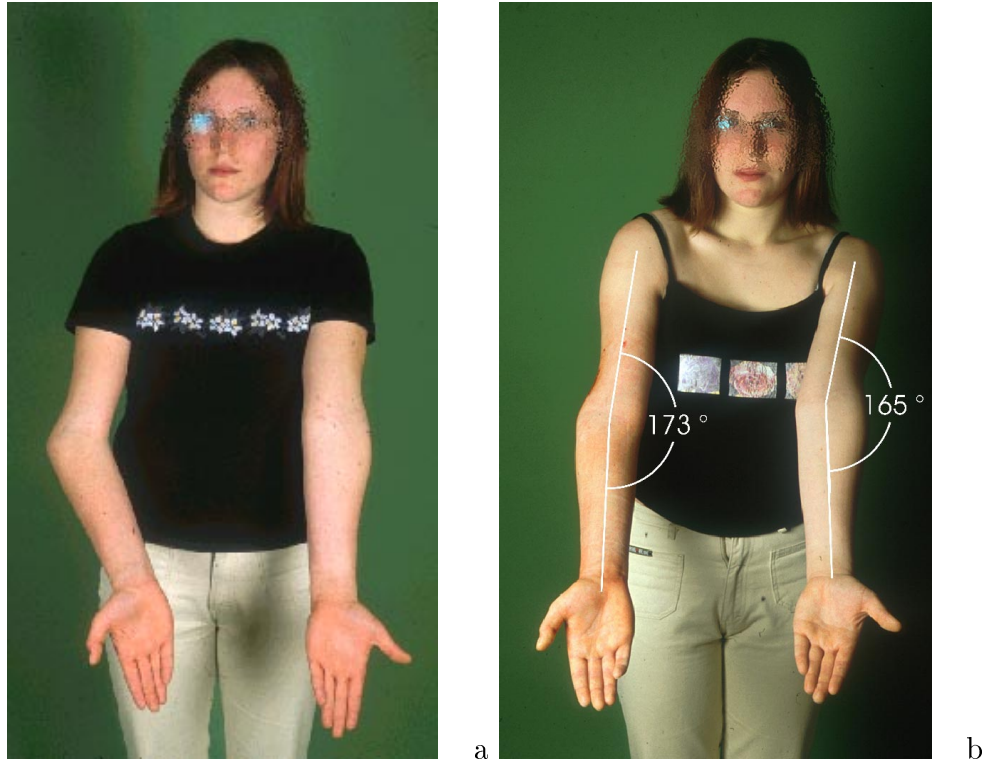


Figure 5.13: Elbow deformity of 14 yr. female, right hand: a) before the operation; b) after the correction

and after its pressing the next button is activated. User actions are guided on each step by using on-line help from the same panel.

5.2.7 Clinical applications

The planning software is implemented for corrections of long bones and hip head rotation. A 14 years old girl had an elbow deformity after fracture at the age of 7 years old (Figure 5.13 a). After a traditional close wedge correction planning on transparent films, the deformity still exists (Figure 5.13 b). The operation results are presented in Figure 5.14. The 3D operation planning shows correct results of the operation by using close wedge or oblique osteotomy corrections (Figure 5.15).

In the next clinical case the hip head rotation was required. The patient



Figure 5.14: Results of the elbow correction: a) frontal view; b) lateral view

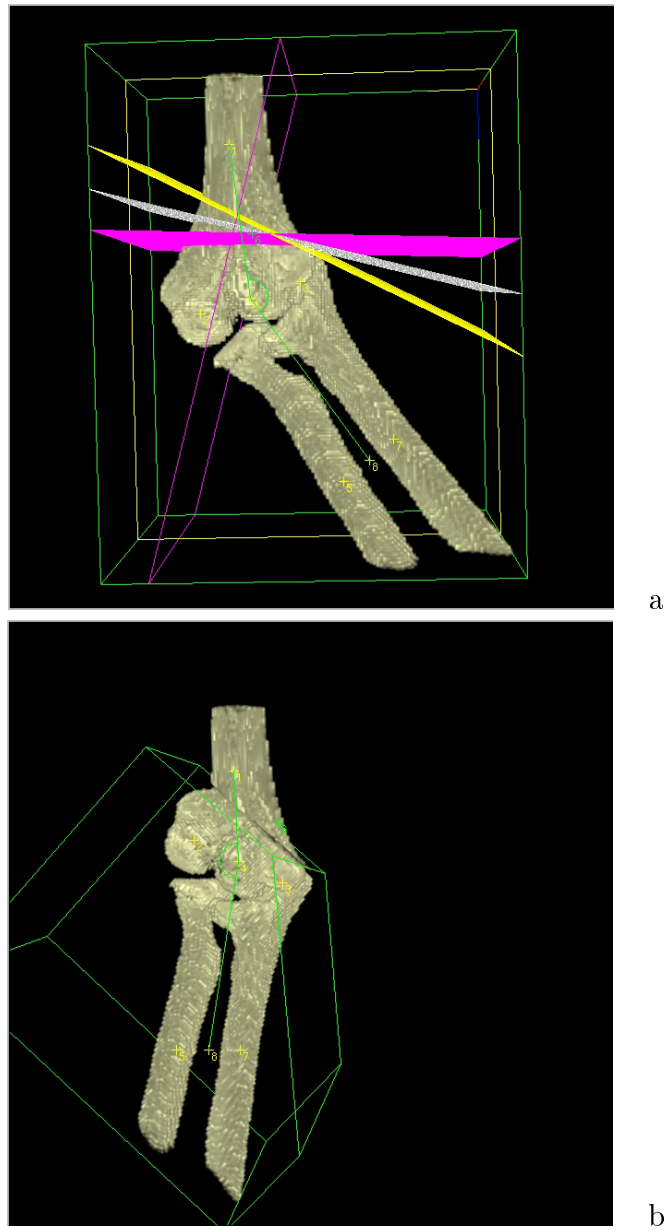


Figure 5.15: Results of planning of the elbow correction: a) frontal view; b) lateral view

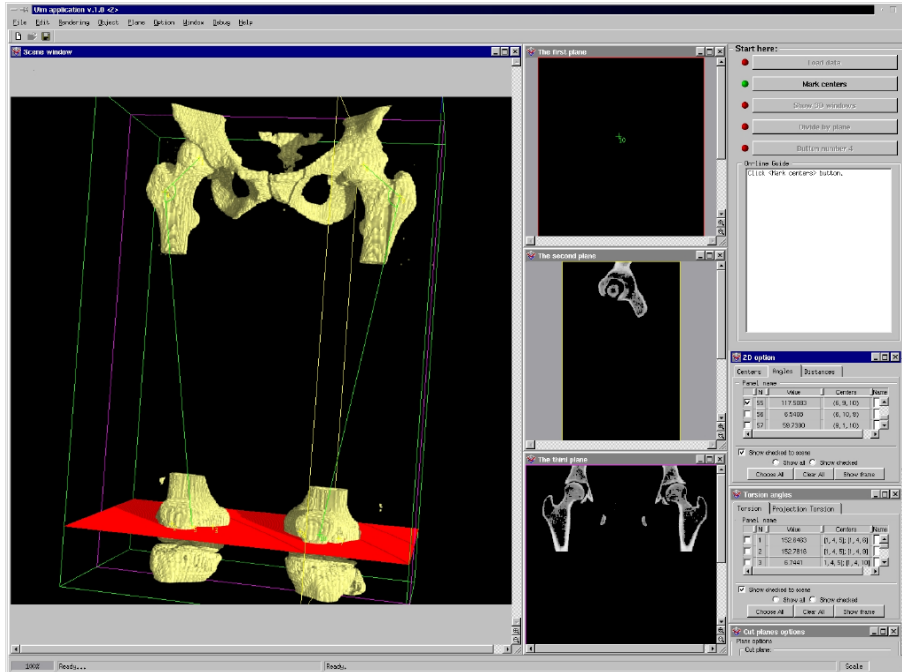


Figure 5.16: Definition of anatomical landmarks to describe the deformity for automatic calculation of the oblique osteotomy.

has a partial cystic deformation of the hip cup and it is necessary to make oblique osteotomy to rotate hip head so that after the operation strain could be applied to surfaces without deformation. Figure 5.18 shows planning and result of oblique osteotomy correction.

5.2.8 Comparison with other systems

There exist many osteotomy planning systems. Mostly they are used for planning using 2D projections. Therefore, I shall compare the developed osteotomy planning system only with some systems, that provide some kind of the computer analysis of the bone geometry.

FRACAS is a computer-integrated system for closed long bone fracture reduction [45], [46]. This system uses similar to my principles to create the bone reference basis. Condyle landmarks and femoral neck axis using local principal axes determination are extracted. Periaxial rotation, i.e. the angle

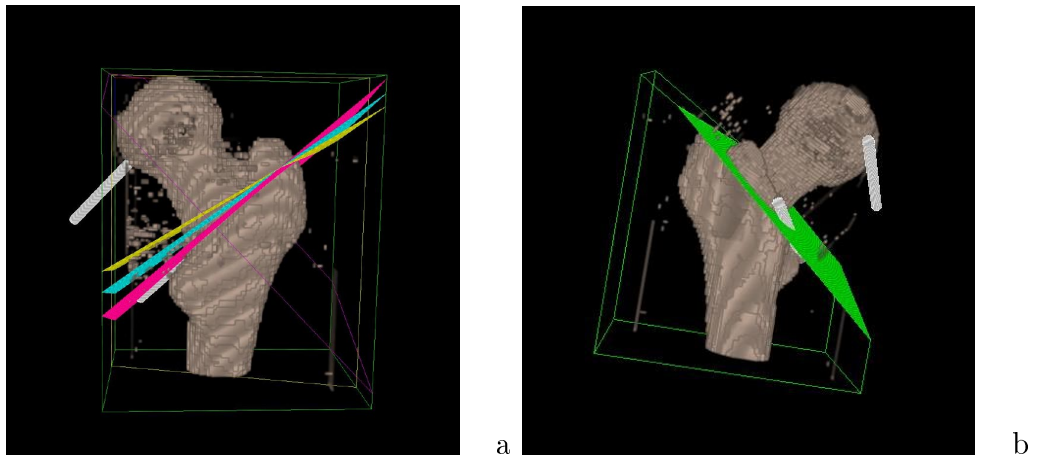


Figure 5.17: Close wedge osteotomy correction: a 10° wedge planning, b) hip head rotation after close wedge correction

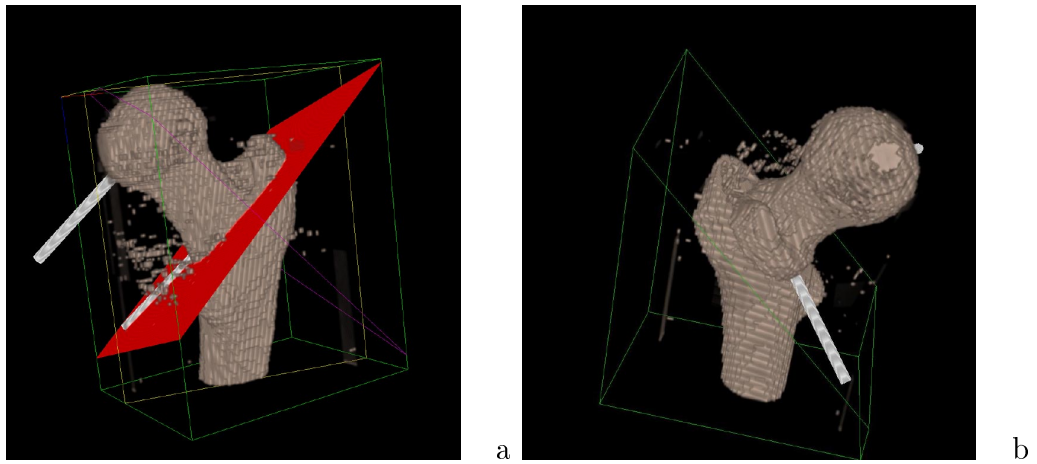


Figure 5.18: Oblique osteotomy correction: a 10° wedge planning, b) hip head rotation after close wedge correction

between the axis of femoral neck and the reference plane, is calculated. The reference plane passes through the extreme dorsal points of the condyles and is parallel to the main axis of femur. Like in the developed by me system, this approach allows to introduce the local coordinate system, which is position scan independent. User interaction to orient of the principle axes according to a preferred orientation is used. After that, the long axis of femur is parallel to the table top. Condyle landmarks are detected as the lowest points with respect to the table top normal. The femoral neck axis is the principal axis of the region of the femur head and neck.

The femur bones is modelled preoperatively and the mesh model is generated. FRACAS system does not require also additional image data. The feature extraction is fully automatic. The correctness of the system was demonstrated using in-vitro tests only [46].

My planning system has a number of advantages. First, the volume based model generation provides more information for a surgeon than the mesh based one. Both the preoperative and the intraoperative segmentation is available. I consider that the manual landmark identification using the developed special interface is preferred than the automatic one. The manual placement provides a flexibility and allows for surgeon to adapt the planning procedure to the existing pathology. The identification is not time consuming for an experienced user. The decision not to use the principal axes determination was accepted by me taking into account the need to the classification of bones not only as dense objects, but also as parts of the skeleton. It is easy to calculate the principal axes during in-vitro tests, when the only one bone model is scanned. In-vivo tests require the bone separation and the moments calculation for a selected part. Presence of artefacts and segmentation errors make such approach very difficult for real medical practice.

Another planning system so called Medi-Cad was developed [47]. This system performs corrective osteotomies to prevent early joint degeneration. First the radiograph is digitised. Then measuring the mechanical axis, angles and distances in metric units are carried out by using CAD module. A special preview function allows to adjust the level of osteotomy as well as to change the amount of correction angle and hinge position. All results and corrective simulations can be saved with data base.

Advantages of Medi-Cad system in comparison with the traditional hand-drawing planning are the implementation of direct image processing features and the high level of automation. The biggest advantage of my system is in the implementation of real 3D measurements, what provides the high

accuracy of planning. An example of the comparison of 3D planning versus 2D planning was given in the beginning of this chapter.

5.3 Operation support system

The first step in the development of the operation support system was devoted to the segmentation of sow-bone surfaces (plastic bone phantom) from US data set and their registration with surfaces of the same bone taken from CT data set. This technology was new and a pessimistic opinion about an automatic segmentation of ultrasound images didn't add inspiration for the researchers. The first report about a successful segmentation and registration of pelvis sow-bone and cadaveric spine in water basin was presented at the 5th CAOS symposium in Davos, Switzerland in February of 2000 [48]. A good visualisation was reached even for the spine, which presents the most complex case because of a high curvature of surfaces (Figure 5.19). This presentation was the only work about the implementation of B-mode ultrasound for navigation and tracking bones at the symposium. There was another work devoted to the implementation of ultrasound for detection of bone borders, but it proposed to use A-mode (one dimensional) signals [49]. One year later at the same CAOS symposium in Davos three works were presented, where B-mode was implemented as a component of the multimodal registration system [55] [56] [57]. It shows an increasing interest in ultrasound for its implementation in computer assisted orthopaedic applications.

Numerous studies were carried out to investigate the segmentation of bone surfaces from US in water basin. The water basin was implemented, because at this moment no OTD is available for the author to detect the position and orientation of an ultrasound probe during images acquisition. Therefore, the algorithms were tested in vitro studies. The system will be completed and applied in the clinic Ulm, when OTD becomes available.

5.4 Future steps

The described software system is required to be extended in the near future to use a computer assistant in various cases (as many as possible). First, the number of supported wedge types will be increased by including a dome wedge correction. Second, the ultrasound is a very attractive tool for the

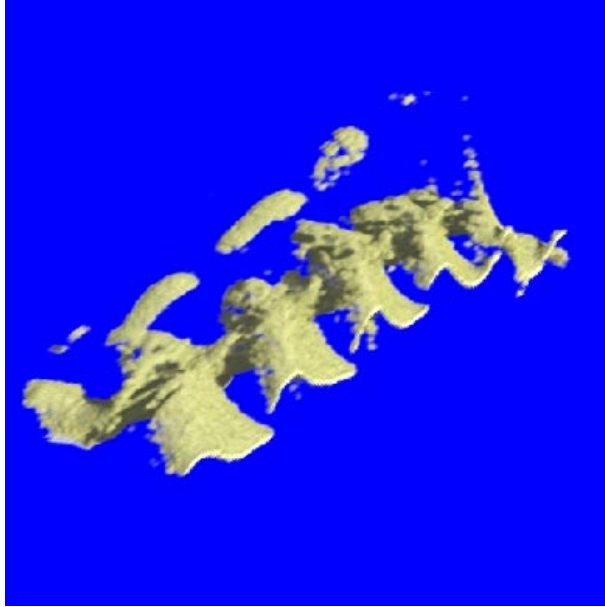


Figure 5.19: Surface reconstruction of the cadaveric spine from US images

generation of bone surfaces. In case of simple anatomy, it will allow to avoid implementation of any X-ray equipment, what makes the operation planning riskless and reduces the expenses (the clinical examination using CT costs approximately in two orders of magnitude than US one in Germany).

5.5 Summary

The prototype of the operation planning system was developed. The planning software has been implemented in clinic Ulm (Unfallchirurgie III) to measure deformities and plan osteotomy corrections. The planning system optimises the work of a surgeon making the planning process more precise and reducing the total time of planning. Thus, an experienced user needs only 10-30 minutes in comparison with more than 3 hours for the traditional 2D planning on transparent films. The presented planning software allows to plane not only traditional open/close wedge corrections but also the oblique osteotomy (single cut) correction. Implementation of the oblique osteotomy results in shorter rehabilitation time for the patient and reduces the total cost of the

operation.

The main advance of the navigation system is that it realises highly accurate and minimal invasive pelvis surgery. Navigation is necessary for placements of screws. The pelvis surgery is very sensitive to accurate screw placement, because frequently the thickness of the screw is comparable with the thickness of the pelvis bone. A similar problem exists and in spine surgery. The complex anatomy of pelvis makes the implementation of fluoroscopy based navigation systems not useful. Thus, with the implementation of the optical tracking system, the ultrasound based navigation system will allow treatment of pelvis fractures with a high accuracy of screw placement and minimal invasive surgery.

Chapter 6

Conclusion

In this thesis the theoretical and practical results were demonstrated. A concept of the operation planning and surgery support system for orthopaedics is proposed. The system implements different image modalities such as CT and US to provide necessary information for a surgeon. All software components can be used on conventional personal computers, what provides a low cost solution for realising the CAOS station.

The planning part of the software for osteotomy corrections was tested in the clinic of Ulm the Trauma Department (Unfallchirurgie III, Klinikum Ulm). It provides a flexible 3D measurement system to calculate on-line the distances, axial and torsion angles. The planning system can be used for measuring the bone deformities and performing the virtual surgery. Currently, three types of osteotomy are supported: the close wedge, the open wedge and the oblique osteotomy. They can be calculated in the semi-automatic or the automatic modes. A special user graphical interface guides a surgeon and optimises the surgical routine. Thus, the planning procedure is carried out by an experienced user for 30 minutes instead of three hours using traditional planning. The high accuracy is guaranteed by the implementation of 3D. The planning system was appreciated by an expert from the clinic of Ulm as useful and accurate.

An effective and high accurate planning is possible with the implementation of fine bone modelling technique from CT data. Therefore, the concept using automatic and interactive segmentation of bones was proposed. The automatic segmentation provides high quality modelling, but is performed off-line. While, the interactive segmentation does not guarantee a high quality, but allows taking into account the pathology of the patient.

To extract bone surfaces from US images, the rainfall algorithm was developed. It allows to segment and to classify segments of the bone surfaces automatically. The implementation of fast image processing allows to extract the bones in near real-time. The maximal depth of extracted bones under skin can be about 7.5 mm using the linear transducer of 5 MHz from Siemens Sonoline.

To register CT and US data sets the *ICP* algorithm was proposed. It is a fast and accurate registration method, which provides a flexibility of registration. Both volume based and surface based data set can be matched by the *ICP* algorithm. An acceleration using the distance coding is proposed. The modification allows to register data sets in real-time. Validation studies show MDE error less than 2 mm, what is acceptable for clinical use.

Thus, the algorithms for a realisation of the surgery support system were developed and tested. They will be incorporated in the complete system during further developments, when a tracking system will be available for the author. The software will be installed and tested in the clinic of Ulm.

Chapter 7

Appendix: Background of the image processing

7.1 Basic mathematical tools for the image processing

Image processing plays a very important role in CAOS. The development of equipment and image processing techniques has made CAOS available for clinical use. The filtration and segmentation algorithms used in current work are based on mathematical morphology. Mathematical morphology is a part of image processing and a very powerful tool for image analysis. Image operations and analysis are based on using structuring elements of different sizes and forms. The native parallel structure of operators gives the possibility to build high performance image processing systems.

Mathematical morphology operates both binary and gray-level images. Binary images are defined by subsets of n dimensional space E^n , where E^n is an Euclidean space R^n or a set of integer values Z^n in discrete case, i.e. $E = R$ or $E = Z$ and

$$E^n = \{a : a = (a_1, a_2, \dots, a_n), a_i \in E, i = 1, \dots, n\}.$$

Gray-level image is defined by a function $f : D \rightarrow V$, where $D \subseteq E^n$ and $V \subseteq E$.

Let vector (x_1, x_2, \dots, x_n) represent spatial coordinates of a pixel and $G = 1, \dots, L$ be a set of positive integer numbers, which denote the intensity of

pixels or gray values. The intensity of pixel with coordinates (x_1, x_2, \dots, x_n) can be represented by the function $f(x_1, x_2, \dots, x_n)$.

A set of neighbour pixels of pixel p in a given neighbour grid is denoted as $N(x)$. A *path* of length n between pixels p_1 and p_n is a sequence of pixels p_1, p_2, \dots, p_n , such that $p_i \in N(p_{i+1})$, for $i = 1, 2, \dots, n$.

7.2 Binary operations

Let X and B be sets from E^n . Dilation of set X by set B is called the set $X \oplus B$, defined as:

$$X \oplus B = \{y \in E^n : y = x + b, x \in X, b \in B\}.$$

Here the addition of vector x and b is treated as addition of their components, i.e. $x + b = (x_1 + b_1, x_2 + b_2, \dots, x_n + b_n)$. The set X represents the initial image and the set B is called the structuring element. In practice, the set B has usually a small size and a simple form. The operation of dilation is commutative and associative operator, i.e. $X \oplus B = B \oplus X$ and $(X \oplus B) \oplus C = X \oplus (B \oplus C)$. These features are inherited from the addition operation.

Let X and B be sets from E^n . Erosion of set X by set B is called the set $X \ominus B$, defined as:

$$X \ominus B = \{y \in E^n : y + b \in X, \forall b \in B\}.$$

The distributivity the erosion operation is expressed by formulae $(X \ominus B) \oplus C = X \ominus (B \oplus C)$. Another pair of basic morphological operators are opening and closing.

Opening and closing of X by structured element B are called sets $X \circ B$ and $X \bullet B$ respectively.

$$X \circ B = (X \ominus B) \oplus B,$$

$$X \bullet B = (X \oplus B) \ominus B.$$

The shift of the set X on item $b \in E^n$ is called set A_b , such as

$$X_b = \{x + b : x \in X\}.$$

Let B denote a central symmetrical set to B , relatively the origin, i.e.

$$\check{B} = \{-b : b \in B\}.$$

The most significant features of the basic morphological operators [1] are:

1.

$$X \oplus B = \{x : \check{B}_x \cap X \neq \emptyset\},$$

$$X \oplus B = \cup_{b \in B} X,$$

$$X \ominus B = \cap_{b \in B} X.$$

It means that dilation and erosion of the set X by the structuring element B shift union and intersection of the set X on element b from B and element $-b$ from B , respectively.

2.

$$X_x \oplus B = (X \oplus B)_x,$$

$$X_x \oplus B_{-x} = X \oplus B,$$

$$X_x \ominus B = (X \ominus B)_x,$$

$$X \ominus B_x = (X \ominus B)_{-x}.$$

This means that dilation is invariant to this shifts of the image and structuring element, and the erosion is invariant to the image shifts.

3. If $0 \in B$, then $X \subseteq X \oplus B$ and $X \ominus B \subseteq X$.

4. Dilation and erosion are increasing operators. The following relationships are true: if $X \subseteq B$ then $X \oplus D \subseteq B \oplus D$ for any D , if $X \subseteq B$ then $X \ominus D \subseteq B \ominus D$, and if $B \subseteq D$ then $X \oplus D \subseteq X \oplus B$.

5.

$$(X \cup B) \oplus C = (X \oplus C) \cup (B \oplus C),$$

$$(X \cap B) \oplus C \subseteq (X \oplus C) \cap (B \oplus C),$$

$$(X \cap B) \ominus C = (X \ominus C) \cap (B \ominus C),$$

$$(X \cup B) \ominus C \supseteq (X \ominus C) \cup (B \ominus C),$$

$$X \ominus (B \cup C) = (X \ominus B) \cap (X \ominus C),$$

$$X \ominus (B \cap C) \supseteq (X \ominus B) \cup (X \ominus C).$$

6. Opening of the set X by the structuring element B is a union of all shifts, such that the shifted structuring element is inside X , i.e.

$$X \circ B = \cup_{y: B_y \subseteq X} B_y.$$

7.

$$X \bullet B = \{x \in E^n : x \in \check{B}_y \text{ such that } \check{B}_y \cap X \neq \emptyset\} = \cap_{y: \check{B}_y \cap X \neq \emptyset} (\check{B}_y)^c.$$

8. Opening of the set X is concerned by X , and closing consists of X , i.e.

$$X \circ B \subseteq X,$$

$$X \bullet B \supseteq X.$$

9. Dilation and erosion are dual operations, i.e.

$$(X \ominus B)^c = X^c \oplus \check{B},$$

$$(X \bullet B)^c = X^c \circ \check{B}.$$

7.3 Gray-level morphology

Two representation of gray-level function is used:

1. Function level representation;
2. Function umbra representation.

Level $T_t(f)$, $t \in V$ of function f is defined as:

$$T_t(f) = \{x \in D, f(x) \geq t\}.$$

The set of levels T defines function f .

Another representation of f [3] [4] [5] [2] is

$$U(f) = \{(x, t) \in D \times V, f(x) \geq t\},$$

$$f(x) = \sup\{t : (x, t) \in U(f)\}, x \in D.$$

Dilation and erosion of functions f and g are denoted $f \oplus g$ and $f \ominus g$ so that:

$$U(f \oplus g) = U(f) \oplus U(g),$$

$$U(f \ominus g) = U(f) \ominus U(g).$$

Let $f(x)$ and $g(x)$ be $f : F \rightarrow V, g : G \rightarrow V$, where $F, G \subseteq D$, then

$$(f \oplus g)(x) = \max_{z \in G_{x-z} \in F} \{f(x-z) + g(z)\},$$

$$(f \ominus g)(x) = \min_{z \in G_{x+z} \in F} \{f(x+z) - g(z)\}.$$

Gray-level dilation and erosion have the following main features:

1. Commutativity

$$f \oplus g = g \oplus f,$$

2. Associativity of dilation

$$(f \oplus g_1) \oplus g_2 = f \oplus (g_1 \oplus g_2),$$

3. Associativity of erosion

$$(f \ominus g_1) \ominus g_2 = f \ominus (g_1 \oplus g_2),$$

4. Conjugation of erosion and dilation

$$g \leq f \ominus k \leftrightarrow f \geq g \oplus k,$$

5. Duality Let $f : F \rightarrow V$, $g : G \rightarrow V$ and $x \in (F \oplus G) \cap (F \ominus \check{G})$. Then $-(f \oplus g)(x) = ((-f) \ominus \check{g})(x)$. Here $\check{G} = \{-y : y \in G\}$, $\check{g}(x) = g(-x)$.

Let $f : F \rightarrow V$ and $g : G \rightarrow V$. Opening and closing of the function f and the structuring element g are denoted $f \circ g$ and $f \bullet g$ respectively.

$$f \circ g = (f \ominus g) \oplus g,$$

$$f \bullet g = (f \oplus g) \ominus g.$$

For opening and closing the following features are true:

1.

$$(f \circ g)(x) \leq f(x)$$

for any $x \in F \circ G$,

2.

$$f(x) \leq (f \bullet g)(x)$$

for any $x \in F$,

3.

$$(f \circ g) \circ g = f \circ g, \quad (f \bullet g) \bullet g = f \bullet g.$$

This very important feature means that opening and closing are the idempotent operators, i.e. their secondary implementation does not change the image f .

4. Duality

$$-(f \circ g) = (-f) \bullet \check{g}.$$

5.

$$(f \circ g)(x) = \max\{t : (x, t) \in \bigcup_{y: U(g)_y \subseteq U(f)} U(g)_y\}.$$

From operation complexity point of view, the basic morphological operators are computationally expensive. Their realisation via convolution of the two sets requires $O(n * m)$ operations, where n and m are set potencies. One approach to the acceleration of the basic operations of mathematical morphology is to replace the convolution by the Fourier domain convolution (using fast fourier transform algorithm), which has complexity of $O(n \log m)$ operations.

In case of the binary structured element,

$$(f \oplus B)(x) = \max\{f(x - z), z \in B\},$$

$$f \ominus B(x) = \min\{f(x + z), z \in B\},$$

$$f \circ B = (f \ominus B) \oplus B,$$

$$f \bullet B = (f \oplus B) \ominus B.$$

The implementation of morphological operators with the binary structuring element allows to create fast a algorithm for their calculation. For this reason, the distributivity of erosion and dilation is used to decompose the structuring element. In this way, it is represented as a set of linear elements, such that the potency of this set equals to the dimension. We have the running operation, i.e. the output of one morphological operator with one linear structuring element is the input for the same operator with the next linear element. The computational complexity of linear morphological operator is also linear, because after shifting the structuring element in one position in a given direction, we need only some comparisons (approximately 3) to find the maximum/minimum value of the current data set. Such acceleration of morphological operators is acceptable for real-time applications even without special hardware.

Chapter 8

Glossary

In this section some terms which are often used in this thesis are listed.

2D - Two-Dimensional

3D - Three-Dimensional

AGP - Accelerated Graphics Port

CAOS - Computer Assisted Orthopaedic Surgery

CT - Computer Tomography

ECG - ElectroCardioGram

EEDM - External Euclidean Distance Map

EEG - ElectroEncephaloGram

EIDT - Euclidean Internal Distance Map

FPS - Frames Per Second

ICM - Iterative Closest Point

MDE - Mean Distance Error

MRI - Magnetic Resonance Imaging

MTD - Magnetic Tracking Device

OTD - Optical Tracking Device

PC - Personal Computer

PET - Positron-Emission Tomography

SPECT - Single-Photon Emission Computer Tomography

US - Ultrasound

VGL - Volume Graphics Library

Bibliography

- [1] R.M. Haralick, S.R. Stenberg, X. Zhuang. *Grayscale morphology*. In: Proc. of IEEE Computer Society Conf., Computer Vision and Pat. Recog. Florida, 1986.
- [2] R.M. Haralick, S.R. Sternberg, X. Zhuang. *Image analysis using mathematical morphology* . In: IEEE Trans. on Pattern Analys. and Mach. Intel., v.9, N 4, p. 532-550.
- [3] J. Serra. *Image analysis and mathematical morphology* . Academic Press, London, 1982.
- [4] J. Serra. *Image analysis and mathematical morphology* . vol.2: Theoretical Advances, Academic Press, London, 1988.
- [5] S.R. Sternberg. *Grayscale morphology* . In: Computer Vision, Graphics, And Image Processing 35, pp. 333-355,1986.
- [6] J. Serra L. Vincent. *Morphological filtering* . Lecture Notes on Morphological Filtering,1989.
- [7] F. Meyer S. Beucher. *Morphological segmentation* . In: Journal Of Visual Communication And Image Representation, Vol. 1. No. 1, September. pp. 21-46.1990.
- [8] S. Beucher F. Meyer. *The morphological approach to segmentation: the watershed transformation*. Mathematical Morphology in Image Processing, RIT, New York, 1992.
- [9] P. F. M. Nacken. *Image analysis methods based on hierarchies of graphs and multi-scale mathematical morphology*. PhD thesis, University of Amsterdam, The Netherlands, 1994.

- [10] S. Sheynin, A. Tuzikov, O. Krivonos. *Computation of the Opening Transform*. In: Math. Morphology and its Applications to Image and Signal Processing, CWI, 1998, pp. 339-346.
- [11] L. Billing. *Roentgen examination of the proximal femur end in children and adolescents. A standartized thechnique also suitable for determination of the collum-, anteversion-, and epiphysial angles. A study of slipped epiphysis and coxa plana*. In: Acta Radiol 1954, Suppl 110.
- [12] J. Rippstein. *Zur Bestimmung der Antetorsion des Schenkelhalses mittels zweier Roentgenaufnahmen*. In: Oerthopaedie 86, 1955, pp. 345-360.
- [13] J.L. Bentley. *Multidimensional binary search trees used for associative searching*. In: Communications of the ACM, 1975, 18(9), pp. 509-517.
- [14] R.J. Hernandez, M.O. Tachdjian A.K. Poznanski, L.S. Dias. *CT determination of femoral torsion*. In: AJR 1981, v. 137, pp. 97-101.
- [15] M. Fidler. *Planing an intertrochanteric femoral osteotomy*. In: Acta Orthop Scand 55, pp. 501-503, 1984.
- [16] D. A. Simon, M. Herbert, T. Kanade. *Techniques for Fast and Accurate Intra-Surgical Registration*. In: Journal of Image Guided Surgery. 1(1):17-29, April, 1995.
- [17] S. Lavallee. *Registration for computer-aided surgery: methodology, state of the art*. In: R. H. Taylor, et Al., eds, Computer-Integrated Surgery, chap 5, pp. 77-97. MIT Press, Cambridge, Massachusetts, 1995.
- [18] M. Blackwell, D. Simon, S. Rao, A. DiGioia. *Design and Evaluation of 3-D Pre-operative Planning Software: Application to Acetabular Implant Alignment* Report CMU-TR-RI-96-44, Robotics Institute, Carnegie Mellon University, Pittsburg, December 1996, 12 pages.
- [19] B. Schneider, J. Laubenbergen, S. Jemlich et al. *Measurement of Femoral Antetorsion and Tibial Torsion by Magnetic Resonance Imaging*. In: BJR 70, 1997, pp. 575-579.
- [20] P. Keppler, W. Strecker, L. Kinzl, M. Simmnacher, L. Claes. *Die sonographische Bestimmung der Beingeometrie*. In: Oertopaedie 28, Springer-Verlag, 1999, pp. 1015-1022.

- [21] T. DiGioia. *What is Computer Assisted Orthopaedic Surgery*. In: 4th CAOSUSA Conference in Pittsburgh, Pennsylvania, 2000, pp. 5-8.
- [22] D. A. Simon, K. T. Foley, J. R. Rampersaud. *The Fundamentals Of Virtual Fluoroscopy*. In: 4th CAOSUSA Conference in Pittsburgh, Pennsylvania, 2000, pp. 57-62.
- [23] D. M. Kahler. *Virtual Frluoroscopy: A Tool for Decreasing Radiation Exposure During Femoral Intramedullary Nailing*. In: *Medicine Meets Virtual Reality 2001*, J. D. Westwood et al (Eds.), IOS Press, 2001, pp. 225-228.
- [24] J. Yao at al. *A Progressive Cut Refinement Scheme for Revision Total Hip Replacement Surgery Using C-arm Fluoroscopy*. In: *Medical Image Computing and Computer-Assisted Intervention - MICCAI'99*, Second International Conference, Cambridge, UK, September 19-22, 1999, pp. 1010-1019.
- [25] R. Hofstetter, M. Slomczykowski, C. Krettek, G. Koeppen, M. Sati and L.-P. Nolte. *Computer-Assisted Fluoroscopy-Based Reduction of Femoral Fractures and Antetorsion Correction*. In: *Computer Aided Surgery 5*, 2000, pp. 311325.
- [26] P. Keppler, D. Moskalenko, O. Krivonos, F. Gebhard, L. Kinzl, J. Hesser, R. Maenner. *Computer Aided Correction of Bone Deformations*. In: *CAOS: Computer Assisted Orthopedic Surgery, Symposium*, Davos, Switzerland, 2000.
- [27] O. Krivonos, D. Moskalenko, P. Keppler, F. Gebhard, L. Kinzl, J. Hesser, R. Maenner. *Computer Aided Correction Of Osteotomies*. In: *10 ICBME, Biomedical Engineering in the New Millennium: Integration and Breakthroughs*, 6 - 9 Dec 2000, Mandarin Hotel, Singapore, pp. 565.
- [28] O. Krivonos, D. Moskalenko, P. Keppler, L. Kinzl, J. Hesser, R. Maenner. *Computer Simulation Of Osteotomy Correction*. In: *Medicine Meets Virtual Reality 2001*, J. D. Westwood et al (Eds.), IOS Press, 2001, pp. 247-249.
- [29] P. Keppler, O. Krivonos, D. Moskalenko, F. Gebhard, L. Kinzl, J. Hesser, R. Maenner. *Virtual planning and simulation of complex post-*

- traumatic deformities*. In: 1th Annual Meeting Computer Assisted Orthopaedic Surgery, Davos, Switzerland, February 7-10, 2001.
- [30] O. Krivonos, P. Keppler, J. Hesser. *Computer-Aided Osteotomy Correction: Planning And Operation Support*. In: 6th Intern. Conf. On Pattern Recognition and Information Processing, 15-17 May, 2001, Minsk, Belarus, pp. 101-105.
- [31] O. Krivonos, P. Keppler, F. Gebhard, L. Kinzl, J. Hesser, R. Maenner. *From Planning of Complex Bone Deformities Correction to Computer Aided Operation*. In: 14th IEEE Symposium on Computer-Based Medical Systems, 26-27 July 2001, Bethesda, Maryland, pp. 210-215.
- [32] W. K. Pratt. *Digital image processing*. John Willey & Sons, Inc., 1991.
- [33] R. C. Gonzalez and R. E. Woods. *Digital image processing*. Addison-Wesley, 1996.
- [34] O. Doessel. *Bildgebende Verfahren in der Medizin von der Technik zur medizinische Anwendung*. Springer, Berlin, 2000.
- [35] C. R. Maurer, J. M. Fitzpatrick. *A Review of Medical Image Registration*. In: *Interactive Image-Guided Neurosurgery*, Edited by R. J. Maciunas. In: Neurosurgical Topics, AANS, 1993, pp. 17-44.
- [36] J. G. Webster. *Encyclopedia of medical devices and instrumentation*. A Wiley-Interscience publication. Vol. 1, 1988.
- [37] J. G. Thomas, R. A. Peters, P. Jeanty. *Automatic segmentation of ultrasound images using morphological operators*. In: IEEE Trans. On Medical Imaging, 10(2), June 1991, pp. 180-186.
- [38] G. Sakas, L. Schreyer, M. Grimm. *Case study: visualization of 3D ultrasonic data*. In: Proceedings of Visualization'94 conference, 17-21 October 1994, Washington/DC, pp. 369-373.
- [39] G. Sakas, L. Schreyer, M. Grimm. *Pre-processing, segmentation and volume rendering of 3D ultrasonic data*. In: IEEE CG & A, Special Issue, vol. 15, No. 4, July 1995.

- [40] G. Sakas, S. Walter. *Extracting surfaces from fuzzy 3D ultrasonic data.* In: ACM Computer Graphics, SIGGRAPH-95, Los Angeles/USA, 6-11 August 1995.
- [41] M. C. Baker. *Evaluation of segmentation for bone structures in 3D rendering of ultrasound residual limb images.* Thesis, 1st Lt, USAF, December, 1996.
- [42] W. Albert, M. Pandit. *Processing of Ultrasound Images in Medical Diagnosis.* Handbook of computer vision and applications /edited by B. Jaehne et al, v. 1. Signal processing and pattern recognition, Academic Press 1999, pp. 387-413.
- [43] R. Frischholz. *Motion Tracking.* Handbook of computer vision and applications /edited by B. Jaehne et al, v. 3. Signal processing and pattern recognition, Academic Press 1999, pp. 329-344.
- [44] R. W. Prager, A. H. Gee, and L. H. Berman. *Practical segmentation of 3D ultrasound.* In: Medical Image Understanding and Analysis, pp. 161-164, Oxford, July 1999.
- [45] L. Joskowicz, C. Milgrom, A. Simkin, L. Tockus, Z. Yaniv. *FRACAS: A system for computer-aided image-guided long bone fracture surgery.* In: Journal of Computer-Aided Surgery, v. 3(6), May 1999.
- [46] O. Ron, L. Joskowicz, A. Simkin and C. Milgrom. *Computer-Based Periaxial Rotation Measurement for Aligning Fractured Femur Fragments: Method and Preliminary Results.* In: MICCAI 2001, pp. 17-23.
- [47] Medi-Cad. <http://www.medicad.de>.
- [48] F. Gebhard, O. Krivonos, U.C. Liener, P. Keppler, L. Kinzl, J. Hesser. *Bone Extraction from Ultrasound Images and Surface Matching with CT.* In: Proc. CAOS: Computer Assisted Orthopedic Surgery, Symposium, Davos, Switzerland, 17-19 February, 2000, pp. 48.
- [49] C. Amstutz, J. Kowal, M. Sati, L.-P. Nolte *A-mode ultrasound as a tool for non-invasive registration* In: Proc. CAOS: Computer Assisted Orthopedic Surgery, Symposium, Davos, Switzerland, 17-19 February, 2000, pp. 49.

- [50] O. Krivonos, J. Hesser, R. Maenner, F. Gebhard, U. Liener, P. Keppler, L. Kinzl. *Minimal Invasive Surgery of the Pelvis using Ultrasound*. In: 4th CAOSUSA Conference in Pittsburgh, Pennsylvania, 2000, pp 203-205.
- [51] O. Krivonos, F. Gebhard, P. Keppler, L. Kinzl, J. Hesser, R. Maenner. *Implementation of Ultrasound for Treatment Of Pelvis Fractures*. In: 10 ICBME, Biomedical Engineering in the New Millennium: Integration and Breakthroughs, 6 - 9 Dec 2000, Mandarin Hotel, Singapore, pp. 479-480.
- [52] O. Krivonos, F. Gebhard, P. Keppler, L. Kinzl, J. Hesser, R. Maenner. *Computer Assisted Treatment Of Pelvis Fractures*. In: Medicine Meets Virtual Reality 2001, J. D. Westwood et al (Eds.), IOS Press, 2001, pp. 242-246.
- [53] O. Schorr, H. Woern. *A new concept for intraoperative matching of 3D ultrasound and CT*. In: Medicine Meets Virtual Reality 2001, J. D. Westwood et al (Eds.), IOS Press, 2001, pp. 446-451.
- [54] J. Tonetti, L. Carrat, S. Blendea, J. Troccaz, Ph. Merloz, S. Lavallee, J-P. Chirossel. *Clinical validation of computer assisted pelvic surgery using ultrasound. A percutaneous safe technique with low radiation exposure*. In: Medicine Meets Virtual Reality 2001, J. D. Westwood et al (Eds.), IOS Press, 2001, pp. 515-520.
- [55] D. V. Amin, T. Kanade, A. M. GiGioia, B. Jaramaz, C. Nikou, R. S. LaBarca. *Ultrasound based registration of the pelvic bone surface for surgical navigation*. In: CAOS'01, 7-10 February, 2001, pp. 48.
- [56] J. Tonetti, L. Carrat, S. Blendea, J. Troccaz, Ph. Merloz, S. Lavallee. *Clinical validation of percutaneous computer assisted surgery using ultrasound. A safe technique with low radiosopic radiation*. In: CAOS'01, 7-10 February, 2001, pp. 48.
- [57] J. Koval, C. A. Amstutz, and L.-P. Nolte. *On B-mode ultrasound-based registration for computer assisted orthopaedic surgery*. In: CAOS'01, 7-10 February, 2001, pp. 47.
- [58] 3Ddoctor <http://www.ablesw.com/3d-doctor>.

- [59] Northern Digital Inc. <http://www.ndigital.com>.
- [60] Mednetix AG. <http://www.mednetix.ch>.
- [61] A. Rosenfeld, J.L. Pfalz. *Distance function on digital pictures*. In: Pattern recognition, 1, pp. 33-61, 1968.
- [62] B. K. P. Horn. *Closed-form solution of absolute orientation using unit quaternions*. In: Journal of the Optical Society of America A. 4(4):629-642, April, 1987.
- [63] L. G. Brown. *A Survey of Image Registration Techniques*. In: ACM Computing Surveys. Vol. 24, No. 4, December 1992.
- [64] P. Besl, N. McKay. *A Method for Registration of 3-D Shapes*. In: IEEE Trans. On PAMI, 14, 2, pp. 239-256, 1992
- [65] E. J. Holupka, H. M. Kooy. *A geometric algorithm for medical image correlations*. In: Med. Phys. 19, pp. 411-417, 1992.
- [66] H. Jiang, R. A. Robb, K. S. Holton. *A new approach to 3-D registration of multimodality medical images by surface matching*. In: Proc. SPIE, Visualization in Biomedical Computing, 1808, pp. 196-213, 1992.
- [67] Ch. Schuetz, H. Huegeli. *Recognition of 3D Objects with a Closest Point Matching Algorithm*. In: IAPRS, v. 30, Part 5W1, ISPRS Intercommission Workshop "From Pixels to Sequences", Zurich, March 22-24, 1995.
- [68] S. A. Dudani, K. J. Breeding, R. B. McGhee. *Aircraft identification by moment invariants*. In: IEEE Trans. Computers, 26, pp. 39-45, 1977.
- [69] M. K. Hu. *Visual pattern recognition by moment invariants*. In: IEEE Trans. Information Theory, 8, pp. 179-187, 1962.
- [70] J. V. Sharp, R. L. Christensen, W. L. Gilman, F. D. Schulman. *Automatic map compilation using Digital Technique*. In: PE&RS, (31) 3, pp. 233-239, 1965.
- [71] J. P. W. Pluim, J. B. A. Maintz and M. A. Viergever. *Interpolation artefacts in mutual information based image registration*. In: Computer Vision and Image Understanding, 77(2), pp. 211-232, 2000.

- [72] C. Studholme, D. L. G. Hill, D. J. Hawkes. *Automated 3D registration of MR and CT images of the head*. In: Medical Image Analysis, (1) 2, pp. 163-175, 1996.
- [73] W. Lorensen, H. Cline. *Marching Cubes: A high resolution 3D surface construction algorithm*. In: ACM Computer Graphics 1987, 21:163-170.
- [74] W. Schroeder, J. Zerge, W. Lorensen. *Decimation of triangle meshes*. In: Computer Graphics (SIGGRAPH'92), 26(2):65-70, August 1992.
- [75] W. Schroeder, K. Martin, W. Lorensen. *The visualization toolkit: an object-oriented approach*. 1996 by Prentice Hall PTR, Prentice-Hall, Inc.
- [76] J. Hesser, C. Poliwoda. *Visualization of volume data*. Handbook of computer vision and applications /edited by B. Jaehne et al, v. 3. Signal processing and pattern recognition, Academic Press 1999, pp. 875-906.
- [77] B. Geiger. *Three-dimensional modeling of human organs and its application to diagnosis and surgical planning*. Thesis, Inria 1993.
- [78] J-D. Boissonnat and B. Geiger. *Three dimensional reconstruction of complex shapes based on the Delaunay triangulation*. In: Biomedical Image Processing and Biomedical Visualization, edited by R. S. Acharya and D. B. Goldgof, SPIE 1993, v. 1905, pp. 964-975.
- [79] Volume Graphics GmbH. <http://www.volumegraphics.com>.
- [80] G. Johansen and J. Bill. *A threshold selection method using information measures*. In: Proceedings, 6th Int. Conf. Pattern Recognition, Munich, Germany, pp. 140-143, 1982.
- [81] P.K. Sahoo S. Soltani A.K.C. Wong Y.C. Chen. *A survey of thresholding techniques*. In: Computer Vision, Graphics and Image Processing. 1988, Vol.41, 233-260.
- [82] N. Otsu. *A threshold selection method for grey level histogram*. In: IEEE Trans Sys Man, SMC- 8, 1978, 62- 66.
- [83] S.S. Reddi S.F. Rudin S.F. H.R. Keshavan. *An optimal multiple threshold scheme for image segmentation*. In: IEEE Trans. on System, Man and Cybern., Vol.14, 661-665, 1984.

- [84] J.S. Weszka A. Rosenfeld. *Histogram modification for threshold selection*. In: IEEE Trans. on Systems, Man and Cyber., Vol.9, No.1, 38-52, 1979.
- [85] C-F. Westin, S. Warfield, A. Bhalerao, L. Mui, J. Richolt, and R. Kikinis. *Tensor Controlled Local Structure Enhancement of CT Images for Bone Segmentation*. In: Proc. MICCAI'98, pp. 1205-1212, ISBN 3-540-65136-5, Lecture Notes in Computer Science, Eds. W. M. Wells, A. Colchester, and S. Delp, Springer Verlag, October 1998.
- [86] M. Viceconti, M. Casali, B. Massari, L. Cristofolini, S. Bassini and A. Toni. *The "Standartized femur program" proposal for a reference geometry to be used for the creation of finite element models of the femur*. In: Journal of Biomechanics 1996, 29(9): 1241.
- [87] R. M. Haralick, K. Shanmugam and I. Dinstein. *Textural Features for Image Classification*. In: IEEE Trans., on Systems, Man abd Cybernetics, Vol SMC-3, pp. 610-621.
- [88] R. Adams, L. Bischof. *Seeded Region Growing*. In: PAMI 16(6), pp. 641-647, 1994.
- [89] T. B. Sebastian, H. Tek, J. J. Crisco, S. W. Wolfe, B. B. Kimia. *Segmentation of Carpal Bones from 3d CT Images Using Skeletally Coupled Deformable Models*. In: MICCAI 1998, pp. 1184-1194.
- [90] A. Yezzi, S. Kichenassamy, A. Kumar, P. Oliver, A. Tannenbaum. *Geometric Snakes for Edge Detection and Segmentation of Medical Images*. In: IEEE Transaction on Medical Imaging, 16, pp. 199-209, 1997.
- [91] M. Bomans, K.-H. Hohne, U. Tiede and M. Riemer. *3D segmentation of MR images of the head for 3D display*. In: IEEE Trans. on Medical Imaging, 9(2), June 1990, pp. 177-183.